DEVELOPING A TRANSIENT PHOTOVOLTAIC INVERTER MODEL IN OPENDSS USING THE HAMMERSTEIN-WIENER MATHEMATICAL STRUCTURE

by

Laura M. Wieserman

BS in Electrical Engineering Technology, University of Pittsburgh at Johnstown, 2012

Submitted to the Graduate Faculty of

Swanson School of Engineering in partial fulfillment

of the requirements for the degree of

Doctor of Philosophy

University of Pittsburgh

2016

UNIVERSITY OF PITTSBURGH

SWANSON SCHOOL OF ENGINEERING

This dissertation was presented

by

Laura M. Wieserman

It was defended on

November 16, 2016

and approved by

Alexis Kwasinski, Ph.D., Associate Professor
Department of Electrical and Computer Engineering

Gregory Reed, Ph.D., Professor
Department of Electrical and Computer Engineering

Jerry Samples, Ph.D., Professor
Department of Mechanical & Chemical Engineering

Jeffrey Vipperman, Ph.D., Professor
Department of Mechanical & Bioengineering Engineering

Dissertation Director: Thomas McDermott, Ph.D., Adjunct Professor
Department of Electrical and Computer Engineering

Co-Director: Zhi-Hong Mao, Ph.D., Associate Professor,
Department of Electrical and Computer Engineering & Bioengineering

DEVELOPING A TRANSIENT PHOTOVOLTAIC INVERTER MODEL IN OPENDSS USING THE HAMMERSTEIN-WIENER MATHEMATICAL STRUCTURE

Laura M. Wieserman, PhD

University of Pittsburgh, 2016

Photovoltaic (PV) modules (direct current) have continued to decrease in price over the past decade causing the number of PV installations to increase [1]. With increase in use of PV renewable resources come more interconnections to the electrical power grid and hence system protection challenges for planning engineers [2]. PV inverters (direct current to alternating current interconnections) do not behave like traditional generators having rotational inertia and long-lived electrical time constants. In contrast, inverters have no inertial mass and very short time constants. Manufacturers do not provide inverter design details. Therefore, current inverter circuit models available for studying inverter behavior and completing inverter grid integration tasks are not adequate. In addition, the inverter models currently used by planning engineers only provide steady state solutions; not accurate time-domain results for rapid load changes especially during electrical circuit fault conditions. Inadequate and inaccurate planning models result in unreliable system protection designs, leading to possible operational failure, mis-coordination of protective equipment [3], and system damage. Valid transient models are necessary to plan for

unusual circuit conditions including overvoltages, grounding conditions, and anti-islanding on electric grid feeders connected to photovoltaic resources or utilities desiring to add photovoltaic resources to an existing feeder.

This research makes an original contribution by providing a modeling solution for solar PV inverter transients using the Hammerstein-Wiener (HW) mathematical structure. The analysis is based on laboratory test data from single-phase, micro, and three-phase inverters. Data was collected during open-circuit, short-circuit and voltage sag events. Each inverter was tested at multiple output power levels and multiple tests were run for each case to account for point-on-wave effects on the transient magnitudes. The HW framework, which integrates linear dynamics and nonlinearities, provides a framework for the transient PV inverter model. The model was incorporated into an open source distribution simulation software; OpenDSS. Test results show that PV inverters cause significant over-voltages and over-currents during transient events, but these have been difficult to predict accurately in simulations. The OpenDSS model provides a solution for modeling these nonlinear behaviors for design and operating studies and can be expanded to incorporate other power system components.

TABLE OF CONTENTS

LIST OF TABLES

LIST OF EQUATIONS

LIST OF FIGURES

xi

xii

xiii

PREFACE

A major research project is never the work of anyone alone. The contributions of many different people, in their different ways, have made this research possible. I would like to extend my appreciation to the following. First, I would like to thank God for his wisdom and guidance during this research project and throughout my life. Second, I want to thank my academic advisor, Dr. McDermott, for accepting me into his group and for his guidance throughout my research at the University of Pittsburgh. He has contributed to a rewarding graduate school experience by supporting my attendance at conferences, engaging me in new ideas, demanding a high quality of work, giving me intellectual freedom in my work, advice throughout research, as well as his pain-staking effort in proof reading the drafts. Also, I would like to thank my committee members Dr. Kwasinski, Dr. Zhi-Hong Mao, Dr. Gregory Reed, Dr. Jerry Samples, and Dr. Jeffery Vipperman for their interest in my research. In addition, this research would not have been possible without the help from my fellow graduate students: Cedric Ofakem and Santino Graziani. Both assisted with the laboratory testing, and Santino also helped with the software implementation.

I also am grateful for the funding provided by Electric Power Research Institute (EPRI) which allowed me to pursue my graduate school studies and made this research possible. Both

1.0   BACKGROUND STATEMENT

Photovoltaic (PV) modules (direct current) have continued to decrease in price over the past decade causing the number of PV installations to increase [1]. With increase in use of PV renewable resources come more interconnections to the electrical power grid and hence system protection challenges for planning engineers [2]. PV inverters (direct current to alternating current interconnections) do not behave like traditional generators having rotational inertia and long-lived electrical time constants. In contrast, inverters have no inertial mass and very short time constants. Manufacturers do not provide inverter design details. Therefore, the current inverter circuit models available for studying inverter behavior as well as completing inverter grid integration tasks are not adequate. In addition, the inverter models currently used by planning engineers only provide steady state solutions; they do not provide accurate time-domain results for rapid load changes and especially during electrical circuit fault conditions. Inadequate and inaccurate planning models will result in unreliable system protection designs, leading to possible operational failure, mis-coordination of protective equipment [3], and system damage. Valid transient models are necessary to plan for unusual circuit conditions including overvoltages, grounding conditions, and anti-islanding on electric grid feeders connected to photovoltaic resources or utilities desiring to add photovoltaic resources to an existing feeder.

Distribution protection has seen many changes in recent years with the integration and increase in the number of Distributed Generation (DG) technologies. A significant portion of this DG increase has been in the form of inverter-based technology, as opposed to the more traditional rotating machine technology. Because inverter technology is relatively new compared to rotating machine, fewer models exist that can properly characterize an inverter's response to electrical events resulting from normal operational switching or fault conditions.

Inverter controls have very complex, and varied, behaviors for dynamic responses. It is very difficult for time-constrained planners to be able to build a detailed model to represent these complex controls for each inverter type. For planning purposes, the objective of this research was to obtain a simplified model that is sufficient for determining a conservative design.

Planning and protection engineers need additional data and better planning tools to assist them in planning and protecting their system. This research provides better prediction of inverter behavior in order to perform protection studies.

Many single and three phase inverter manufacturer circuit models exist, but these models represent the steady state operation of the inverter and consequently only have a single operating point. However, the transient operation (fault conditions) of the inverter causes the operating point of the inverter to leave the linear region around the steady state operating point. Once the inverter leaves its steady state operation (its defined steady-state operating point), the existing circuit models are no longer accurate. Due to the inaccuracy of using steady state PV inverter models to simulate transient events, this research developed and implemented into open source software a transient PV inverter model. The model developed in this research uses a moving operating point which tracks the transient operation of the inverter under events typically seen on

the power system including the extremes of load rejections (open circuit) and fault contributions (short circuit).

The transient photovoltaic inverter model was constructed using the load rejection and fault contribution test data collected in the Electric Power Systems Laboratory (EPSL) on four single-phase inverters, three micro-inverters, and a three-phase inverter; each from different PV inverter vendors. Multiple inverters were tested in order to incorporate their differences into the transient inverter model. Multiple data sets were collected during both open-circuit, short-circuit, and voltage sag transient events. Each inverter was also tested at four different output power levels (25%, 50%, 75%, and 100%) and tests are made at fifteen degree increments (90deg to 255deg) for each case to account for point-on-wave effects on the transient voltage and current magnitudes.

The model will follow the Hammerstein-Wiener (HW) mathematical structure. The Hammerstein-Wiener nonlinear continuous-time model is constructed using inverter input and output data collected from the inverter testing regime. <u>The Hammerstein-Wiener modeling provides a framework for simulating non-linear and time-varying transients produced by PV inverters.</u> <u>It does this by separating linear, non-linear and possibly time-varying features of the inverter into three cascaded sub-modules</u> [4]. The submodules consist of an input nonlinearity module, linear module, and an output nonlinearity module. If the nonlinearity blocks have nonlinear estimators set to unity, the linear block would remain, which simulates the steady state operation of the PV inverter [5]. However, by using nonlinearity estimators (see section 4.2.2.3) it is possible to move the operating point of the PV inverter model to track the transient operation of the inverter electrical characteristics. Multiple nonlinear estimators were tested to determine which seemed best to describe the input and output nonlinearities of the inverter system; the

nonlinear estimator that best simulates the PV inverter transients is the piecewise linear estimator.

The transient inverter model developed in OpenDSS allows the user to choose from either a micro-inverter or a single-phase inverter model already incorporated into the OpenDSS library, or create their own customized transient model. If a transient model is desired for an inverter manufacturer which was not included in this research, the user only needs to have access to the inverters transient input and output response. This data can currently be requested from the inverter vendor, however, due to ongoing changes to the IEEE standards, the vendors may eventually be required to provide this data. If access was not available to the data, the inverters transient response could easily be captured by preforming the same tests outlined in this research. The data can then be incorporated at low fidelity by using the MATLAB® script created in this research, however for a higher fidelity model, each inverter model will need to be tuned by choosing the number of breakpoints necessary for the inverter nonlinearity estimators.

Since the transient PV inverter model developed through this research was also incorporated into OpenDSS software, electric utilities will be able to easily incorporate the model into their feeders in order to accurately simulate the impact the PV inverters on the feeder during transient events.

While characterizing the behavior of photovoltaic (PV) inverters under various transient conditions, the objective is to enable more accurate planning and interconnection studies by power system engineers [1, 2]. However, potentially powerful transient models have four significant barriers to widespread use:

(1) There is little or no portability between different computer programs.

(2) High learning curves exist for both the vendor and user.

(3) Validation and convergence issues occur when used outside of its tested range.

(4) Vendors have concerns over possible reverse engineering proprietary design details.

With these concerns in mind, this research meet the objectives in three ways:

(1) Identified new PV inverter behavior tests and analysis methods to help inform the interconnection standards now under revision by the IEEE Standard 1547 working group.

(2) Identified and validated new PV inverter model extraction procedures, from data that is likely to be available and for tools that are likely to be available to power system engineers.

(3) Developed a transient model of the PV inverter in open source software that mimics both the inverter's steady state dynamics and its nonlinear transient behavior for a user defined range of inputs. (DC input voltage, AC grid voltage, Power output level)

In summary, there are many steady state models for inverters [6, 7]. Remembering that a steady state model is defined around a linear range of a single operating point, this model can only be used under conditions close to the operating point. In practical operations, inverter operating conditions can change suddenly from steady state to faulted conditions such as islanding, short circuits, open circuits, and power fluctuations. In order to understand the operation and impacts of the PV inverters on the power system during transient conditions, laboratory testing, modeling and simulation of the inverter is necessary.

This dissertation is different from software based research since it is not solely based on software simulation. Enabled by the recent construction and opening of the Electric Power System Laboratory, data was collected in the laboratory and then mathematically constructed

through data analysis techniques into a model structure. Then, the collected data is compared to the proposed model output for comparison. In this manner, all simulations and models were compared against "real-world" data.

This dissertation research makes an original contribution by providing a modeling solution for the transient behavior of photovoltaic inverters under load rejection and fault contribution transient events. The solution, a Hammerstein-Wiener mathematical structure, provides a non-linear time-varying solution for the transients produced by photovoltaic inverters. The Hammerstein-Wiener mathematical model provides a solution for developing the photovoltaic inverter transient model. Advantages of the Hammerstein-Wiener model include being able to describe both the linear and non-linear transient effects of the inverter and allowing a possible avenue for describing the internal control of the inverter during the transient events. This dissertation not only provides a solution for the photovoltaic transient model, but also implemented the model in both MATLAB and a distribution simulation software platform called OpenDSS. This implementation allows the modeling solution to be used at the present time by planning engineers.

The remainder of the dissertation is outlined in the following sequence: This section provided the background on why this research was necessary and the approach followed to provide a transient PV inverter model. Section 2.0 provides a literature review constructed to give an outline of the current and past research in the field of transient inverter characterization. Section 3.0 provides an overview of the laboratory facility, testing procedures, data processing, and test results from the PV inverter transient testing. Section 4.0 takes the reader through the process of comparing the PV data to multiple mathematical structures. This process produced the mathematical structure used to create and develop the PV transient inverter model that is

presented in section 5.0 . After the appropriate structure was found and the mathematical model developed, the model was incorporated into open source distribution simulation software; OpenDSS. The implementation of the model into OpenDSS as well as example test cases is shown in section 6.0. Lastly, section 7.0 provides a summary of the dissertation by providing answers to the following questions: 'What has this research accomplished?', 'What is the impact of this research?', and 'What future work and research can be done to further what this research accomplished?'. The appendix gives voltage sag results, model results from the sag events, and an example of using the developed model on an IEEE test feeder.

1.1   ACCOMPLISHMENTS SINCE THE PROPOSAL EXAM

In order to aid the reader on what research was completed since the oral proposal exam in December 2015, this section outlines the major accomplishments over the last year that are outlined in detail within this dissertation.

First, each single-phase and three-phase inverter was re-tested under both open-circuit and short-circuit results using the voltage sag generator from EPRI. This eliminated the break-before-make operation of the EPSL addressed at the oral proposal exam. In addition, three micro-inverters were added to the list of tested inverters.

Second, in addition to open-circuit and short-circuit testing, each inverter was tested during voltage sag events. The single-phase and three-phase inverters were tested at 60%, 70%, 80%, and 90%. The micro-inverters were tested at 40%, 60%, 80%, and 90%.

Third, the HW framework originally proposed was validated and used to create transient inverter models in MATLAB. Then, the HW framework and inverter models were implemented and tested in OpenDSS. This required learning the OpenDSS software and the pascal programming language.

Lastly, a journal paper was submitted to IEEE Transactions on Power Delivery and outlined the open and short circuit testing. A second journal or conference paper is in progress which will outline the sag event testing, the HW modeling framework, and results from the developed transient PV model demonstrated in IEEE test feeders. In addition, EPRI extended the project since the proposal and one of their groups is considering using our HW modeling structure for transmission-connected wind and PV generation.

2.0   LITERATURE REVIEW

Harnessing electricity from one the greatest alternative energy resources in our world, the sun, has been a part of history since the late eighteen hundreds. In 1876 William Grylls Adams, along with his graduate students, discovered that the energy from the sun could be converted into electricity through selenium [8, 9]. This discovery started the search for other materials in order to make the conversion process more efficient. However, not until 1953 was the silicon cell used for solar energy conversion, and within a year, the "solar cells" were sold commercially [10]. Since the technology and the process of refining the silicon was new, the cost was very high ($300/Watt) [11]. The initial solar cells were only used for research and space application due to retail costs, but by the 1990s the cost of solar had decreased to approximately $20/Watt. Depending on geographic location and application, solar can be completely installed with backup batteries for around $7/Watt [12]. There is also a current research target to decrease the cost of solar to $1/Watt by 2020 [13] , however, the there is some hesitation by researchers that the installation prices may not permit this low of a price by 2020. Time will tell.

With the price of solar becoming an economical option by the late 1990's, the number of home solar installations has continued to increase over the past couple decades [14]. With the increase of solar installations on homes, comes the need to convert the direct current (DC) output of the panels to alternating current (AC) to interface to the home and grid electrical

infrastructures. (This increase in solar installations on the electrical grid is most commonly referred to as "solar penetration"). In order to complete this electrical transformation from DC to AC, the photovoltaic inverter is necessary.

Since grid-tied photovoltaic inverters are currently necessary for home and utility solar installations that use AC, and with the electric power grid still required to maintain reliability, there is concern by utilities about the effect the increase in solar installations will cause. For example, when the sun is shining, the solar energy conversion can help support the grid, but during cloudy days the grid is required to provide more power to the loads.

The power utilities are also concerned with the effect the PV inverters will have if the grid experiences transient conditions such as electrical faults. This concern caused requirements for grid-tied solar inverters to be incorporated into both UL-1741 and IEEE Standard 1547, requiring the inverter to disconnect during conditions where the grid itself may be temporarily disconnected [15]. In addition, the Institute of Electrical and Electronics Engineers (IEEE) wrote a Standard for Interconnecting Distributed Resources with Electric Power Systems (IEEE 1547) providing requirements for performance, operation, testing, safety considerations, and maintenance of the interconnection of the installation of grid-tied solar inverters [16].

Photovoltaic inverters have been around since the late 1900's, and their operation and electrical structures are not new to the power engineer [17, 18, 19]. For this reason, the photovoltaic inverters during steady state operations will not be discussed in detail. Therefore, this literature review will turn its focus to the transient operation of the photovoltaic inverters.

Most of the recent research has been focused on the transients caused by fluctuation in solar output due to cloud movements. In [20], transient modeling and analysis of a pulse-width modulated inverter was published, however the transient placed on the inverter came from small

changes in the load. This only creates a small perturbation from the steady state operating point and is consequently accurate for only "small-signal" changes. Adding to the field in terms of modeling techniques was shown in [21], which produced a black-box model of Three-Phase Voltage Source Inverter (VSI) based on transient response analysis. It proved that the black-box modeling approach can be applied to VSI's. However, the transient applied was a load step response and the result was in the form of a Linear Time Invariant (LTI) transfer function (a linear system). Mention was made that nonlinearities exist, but were not included in the model. Similar research, [22], claimed to create transient models of photovoltaic inverter operations, however, the transient have been limited to small changes in either the DC voltage due to cloud movement, or small AC changes due to load fluctuations. The major problem in PV inverter modeling is that the models have not been verified in laboratory environments to develop a detailed computational model representing the dynamic characteristics of vendor-specific devices. As part of a new PV Distributed Generation (DG) plant interconnection impact study [23] and on-going steady-state voltage and power flow analysis, most utilities are requiring an in-depth investigation of potential dynamic impacts of inherently variable PV-DG units on transient feeder voltages under various load and generation conditions. New study tools and dynamic models are needed to help engineers investigate the potential impact of PV generation on the grid; the solution provided by this dissertation.

The expansion of PV-DG is expected to continue. Therefore, it is critical for distribution utilities to understand the associated impacts of integrating PV-DG plants on distribution system planning and operation, but also for the impacts associated with PV integration. The steady state operation of the photovoltaic inverters are well known, but there is a gap in the knowledge of

11

their operation during transient events such as load rejection (open circuit) or fault contribution (short circuit) conditions. Again, the goal of this research.

In 2014, I along with Dr. McDermott published a paper showing fault current and over-voltage calculations for inverter based generation using symmetrical component analysis [24]. The calculations analyzed a test feeder with PV distributed generation, and focused on calculating the theoretical overvoltage and overcurrent associated with balanced and unbalanced faults on the feeder. In addition, the effects on the overvoltage's and overcurrent's due to PV inverter grounding was also addressed. The paper was presented in September 2014 at the Energy Conversion Congress and Expo (ECCE) conference. The fault testing completed in this dissertation is a continuation of this paper and the theoretical results can be verified in the laboratory. Due to the transient overvoltage and overcurrent experienced during faults, a dynamic transient model needs to be used for planning and understanding the effects of PV on distribution feeders.

One current benchmark of this research [24], supported by a NSF CAREER grant, proposed a single-phase grid-connected photovoltaic system modeled in MATLAB Simulink. The model includes the PV array and integration of Maximum Power Point Tracking (MPPT) with an averaged model of the power electronics. In addition, the Electric Power Research Institute (EPRI) has made strides to characterize the inverters response to electrical events for both normal operation switching and fault conditions [25]. EPRI has also supported both inverter testing and modeling efforts of inverters that can be used in distribution planning and protection studies. However, [24, 25], are not really practical for widespread use, by electric utilities or others. In addition, the research also recognizes that a nonlinear model is needed and necessary, but does not provide one.

12

Barker [27] and an IEEE Working Group [28] have summarized the protection issues with any type of distributed generation (DG), including overvoltages, fault current contributions, device coordination, islanding, etc. Arritt and Dugan [29] summarized the effects of interconnection transformers on overcurrents and overvoltages from DG, and provided guidance on selecting transformer neutral impedance where applicable. In this prior work, the DG characteristics are important, but so are the balance-of-system components like transformers, loads and capacitor banks. The faulted behavior of rotating machine DG is well understood, but that of PV inverters is less well understood and that is our focus here.

For example, Bravo et. al. performed a load rejection test on a PV inverter with two different inverter software versions [30]. They found an overvoltage of 230% for five cycles with the old software, and then an overvoltage of 177% for two cycles, albeit with a higher impulse voltage, with the new software. Expanding the test regime to three inverter specimens, they found load rejection overvoltages ranging from 190% to 225% for one-half to three cycles [31]. One of the inverters failed during the test, but the other two produced three-phase short circuit currents of 120% to 178% for one cycle, followed by 100% for up to eight cycles. The single-phase short circuit current ranged from 110% to 200% for nine cycles. These results illustrated that PV inverter behavior during open and short circuits will depend on the vendor, control settings and even the version, in ways not presently documented in the catalog data or standard tests. Their results also support a commonly used rule-of-thumb that PV inverters may contribute two times rated current to an external short circuit, but in some cases the currents were higher.

Bravo et. al. emphasized the need for good PV inverter models to perform impact studies [3]. A recent survey of utilities confirms the need for good models; 25% of respondents were primarily concerned about overvoltages from DG, second only to islanding [32]. Nearly 30%

13

reported surge arrester failures from DG-caused overvoltages. Of those who had required direct transfer trip on DG, nearly 20% listed protective device coordination as a reason.

Rotating machines can be modeled with a voltage behind impedance, or Thevenin equivalent. In contrast, PV inverters act more like a controlled current source. It is possible to analyze a circuit with PV inverters modeled as a current in parallel with impedance, or Norton equivalent, and then simulate the impacts of loads, transformers and capacitor banks [23]. However, that approach ignores inverter control dynamics. A full transient model of the inverter can provide better results [33]. However, that approach requires inverter design details and simulation software licenses that are not available to most users. A practical middle ground might involve time-dependent Norton equivalents, analogous to the time-dependent Thevenin equivalents (i.e. synchronous, transient and sub-transient) that apply to rotating machines.

More recently, a group funded by DOE and SolarCity reported on a series of load rejection tests on five inverters [34]. The amount of retained load was varied as a test parameter, and the overvoltage varied from 106.9% to 184.5%, depending on the inverter type, DC link voltage and retained load. That group also reported ground fault overvoltage tests and simulations on three inverters [35], with variations in the interconnection transformer and the presence of anti-islanding detection. They found that wye-grounded / wye-grounded interconnection transformers are the best choice for PV inverters, but that ground fault overvoltages can still occur.

This project contributes test results on a set of eight PV inverters that have not been tested this way before. More importantly, our approach differs in attempting to characterize the PV inverter behavior on its own, so that balance-of-system components can be modeled separately. System parameter variations are not included in the test program. Instead, we aim to

14

develop PV inverter models that are suited for system-level studies, and also to suggest standard tests that could help define such models.

The research discussed in this dissertation was funded by EPRI, and is a continuation of their inverter testing and modeling efforts to create a model useful for widespread use by electric utilities for distribution planning and protection studies.

3.0   LABORATORY FACILITY

The laboratory testing uses the Electric Power System Laboratory (EPSL) located in Benedum Hall at the University of Pittsburgh [26]. The EPSL is supplied by a 75 kVA feeder at 480V and incorporates multiple types of generation including photovoltaic generation and traditional grid tie. The EPSL, Figure 1, includes six experiment stations with configurable loads, motor drives, meters, relays and controllers. The laboratory also includes a local area network (LAN), programmable logic controller (PLC) equipment, custom-built surge and sag generators, uninterruptible power supply (UPS), hardware development tools, smart meters and other test equipment. Both 480V AC and 208V AC systems are available, along with a DC system connected to photovoltaic arrays installed on the roof. The six test benches provide a total 30 kW of adjustable RLC load, including harmonic-producing compact fluorescent lights. A 25-kW synchronous generator and 10-kW controllable DC power supply (PV emulator) enable dedicated micro-gridding in the EPSL.
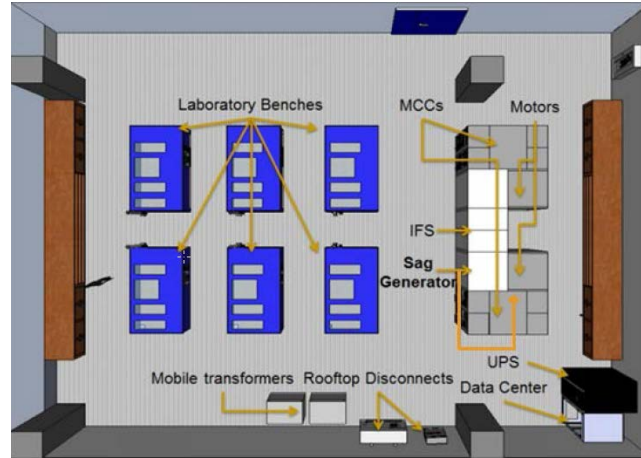
Figure 1. EPSL Laboratory Layout [9]

Multiple single-phase and three-phase PV inverters from different vendors are also available for testing; these range in size from 2 kW to 10 kW. Six configurable three-phase transformer banks, each rated 6 kVA, are available for grounding and interconnection studies. A three-phase bank of variable transformers is available for short-circuit testing at reduced voltages.

Through the EPSL variable system strength, the generation sources can feed a variety of loads, centered on laboratory workbenches, combining passive and motor loads in a system with advanced metering and control. The key components of the EPSL used for testing are the laboratory workbenches, integrated sag generator, 10 kW Photovoltaic Emulator, PV Inverters, and motoring equipment. Each of the testing equipment used in this research are described in further detail in the following sections.

3.1   LABORATORY WORKBENCHES

There are six laboratory workbenches located in the EPSL. Each workbench, Figure 2, is capable providing 5kW of varying types of loads. The benches provide adjustable resistive, reactive, capacitive, and harmonic loads. In addition, the benches can be monitored through a local area network (LAN) or a programmable logic controller (PLC).

Figure 2. Single EPSL Workbench

3.2   PHOTOVOLTAIC EMULATOR

In order test the photovoltaic inverters, a photovoltaic source in the form of a photovoltaic emulator (programmable solar source) is utilized. The photovoltaic emulator is a TerraSAS10-kW, 600Vdc controllable DC power supply as shown in Figure 3. The emulator is controlled by a personal computer (PC) via a graphical user interface (GUI) display. Programmable parameters

such as the solar irradiance level, temperature value, voltage, current, and temperature coefficient allow full control of a photovoltaic panel for laboratory testing and analysis.

Figure 3. 10kW Photovoltaic Emulator

The entered set of VI curves, via the parameter settings, is displayed on the emulators software GUI interface to monitor the output of the emulator. The actual measured data is then overlaid on the PC screen so that the operating point can be viewed in real time. A screenshot of the emulator software interface is shown in Figure 4.
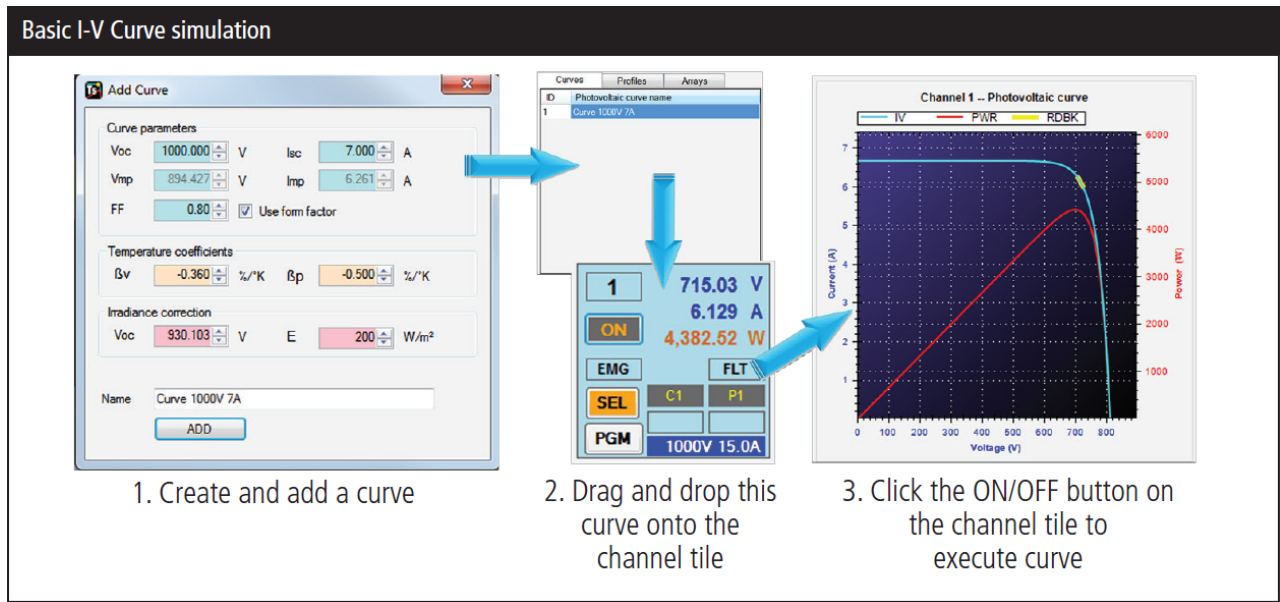
Figure 4. Simulator Real-time Interface [36]

Through programming PV voltage-current (VI) curves, or entering the PV panel parameters individually, the emulator becomes a fully controllable solar panel. Although the emulator is rated for 10kW, it has an internal fill factor making the obtainable output of the emulator around 8kW instead. The only change this caused is that the one 10kW inverter was only tested up to the 8kW instead of the full output power range like all the other inverters. This however, did not affect the testing results needed for the modeling.

3.3   SAG GENERATOR

In order to form fault contribution (short circuit) conditions in a laboratory setting, a voltage sag is necessary. A voltage sag is defined as a decrease in voltage magnitude to a certain percent.

There were two sag generators used for the testing. The first sag generator used was the one incorporated in the EPSL and operated via silicon-controlled rectifier (SCR) technology. This sag generator was used to collect the data for the preliminary defense, however it was noted at the defense that the sag generator switching was too slow. The second was a portable sag generator we borrowed from EPRI which operated/switched much faster due to its use of IBGTs. All the PV transient tests were performed again on the second sag generator to remove the transients caused by the switching of the first sag generator. Both sag generators are described below along with the reason for retesting with the EPRI sag generator.

The first sag generator used for this research is located in the Electric Power Systems Laboratory and was designed to be controlled by a touch-screen programmable logic controller (PLC) interface [37]. From the PLC, the user can select the desired sag duration in terms of percent retained voltage. A sag can be set on each phase separately since the sag is created using three separate tapped transformers with thirteen increments per phase. The PLC utilizes Eaton SmartWire-DT technology to control contactors to select the transformer taps remotely, and controls the SCR gate drivers through a digital output module. To decrease the loading on the SCRs, a large three-phase contactor is placed in parallel with the SCR paths when a sag event is not being run. Electrically, the sag generator is in series with the power source, the motors, and lab benches. A selector switch on the front panel of the EPSL system is used to control the contact position to choose the type of source: normal, sag, or to open circuit both. A one-line diagram of the electrical location of the sag generator with respect to the building electrical input is shown in Figure 5.
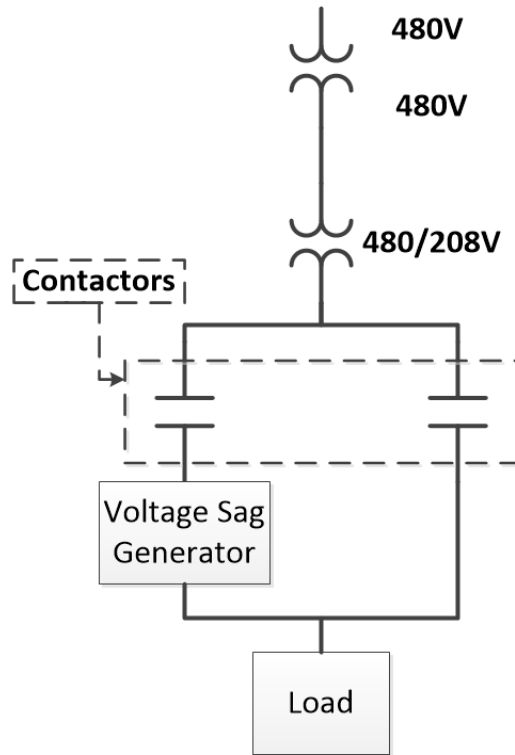
Figure 5. Sag Generator Location One-line

The electrical schematic of each phase is shown in the one-line diagram, Figure 6. The two SCRs are rated at 250 A and 1600 V. The top SCR is the bypass SCR and is shown in parallel with a contactor to its left in the one-line diagram. The bypass SCR is controlled by the two gate drivers on the right of the group of four at the top of the board. The gate drivers are Applied Power Systems SCR gate driver boards. The sag path SCR is controlled by the two gate drivers and is in series with the autotransformer and tap selection contactors.
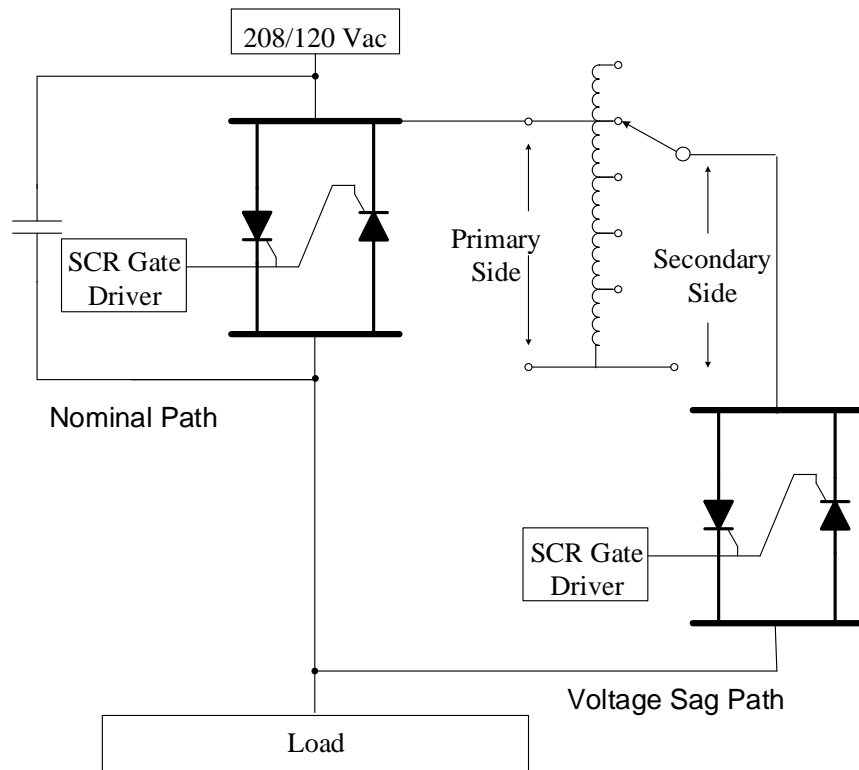
Figure 6. Sag Generator One Line Diagram (per phase)

On the far left of the one-line diagram, Figure 6, is shown a normally open contact. This contact represents the three-phase 200A series bypass contactor which is in parallel with each of the bypass SCRs. This contactor is closed whenever the PLC is powered and a sag event is not in progress to take the normal load away from the SCR bypass path. This contactor opens before the SCR switching sequence occurs, however, so that the power electronics handle the actual sag event.

There are thirteen tap selection contactors for each phase. One of these contactors at a time will close to select a transformer tap to feed to the sag SCR. The bottom of each contactor is wired to one of the transformer taps, and the contactors then feed the line side of the sag path

SCR. The 100% tap of each contactor is fed from the line side of the bypass SCR. These contactors are controlled by the PLC by using the GUI touch screen located in the lab.

The GUI interface is shown in Figure 7 and can be set to apply the sag for a duration between 3 and 180 cycles. In addition, each phase can be individually programmed for a voltage magnitude from 0% (short circuit) to 120% (voltage swell).
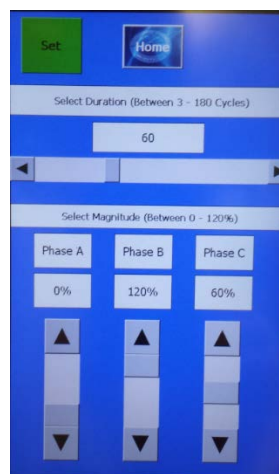
Figure 7: Sag Generator GUI

The issue we had to address when using the EPSL sag generator was a "break-before-make" phenomenon. Since the SCR switches used in the EPSL are controlled independent of each other (not timed precisely) while forming the sag event, the SCR switches open before the auto-transformer contacts are enabled to create the voltage sag. This causes a momentary open circuit before the short is actually applied. Although this is fast enough to demonstrate sags in a laboratory environment, it produces erroneous transients that make a large difference when accurate transient models are trying to be reproduced. This led us to borrow the sag generator from EPRI's laboratory facility, Figure 8, which has a much faster 200A Tri-Mode sag generator

which does not experience this problem due to the faster switching of their IBGTs. EPRI's sag generator has built-in data acquisition at 12-bit resolution and a sampling rate of 5 or 10 kHz. The difference between the University's sag generator and EPRI's is shown in Figure 9.

Figure 8. EPRI Portable Sag Generator
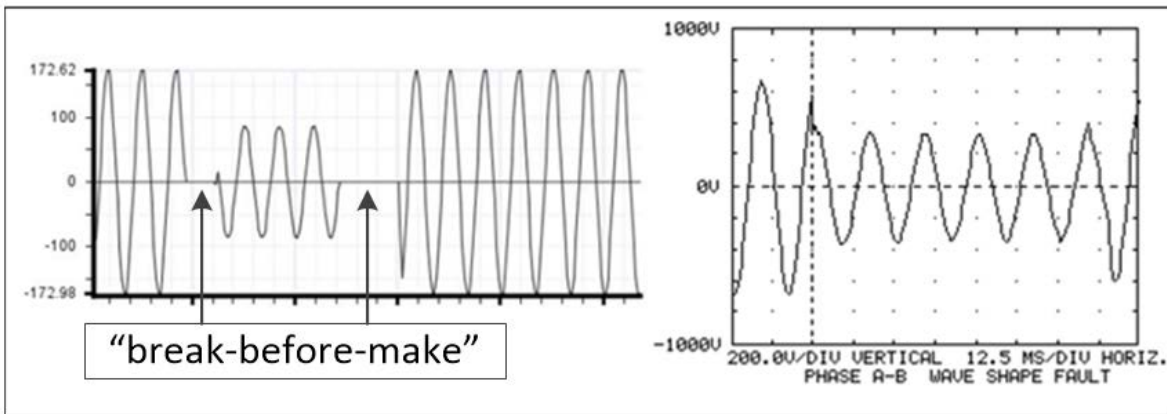
Figure 9. EPSL Three-cycle 50% Sag Event (left) [37] and EPRI 40% Sag Event (right) [38]

The "break-before-make" operation (each sag beginning with approximately ¾ cycle of dead time) of the EPSL sag generator is clearly shown by the dead bands of zero voltage when the sag is enabled and removed. The dead-band voltage is zero if there is no source active in the EPSL; as in Figure 9. With a PV inverter under test, back-feeding will cause an unwanted overvoltage

during the break-before-make period. However, a temporary solution to this problem was addressed by connecting autotransformers to the resistive load of the laboratory benches in order to enable a load matching the output of the photovoltaic inverter. For example, if one of the 2kW inverters is being testing at 100% power output, the load bench was tuned using the autotransformers to a 2kW load. Since each bench is capable of providing 5kW of load, multiple benches were used to create a load for the larger 10kW inverter. This method provided constant voltage magnitude during steady state and just before the fault was applied. This provided voltage stability even during the "break-before-make" operation of the EPSL sag generator. As seen in Figure 10, the matched load helps the "break-before-make" operation have minimal-to-no impact on the test data (Note: the voltage magnitude remains in steady state before the fault when the matched load is used.). Even though a matched load provided voltage stability for riding through the break-before-make, if the loads were not tuned precisely, inaccurate transients could be observed and collected.
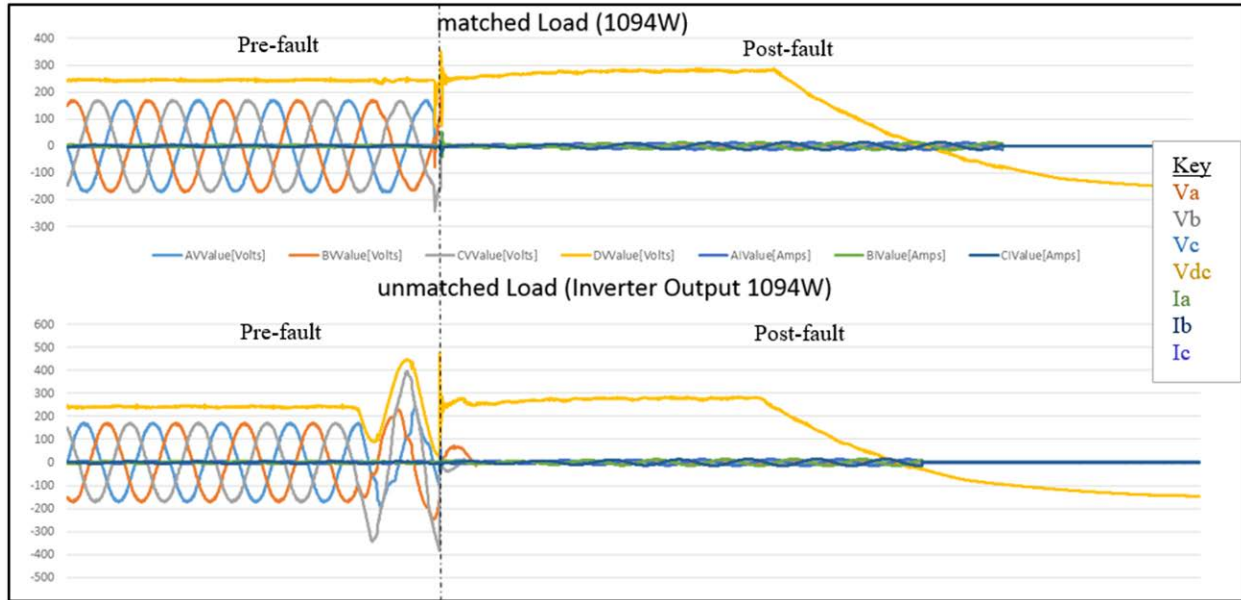
Figure 10. Bench Load equal to Inverter Output (top) and No Bench Load (bottom)

Since the goal of this dissertation was to provide an accurate transient model for the PV inverters, second class transient data is not acceptable if better data could be obtained. Therefore, ALL the transient events performed using the EPSL sag generator were recreated using the borrowed sag generator and allowed for the collection of accurate transient data.

3.4   METERING

This section describes the processing of collecting, storing and analyzing the data collected during the inverter transient testing.

For the open circuit tests, the PowerXplorer PX5, (Figure 11) was utilized. The PX5 is a three-phase power quality analyzer and is used for triggering and capturing the transient event data collected in the laboratory. By using internal voltage and current triggers for open circuit

27

and short circuit tests respectively, the entire event can be captured by recording the number of pre and post cycles required to view the entire event. The meter is capable of collecting data on eight channels, four voltages and four currents. It has 14-bit resolution and 1 MHz sampling for transients, plus 16-bit resolution and 256 samples per cycle for rms. The captured data can be viewed on the scope directly after the event, but is also captured on an external Compact Flash (CF) card inserted in the scope, which allows the data to be easily downloaded to a personal computer (PC).

Figure 11. PowerXplorer Analyzer

Once a set of events are captured, the data is then opened in the PX5 supported software; DranView 6.0 [39]. The software allows the user to view the data event-by-event based on the time of the event. A screen-shot of the event window in the DranView software is shown in Figure 12. The DranView data could be exported in CSV format and imported into Excel where it can easily be exported into MATLAB for mathematical processing via a MATLAB script.
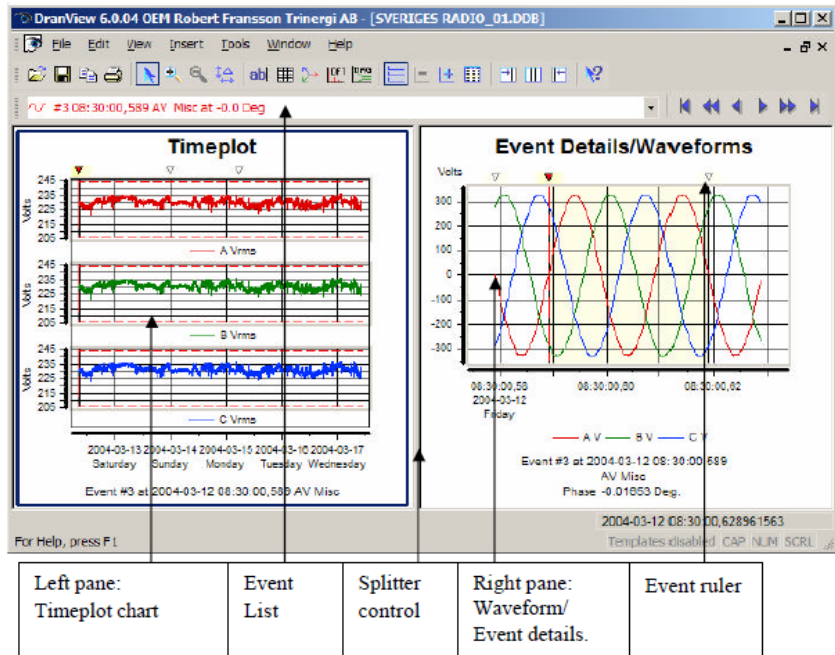
Figure 12. DranView Software Interface [39]

For the short circuit tests, the data was initially stored using the PX5 when utilizing the EPSL sag generator. However, when the tests were performed using EPRIs sag generator, the data was collected via software already incorporated into the Sag Generator software, called Portosag. The Portosag software stored the data as comma separated value (CSV) format directly. Due to the CSV collection format, the short circuit data could be easily imported, manipulated, and analyzed directly in MATLAB without having to use the created conversion scripts needed for the open circuit tests. The data export and data analysis processing is discussed in further detail in the Data Processing Section 3.7.

3.5 LABORATORY SET-UP

This section will briefly describe the test set-up used to test the photovoltaic inverters in the Electric Power Systems Laboratory. The inverter test set-up for the single-phase inverters is shown in Figure 13 (the same wiring is followed for the three-phase inverters except there are three AC output voltages from the inverter, one per phase).

Figure 13. Laboratory Test Set-up for Inverter Transient Testing

The switch, shown on the top right of the diagram, is connected to the AC output of the inverter and allows the AC side of the inverter to be easily connected or disconnected from the EPSL for the open circuit cases. For the short circuit tests, the sag generator is used in place of the switch. The DC input of the inverter is connected to the output of the PV emulator shown on the top left. The power quality analyzer is shown in the bottom center, and the eight channels of the instrument

monitor the inverter's DC input voltage, the AC output voltages, and the corresponding AC line currents. The following section outlines the testing procedure used to test the inverters with this test set-up.

3.6   TESTING PROCEDURE

The testing procedure described in this section uses the laboratory set-up described in Section 3.5. The testing includes load rejection (open circuit) and fault contribution (short circuit) tests on four single-phase inverters, three micro-inverters, and a three-phase inverter. Photos of the testing setup are shown in Figure 14 and Figure 15.
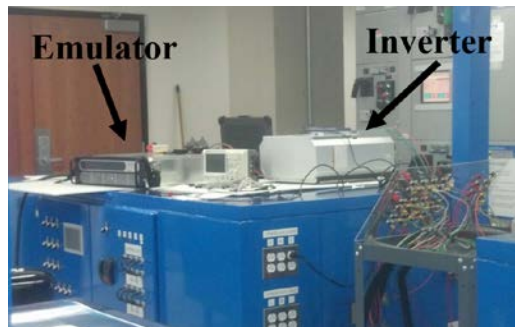
Figure 14. Inverter Test Set-up in the EPSL
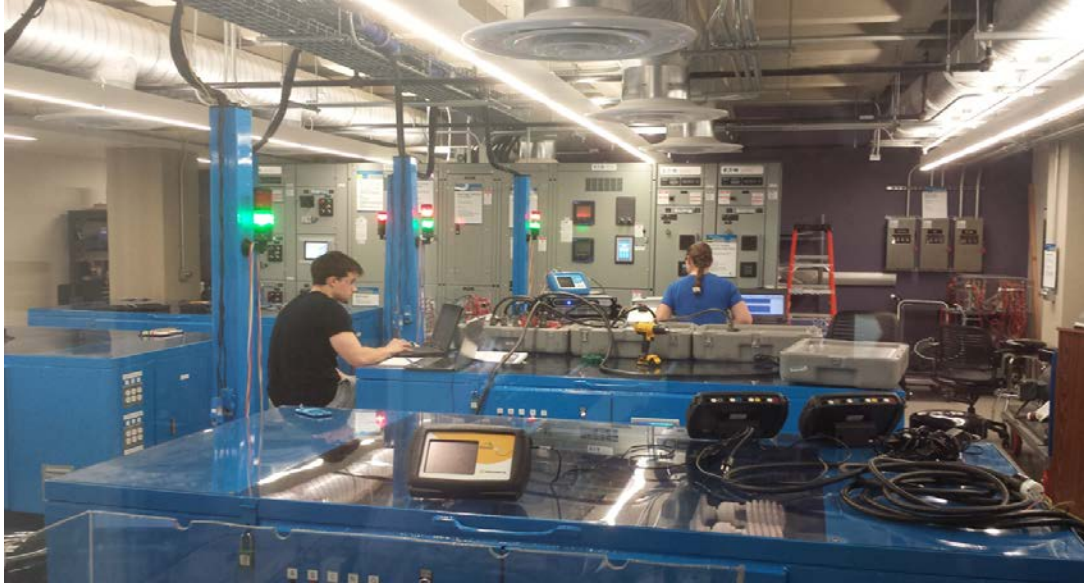
Figure 15. Preforming Sag Testing in the EPSL

Each inverter is tested at four different output levels, namely 25%, 50%, 75% and 100% of rated output. In addition, multiple shots are performed to statistically quantify point-on-wave effects. Each test type, load rejection and fault contribution, is described below. The rated power levels for the inverters are indicated in Table 1. Each inverter was tested under both short circuit and open circuit conditions.

Table 1. List of Tested PV Inverters

Inverter	Type	Size
Inverter A	Single-phase	2kW
Inverter B	Single-phase	3kW
Inverter C	Single-phase	2.8kW
Inverter D	Single-phase	2kW
Inverter E	Three-phase	10kW
Inverter F	Single-phase Micro	190W
Inverter G	Single-phase Micro	215W
Inverter H	Single-phase Micro	250W

For the load rejection tests, each inverter is energized by programming the PV emulator to the corresponding load level, 25%, 50%, 75% and 100% of rated output power respectively. The metering equipment is set to record the inverter input (DC) voltage and the output (AC) voltages and currents. Once the corresponding inverter output power level is reached, the switch between the inverter output and laboratory bench B is opened to initiate the load rejection at the output of the inverter. All input/output event data is stored on a CF card for future data analysis via the scope triggering within the power quality analyzer. Each load rejection test is completed three times per inverter power output level to account for point on wave effects.

For the fault contribution tests, each inverter is energized by programming the PV emulator to the corresponding load level, 25%, 50%, 75% and 100% of rated inverter output power respectively. The metering equipment is set to record the inverter input (DC) voltage and

the output (AC) voltages and currents. Once the corresponding inverter output power is reached, the sag generator is triggered to produce a 100% sag on all three phases. This produces zero volts at the output of the inverter, creating an equivalent short circuit. All input/output event data is stored for future data analysis via the scope triggering. Each load rejection test is completed fifteen times per inverter power output level to account for point on wave effects.

3.6.1   Photovoltaic Inverter Manufacturer Interaction

As noted in the previous section, there were hundreds of inverter tests performed in the laboratory, however, the inverter firmware imposed five minutes dead time between tests per IEEE 1547. In order to reduce the time required to test in the lab and the unnecessary five minutes between tests waiting for the inverter to reconnect, each manufacturer had to be called in order to solve this problem. Each inverter is equipped with a "Grid Guard-Code" (GGC) that can be used to override this waiting time during laboratory testing. Some inverter vendors willingly provided the code over the phone, whereas other vendors required paper work to be filled out and signed stating that the code was being used for laboratory testing only. Others required download of their software to control the inverter. We were able to set each inverter with a GGC to reconnect after three seconds and reduced the laboratory testing time by days.

An additional problem encountered was enabling the emulator to energize the input of some of the inverters. We believe the problem was due to the switching of the power electronics within the emulator causing high frequency noise, in turn causing the arc fault circuit interrupter (AFCI) to "falsely" trigger in the inverter. We were able to solve this problem by disabling the AFCI during testing through the use of the GGC. For some of the inverters, the voltage and

frequency grid connection range had to be slightly increased as well to allow the emulator and IUT to connect to the AC grid. One of the vendors would not provide the GGC nor admit it could be changed due to the age of the inverter. This reduced our number of testable single-phase inverters by one since it could not be energized by the emulator. However, enough data was collected from the other seven inverters to complete the mathematical analysis and obtain trends based on manufacturer designs.

3.7   DATA PROCESSING

As indicated in Testing Procedure, Section 3.6, all inverters listed in Table 1 were tested under both OC and SC events at multiple output power levels. *For the OC events*, the data was stored using the Compact Flash (CF) card internal to the power quality analyzer and is downloaded to a PC. The data from the meter can be viewed using the DranView software, however the software does not allow the data to be mathematically processed. In order to make the data into a useful format for analysis, a software script was created using AutoHotkey (AHK) software to export the DranView scope data into comma-separated value (CSV) files. Then, a MATLAB script was created to import the CSV files created by AHK into MATLAB. A block diagram showing the flow of data processing is shown in Figure 16.
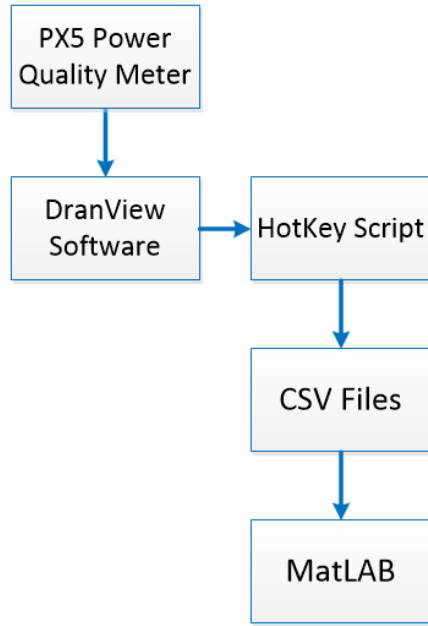
Figure 16. Flow of Data Processing

The script in MATLAB was written so that the data could be viewed, plotted, and analyzed with respect to the inverter manufacturer (Inverter A-H), type of test preformed (open-circuit, short-circuit test), and the inverter output power (25%, 50%, 75%, 100%).

For the SC events, the data was initially stored using the PX5 when utilizing the EPSL sag generator. However, when the tests were performed using EPRIs sag generator, the data was collected via software already incorporated into the Sag Generator software, called Portosag. The Portosag software stored the data as comma separated value (CSV) format directly. Due to the CSV collection format, the short circuit data could be easily imported, manipulated, and analyzed directly in MATLAB without having to use the created conversion scripts needed for the open circuit tests.

All mathematical processing was done using MATLAB scripts and toolboxes. After the mathematical analysis on the data was successfully built and proven in MATLAB, the PV

transient model was coded into a transient PV model in OpenDSS. OpenDSS is a distribution simulation software used by planning engineers. With increase in PV penetration, it is now necessary for engineers to ensure the power grid operates safely with increase in PV installations. Therefore, transient models are needed for the PV systems. More details about OpenDSS and the created model will be discussed in later sections.

3.7.1   MATLAB Issues in Data Processing

As described in the previous section, all the data was imported into comma-separated-value (CSV) format so it could easily be processed in MATLAB. One main toolbox used in MATLAB was the System Identification (SI) Toolbox [40]. This SI toolbox claims to be able to help visually identify the HW filter order necessary to recreate the data; given a specific nonlinear estimator size. The toolbox is usually capable of fitting the data to an accuracy between 50-60%. However, the user then needs to fine tune the model by changing the nonlinear estimator size and filter size to obtain greater accuracy. A MATLAB script was created which used the toolbox to help initialize the model, then additional processing is done to increase the accuracy of the model. This process of allowing the toolbox to help visualize the curve fitting works for some sets of data and not others. For example, the toolbox is helpful in determining the filter size necessary for the micro-inverter short-circuit response since the inverter only has a momentary current spike then ceases. The micro-inverters tend to require a filter order in the twenties and nonlinear piecewise estimators (input and output) having ten breakpoints. However, the toolbox breaks down when inverter short-circuit current lasts for a couple cycles after the initial momentary current spike (single-phase and three-phase inverters). When the current lasts

past the time of the initial fault, the model has to mathematically contain energy storage (the input energy ends at the time of the fault). The need for mathematical energy storage causes a need for an increase in filter order. The SI toolbox is only capable of modeling a filter order in the fifties, but it is estimated we will need orders larger than one-hundred for some single-phase responses and even greater for three-phase inverter responses. Therefore, the single-phase and three-phase inverters require a filter order much greater than the toolbox limit.

Technical support advised that they would have to change their code for the toolbox to allow it to handle larger order models (needed for PV transient data). Developmental engineers from MATLAB confirmed that their toolbox needs to be updated to support larger models. However, they have no plan in the near future to fix this issue, they just recommended modeling smaller order data. Therefore, the toolbox in MATLAB is incapable of predicting models that require energy storage (single-phase inverter short-circuit responses and all three-phase inverter responses), but does a good job of modeling micro-inverter short circuit responses and most open-circuit events.

The job of the SI toolbox is to aid in predicting orders for the filter and nonlinearities for the HW models. However, because of the limitation of the SI toolbox, some HW models could not be initially constructed using the toolbox and required extensive scripting in MATLAB. Future work will include fixing the limitation or eliminating the toolbox in creating the models.

3.8   TEST RESULTS

As noted in the testing procedure, the open circuit tests were completed three times per inverter per load level. The short circuit tests were conducted fifteen times per inverter per load level. The short circuit tests were performed in increments of 15 degrees from 90 degrees to 255 degrees, with respect to Phase A Voltage of the AC grid, to account for point-on-wave effects. The open circuit tests were random in nature, meaning that the switch was manually opened for each test irrespective of the point-on-wave. The number of shots and the degrees increments were based on conversations with EPRI and common testing practices.

This section gives an overview of both the open circuit and short circuit results from each of the eight inverters tested. (Each inverter along with type and size was listed earlier in Table 1). One method used for viewing over-voltages and over-currents from open circuit and short circuit tests is by considering the peak transient, duration, and pre and post rms currents and voltages respectively. These parameters will be addressed in the following sections. As will be seen, the short circuit overcurrents tend to be similar across a broad range of inverter sizes and vendors, and the open circuit results are very different.

3.8.1   Short Circuit Test Results

This section summarizes the short circuit results obtained for each inverter tested. Table 2 shows the pu peak transient (ITR) and rms (IRMS) currents obtained for each inverter. Point-on-wave affected I_{TR} for most of the inverters, as shown in the third column, labeled ΔPOW, for the minimum value over all points on wave. Point-on-wave did not appear to affect rms currents.

39

The micro-inverters F, G, and H did not stay on long enough to record post-fault rms current, but the others produced measurable rms currents for up to 9 cycles. Therefore, Table 2 separates the peak I_{RMS} into time ranges of zero to one cycles, one-to-four cycles and four-to-eleven cycles after the fault. Inverter E could produce 1 pu I_{RMS} beyond four cycles, but the others did not. Inverter C produced less than 1 pu I_{RMS} in all tests.

Table 2. Short Circuit Test Results – Extreme Values

IUT	I_{TR} [pu]	ΔPOW [pu]	0-1 Cycle I_{RMS} [pu]	1-4 Cycle I_{RMS} [pu]	4-11 Cycle I_{RMS} [pu]
A	3.75	2.28	1.17	1.00	0.16
B	2.91	1.68	1.06	1.11	0.01
B*	2.86	1.86	1.13	1.08	0.09
C	2.68	1.51	0.62	0.07	0.07
D*	7.53	0.65	1.91	1.52	0.21
E	1.47	0.16	0.92	0.96	1.00
F	3.95	2.95	0.00	0.00	0.00
G	3.49	1.72	0.00	0.00	0.00
H	3.00	2.00	0.00	0.00	0.00

Table 3 shows correlation coefficients between the pre-fault output level, I_{SS}, and the pu peak values of I_{TR} and I_{RMS}. This table also reports the number of test samples available for each IUT. I_{SS} has little impact on I_{TR}, but it does have significant correlation to I_{RMS}, especially in the first cycle.

Inverter D was tested with the SCR-based sag generator, and then it failed before it could be tested with the IGBT-based sag generator. Results from the SCR-based sag generator are italicized in Table 2 and Table 3. Note that Inverter D had the highest I_{TR} and I_{RMS} values, so the impact of the sag generator on test results for Inverter B was compared. The results are

40

comparable for Inverter B with both sag generators, so the results for Inverter D could be useful (e.g. duration). However, the same degree of confidence in both is not possible (e.g. I_{TR} and ΔPOW).

Table 3. Short Circuit Test Results - Correlation Coefficients to Output Power

IUT	Samples	I_{SS} to I_{TR}	I_{SS} to I_{RMS}		
			0-1 Cycle	1-4 Cycle	4-11 Cycle
A	48	0.13	0.77	0.23	0.98
B	48	0.32	0.99	0.95	0.71
B*	60	0.33	0.79	0.46	0.90
C	48	0.10	0.79	0.46	-0.02
D*	71	0.39	0.70	0.28	-0.02
E	36	0.002	0.98	0.99	0.70
F	12	-0.51	n/a	n/a	n/a
G	12	0.01	n/a	n/a	n/a
H	12	-0.08	n/a	n/a	n/a

Inverters can produce overvoltages that exceed 2.0 pu peak and 1.9 pu first-cycle rms during an open circuit event. To further view the short circuit transient responses of all the inverters, an example plot for each inverter is shown below in the next section.

Example Short Circuit Waveforms for Each Inverter Tested

Below are example short circuit waveforms from each inverter. Figure 17 shows the short-circuit response of Inverter A when operating at 75% output power. The arrow on the plot indicates the time at which the fault was applied. Note the momentary current spike at the time of the fault followed by sustained current for 1.5 cycles as it decays to zero. The transient peak was

probably caused by the discharging of a DC link capacitor, and the decay follows the RLC filter response of the inverter.
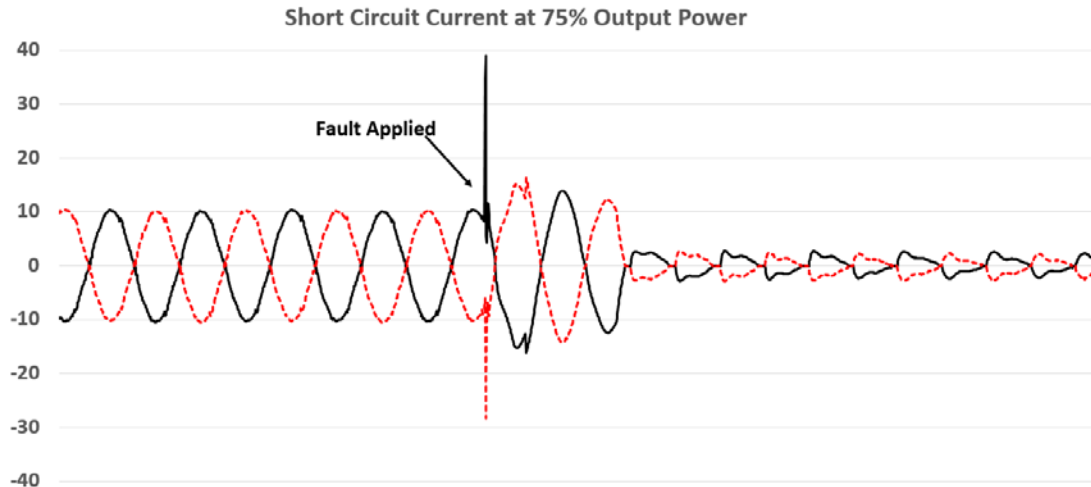

Figure 17. Short Circuit Response of Inverter A

Figure 18 is an example of the short circuit current results from Inverter B operating at 25% output power. The arrow on the plot indicates the time at which the short circuit event occurred. The current initially spikes as a 2.1 per-unit transient overcurrent, followed by the inverter rms current increasing to 1.3 per-unit for 1.5 cycles. The inverter attempts to maintain pre-event output after the fault, causing the current to increase after the fault. However, within one cycle after the event, the current quickly decays to zero due to the inverter tripping as a result of the fault (i.e. voltage lost). Figure 19 shows a zoomed in view of the transient from Figure 18. From the zoomed in view it is possible to see where the fault was applied and the momentary overcurrent. After the current spike at the fault, the inverter attempts to maintain rated output by increasing the output current until the inverter controls trip the inverter due to

42

voltage loss. Note that a current transient peak of 2.1 per unit was experienced during the single-phase transient event and was probably caused by the discharging of the filter within the inverter (i.e. possibly a DC link capacitor). An overcurrent of 2.0 per unit is typically assumed to be the rule of thumb for distribution planning for inverter transient overcurrents. As will be shown in the test results in this section for both the single-phase and three-phase inverters, this assumption underestimates the overcurrents produced by photovoltaic inverters.
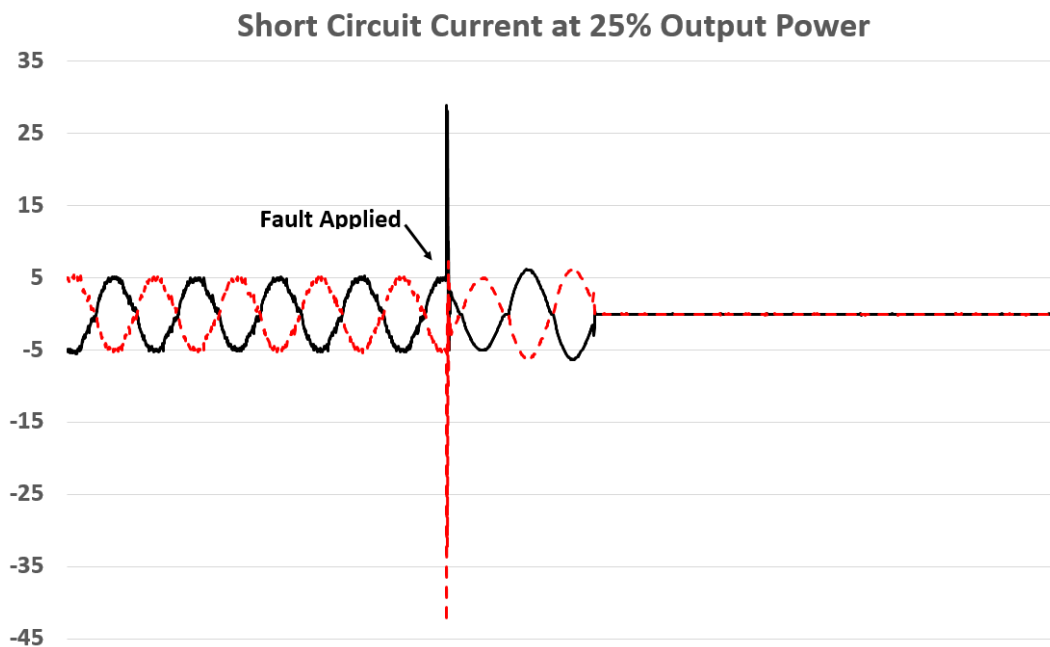

Figure 18. Short Circuit Response of Inverter B
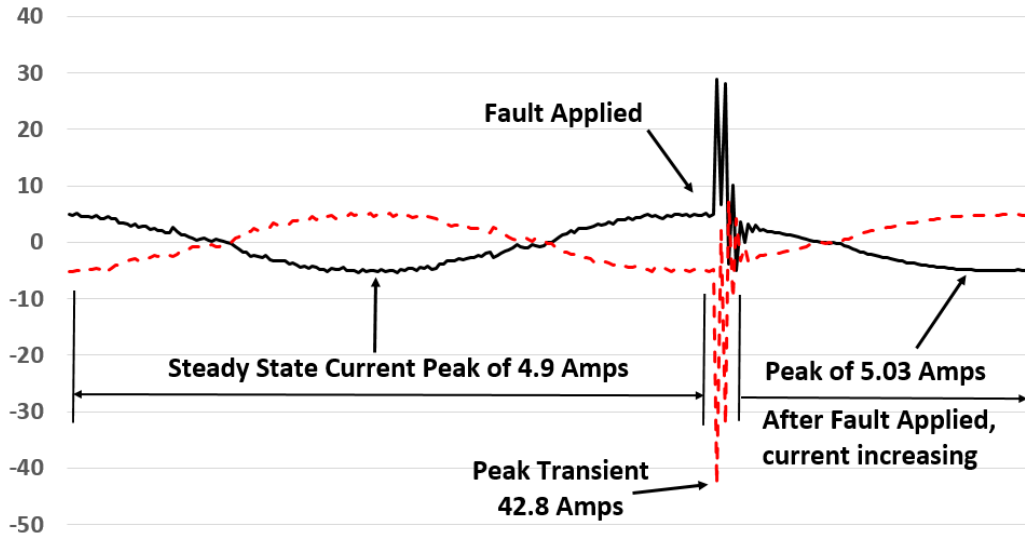
Figure 19. Zoomed-in View of the Short-Circuit Current Transient

Inverters C and D, shown in Figure 20 and Figure 21, contribute similar fault currents as both Inverter A and B. The inverters attempts to maintain pre-event output after the fault, causing the current to increase after the fault. However, within one cycle after the event, the current quickly decays to zero due to the inverter tripping due to the fault (i.e. voltage lost).

44

Figure 20. Short Circuit Response of Inverter C

Figure 21. Short Circuit Response of Inverter D

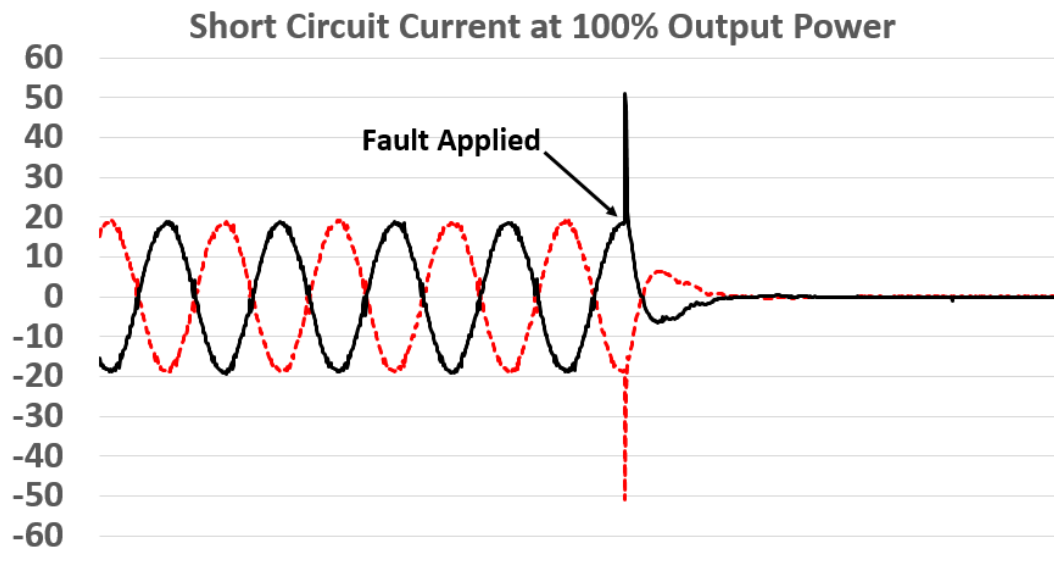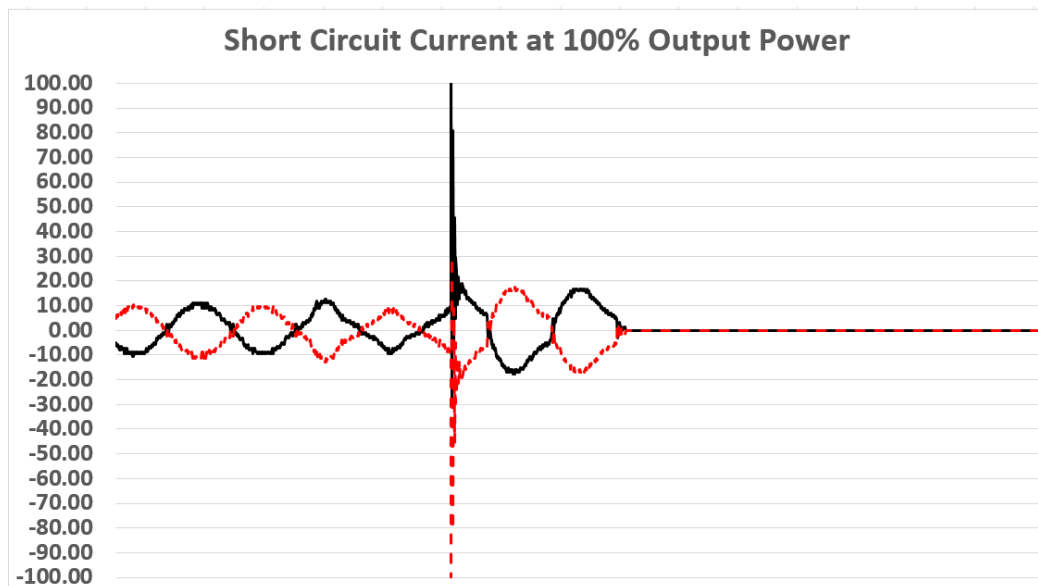Figure 22 is an example of the three-phase short circuit current results with Inverter E operating at 75% output power. The arrow indicates the time at which the 0% voltage sag occurred. Once the sag event was triggered, an initial momentary overcurrent was followed by the fault current increasing to rated current. The current increases after the fault due to the inverter trying to maintain rated output. The sustained rated current remains for approximately four cycles until the internal controls cause the inverter to trip. The three-phase inverter continued to produce current after the sag for six to ten cycles, depending on the point-on-wave and the power output of the inverter when the fault was applied. Note that the transient overcurrent reaches 1.45 per-unit at the initiation of the short circuit event, and the RMS current reaches 1.02 per-unit of rating (1.36 per-unit of the pre-fault current) for the last several cycles.
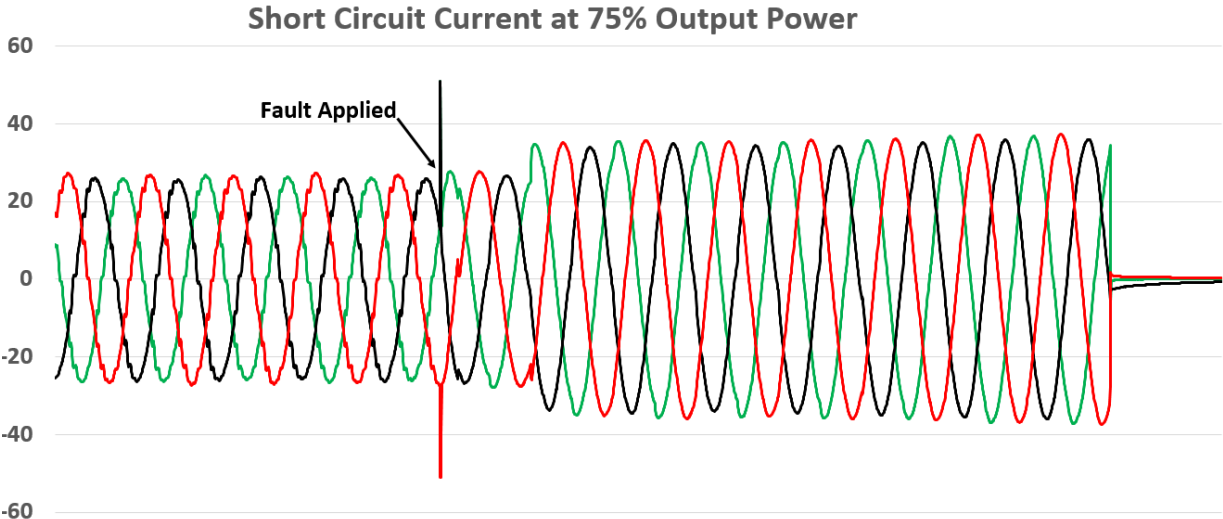
Figure 22. Short Circuit Response of Inverter E

As was seen in the open circuit results, each micro inverter also behaves the same during short circuit events. Figure 23, Figure 24, and Figure 25 show the short circuit responses of the micro Inverters F-H. Once the fault is applied, the current momentarily spikes up to 5.6 pu an then goes directly to zero.

Figure 23. Short Circuit Response of Inverter F

Figure 24. Short Circuit Response of Inverter G

Figure 25. Short Circuit Response of Inverter H

In summary, the short circuit responses of PV inverters tend to follow similar patterns. An initial transient overcurrent, followed by a sustained current increasing to rated current before the inverter trips due to voltage loss. Laboratory testing showed that the sustained current lasts between one and ten cycles depending on the inverter, power output le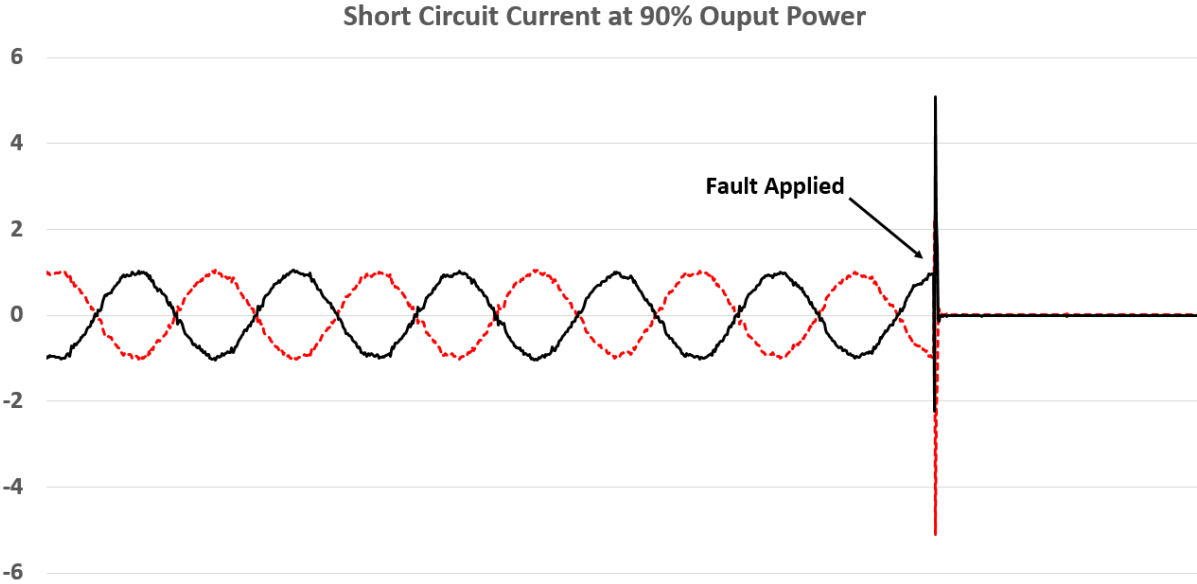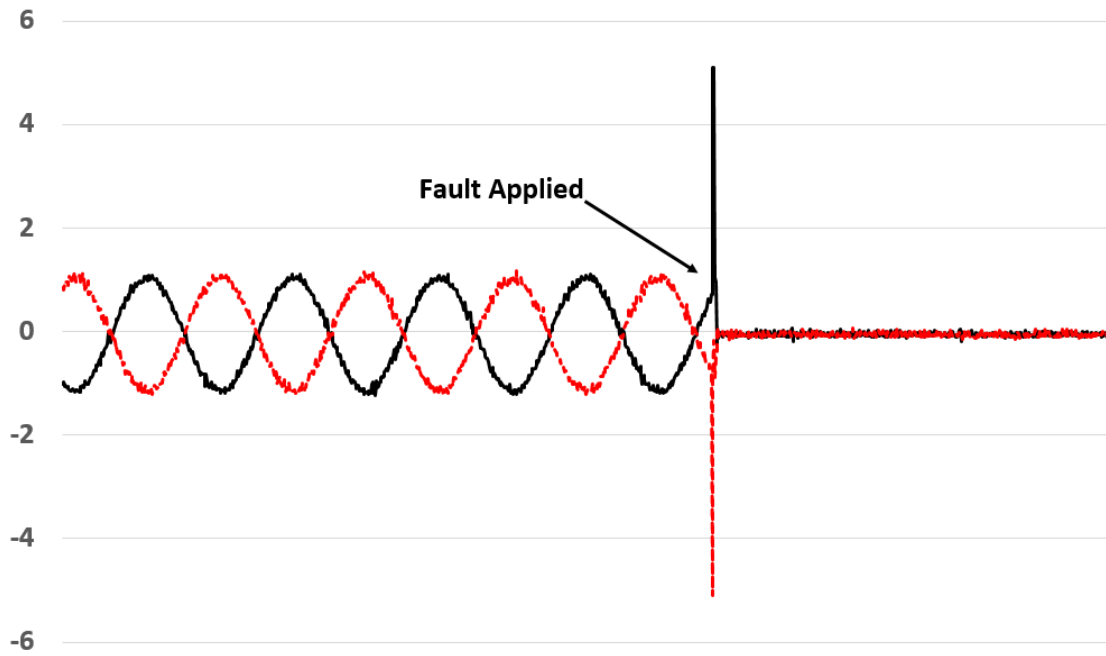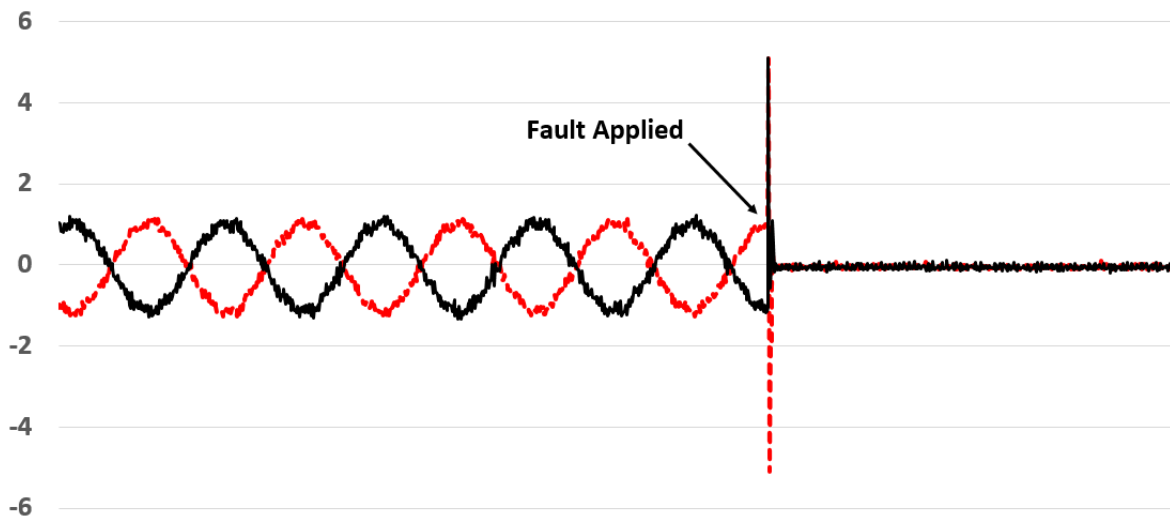vel, and the triggered point-on-wave. In summary, the transient overcurrents ranged from 1.47 to 7.53 pu while the sustained overcurrents ranged from nothing to 1.91 pu.

3.8.2   Open-Circuit Test Results

The open circuit results are summarized in Table 4. The highest peak transient overvoltage (V_{TR}) appears in column 2, and the effects of point-on-wave (ΔPOW) and power output (P_{DC}) appear in columns three and four. For example, V_{TR} for Inverter A could vary by 0.10 pu with point-on-wave, but power level had little impact. For inverters B-E, the highest V_{TR} was found, by a significant amount, at less than full output power. Some of the inverters could produce a sustained overvoltage for several cycles. Therefore, V_{RMS} was separated into time ranges of zero to one cycle and one to eleven cycles after the switch opening. Only Inverter C produced less than normal voltage within one cycle. The micro-inverters behaved differently, as their voltages decayed exponentially from V_{TR}.

Table 4. Open Circuit Test Results – Extreme Values

IUT	VTR [pu]	ΔPOW [pu]	Worst P_{DC}	0-1 Cycle V_{RMS} [pu]	1-11 Cycle V_{RMS} [pu]
A	1.46	0.10	Any	1.91	1.93
B	1.78	0.40	75%	1.67	1.72
C	1.65	0.15	50%	1.42	0.27
D	1.58	0.29	25%	1.27	1.30
E	2.08	0.50	75%	1.74	1.00
F	1.88	0.41	n/a	Exponential dc decay	
G	1.86	0.23	n/a	Exponential dc decay	
H	2.07	0.41	n/a	Exponential dc decay	

Correlation coefficients of I_{SS} to V_{TR} and V_{RMS} are not presented for the open circuit tests. The micro-inverters were tested at just one power level, and the others had at most three open-circuit test samples at each P_{DC} value. As mentioned previously, the short circuit current responses of the photovoltaic inverters tend to be similar, but the open circuit responses are very diverse.

For Inverter A, the largest overvoltage was 1.46 per unit and occurred at 100% power output level. The lowest overvoltage occurred at 25% power output level and had an overvoltage of 1.35 per unit. The peak TOV was relatively consistent across its entire range of output power; the average overvoltage is about 1.4 pu. The overvoltages seemed to be independent of point-on-wave effects.

For Inverter B, the highest overvoltage of 1.78 was seen at a 75% output power level and the largest change in overvoltage caused by POW is 0.4 at 75%. The vertical spreading of the data points show the significance of the POW effects, especially at 75% output power.

For Inverter C, the largest overvoltage for was 1.65 per unit and occurred at 50% power output level. The lowest overvoltage occurred at 25% output power level. Furthermore, in

contrast with Inverter B, the peak TOV range of Inverter C compresses with the increase of power output level. At higher power levels, point-on-wave effects seem less significant.

For Inverter D, the largest overvoltage was 1.58 per unit and occurred at 25% power output level, also the lowest overvoltage occurred at 25%.and had an overvoltage of 0.98 per unit. Besides at 25%, the overvoltage increases with inverter output power level and is not affected much by point-on-wave effects.

For Inverter E, the largest overvoltage was 2.08 per unit and occurred at 75% power output level. Inverters F-H (micro) had peak transient voltages of 1.88, 1.86, and 2.07 pu voltage respectively. An example of the open circuit waveforms obtained for each of the inverters are shown and discussed in the following section.

Example Open Circuit Waveforms

Below are example open circuit waveforms from each inverters. The open circuit response of Inverter A is shown in Figure 26. When the fault (open circuit) is applied to the output, there is an overvoltage followed by a cycle of a square pulse followed by a slow voltage decay to zero. This square pulse and slow voltage decay is caused by a DC link capacitor on the output of the inverter which is attempting to hold the voltage at rated. However, since the AC grid voltage was removed, what we actually see is the decay of the DC link capacitor. The voltage peaks at 1.27 per-unit for the first cycle after the open circuit. However, the voltage does not decay quickly. The decay rate is much slower than the other tested inverters (as will be seen in following figures), i.e. the time constant is 0.3 s. This slower rate of decay is probably caused by a DC link capacitor internal to the inverter causing a longer sustained voltage after the event.
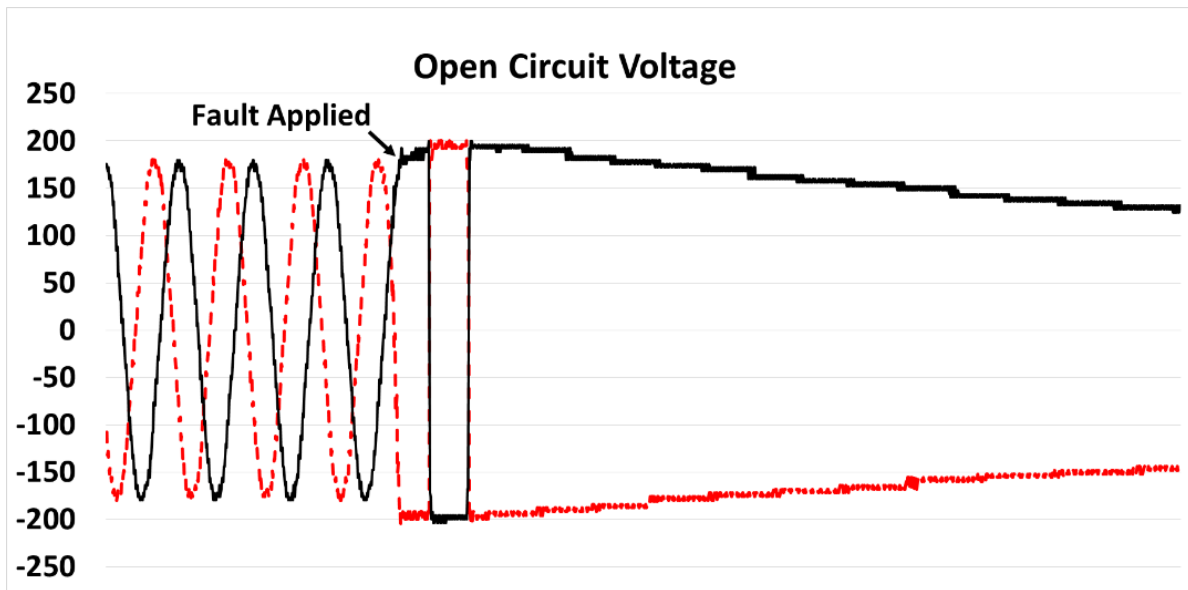
51

Figure 26. Open Circuit Response of Inverter A

The open circuit response of Inverter B is shown in Figure 27. When the fault is applied to the output, there is immediately an overvoltage followed by a rapid voltage decay to zero. Unlike Inverter A, this inverter does not contain a DC link capacitor. The arrow on the figure indicates the time at which the switch was opened. During the open circuit event, an overvoltage of 1.59 per-unit occurs on two phases, then the voltages exponentially decay to zero within three cycles (i.e. time constant is less than one cycle). This rate of decay was probably based on the internal RLC filter within the inverter. Each inverter will respond differently. We can also conclude from the non-sustained overvoltage that this inverter does not have an internal DC link capacitor and is transformer-less.
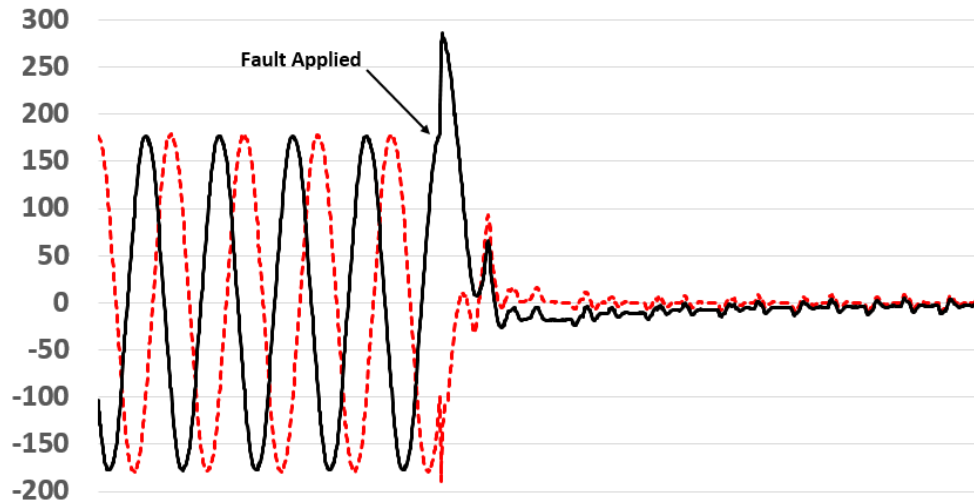
Figure 27. Open Circuit Response of Inverter B

The open circuit response of Inverter C operating at 75% output power is shown in Figure 28. When the fault is applied to the output, the voltage attempts to go to zero, but is immediately followed by an overvoltage decaying to zero; (similar to Inverter B). However, unlike Inverter B, this inverter rings for an extra cycle before returning to zero. The arrow indicates the time at which the switch was opened and the open circuit event occurred. Note the overvoltage of 1.72 per unit during the transient event. The overvoltage remains for less than one cycle, then quickly decays within a cycle. This plot looks almost like an underdamped second order response. Again, the overvoltage peak and the decay rate is probably inherent to the inverter's internal RLC filter. We can also conclude from the non-sustained overvoltage that this inverter does not have an internal DC link capacitor and is transformer-less.

53

Figure 28. Open Circuit Response of Inverter C

The open circuit response of Inverter D is shown in Figure 29. When the fault is applied to the output, an overvoltage is seen for about 1.5 cycles before quickly decaying to zero. However, the 1.5 cycles after the fault are square in nature and it appears that there may be an internal transformer at the output of the inverter that is saturating during those cycles. After the 1.5 cycles, the inverters internal control cause the inverter to trip causing the voltage to quickly go to zero.
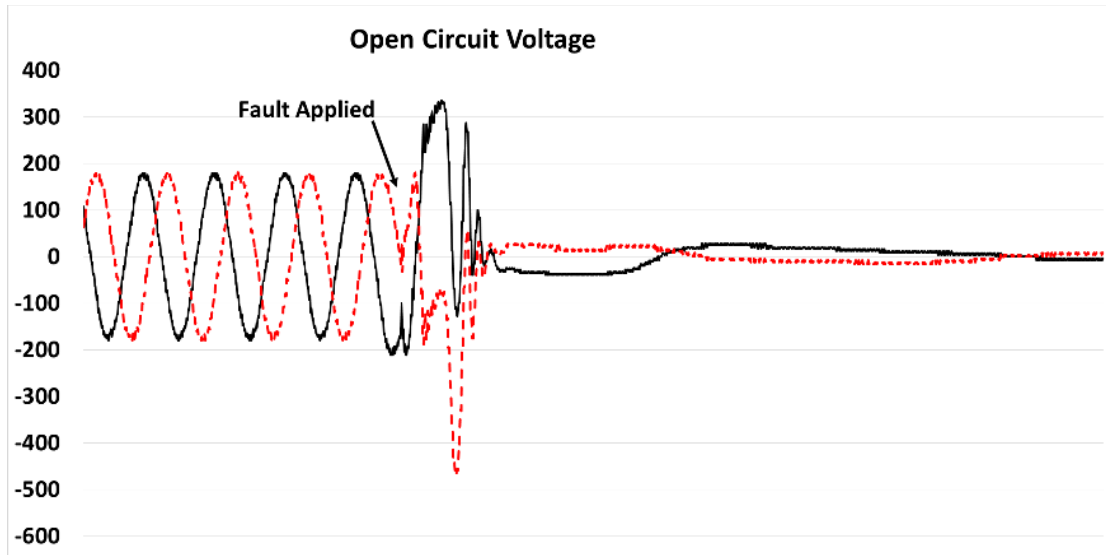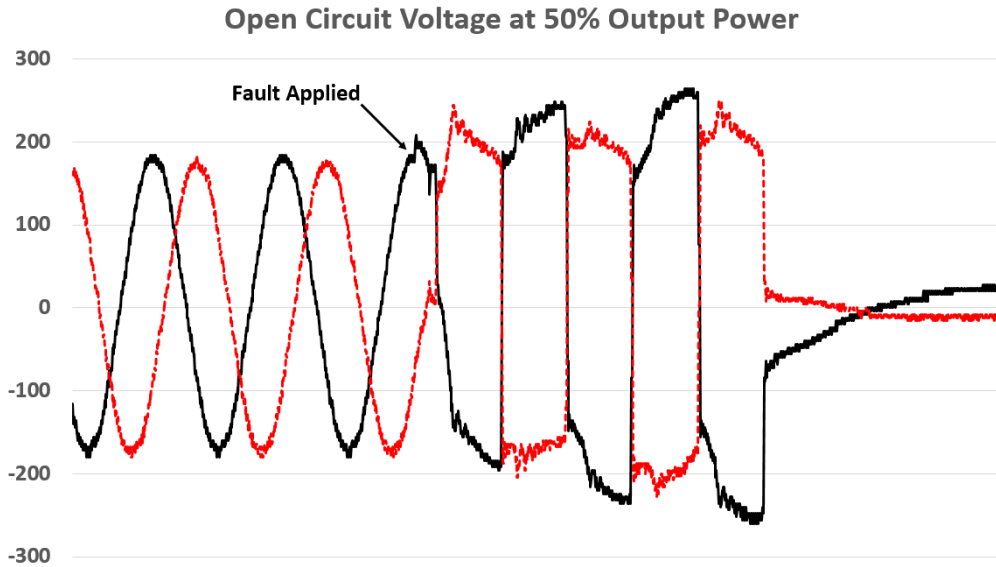
Figure 29. Open Circuit Response of Inverter D

The open circuit response of Inverter E is shown in Figure 30. When the fault is applied to the output, an overvoltage is seen on two phases followed by the voltage decaying to zero. The decay rate is based on the internal RLC filter of the inverter. Note that there is neither a DC link capacitor nor transformer on the output of the inverter.

55
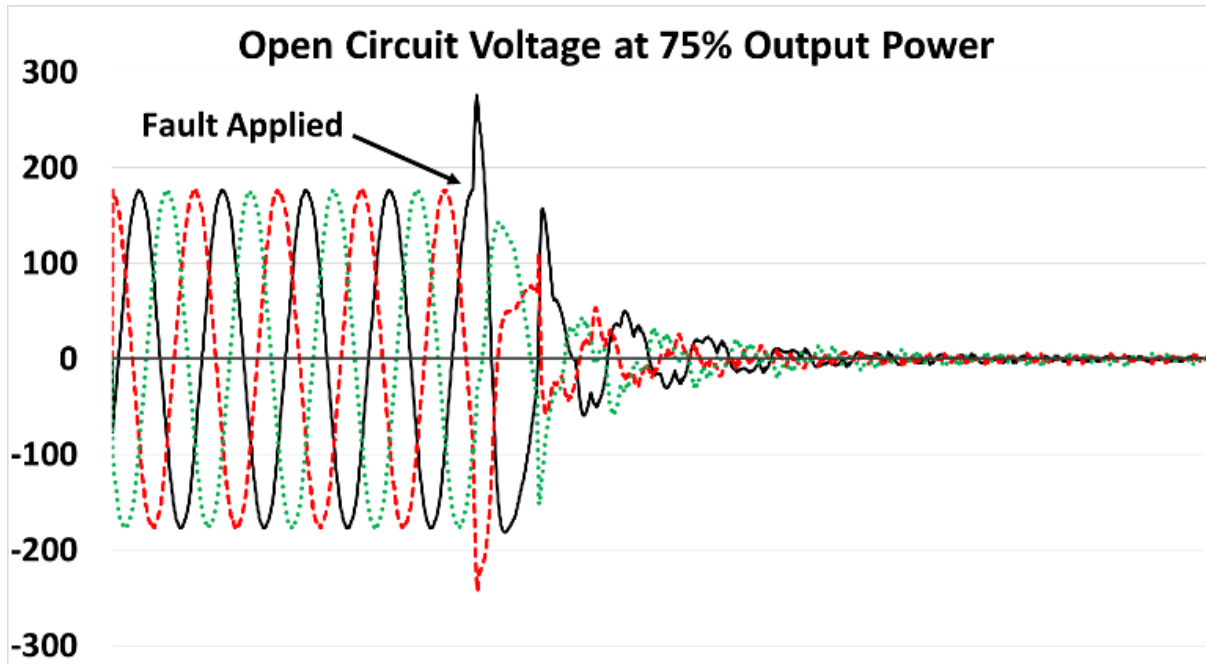
Figure 30. Open Circuit Response of Inverter E

The open circuit response of Micro Inverters F-H are shown in Figure 31, Figure 32, and Figure 33. The response of the micro inverters were very similar. Each inverter produced a momentary overvoltage followed by a slow voltage decay to zero. We can infer from their response that the micro inverters are indeed transformer-less, but that that they do contain a DC link capacitor on their output.

Open Circuit Voltage at 90% Output Power

Fault Applied
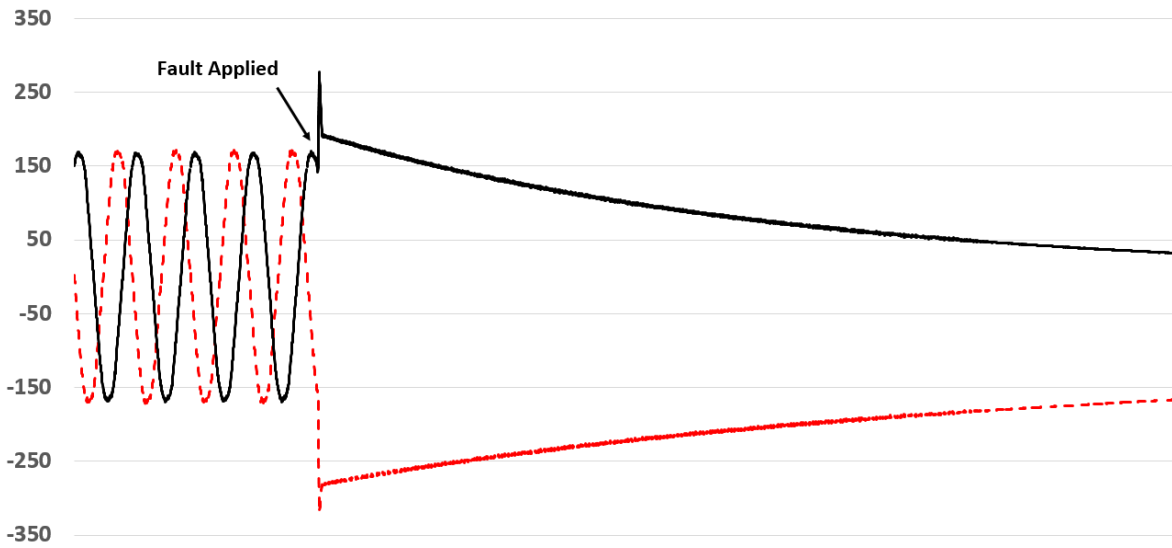
Figure 31. Open Circuit Response of Inverter F

Open Circuit Voltage at 79% Output Power

Fault Applied
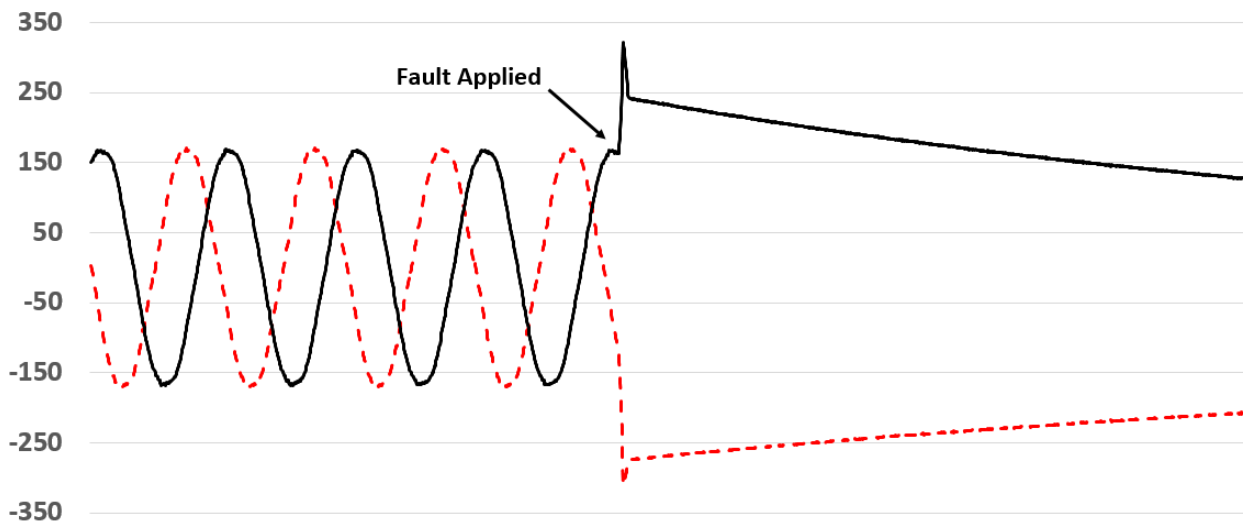
Figure 32. Open Circuit Response of Inverter G
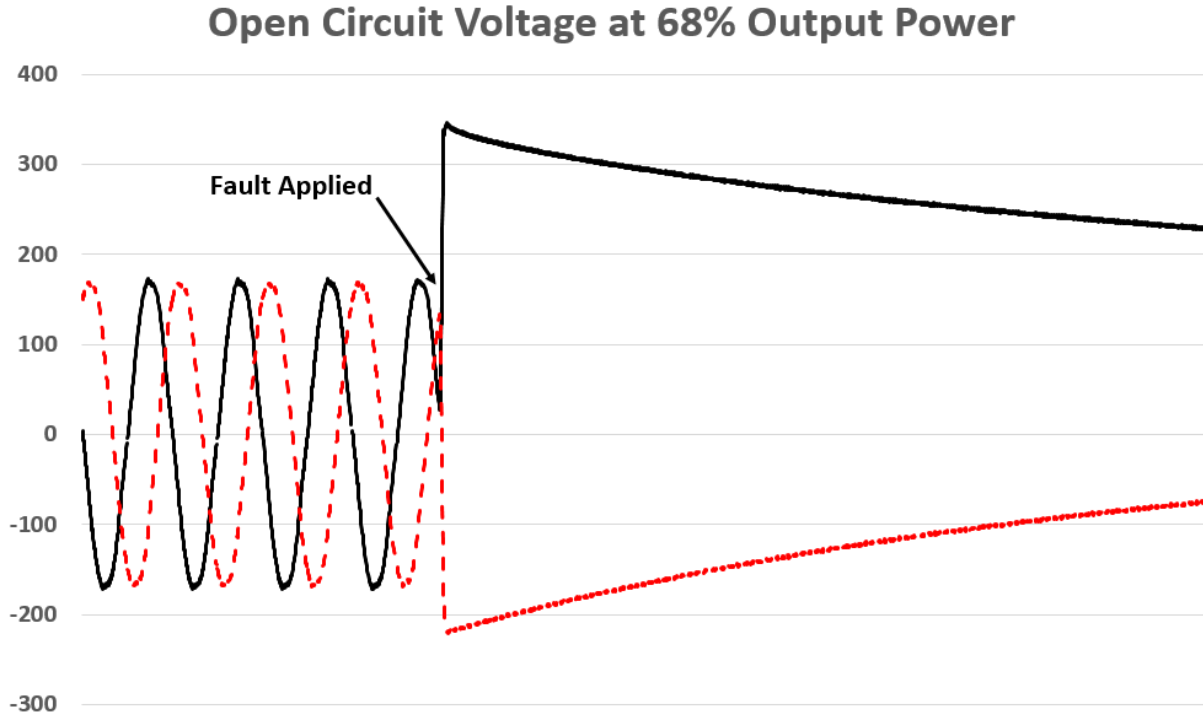
Figure 33. Open Circuit Response of Inverter H

Open Circuit Summary

In summary, each inverter produced a different open circuit result based on whether the inverter had a DC link capacitor, transformer, or just its internal RLC filter structure. The only exception was the micro inverters since they all appeared to have a DC link capacitor. In addition, the value of the initial overvoltage is dependent on the inverter manufacturer, power output level, and the point-on-wave where the event occurs. Maximum values ranged from 1.46 to 2.08 per-unit over the set of eight inverters tested. The exponential decay of the voltage is dependent on the size of the DC link capacitor within the inverter. The first-cycle rms voltage peak ranged from 1.27 to 1.91 pu. The transient PV model designed and demonstrated later in this dissertation will show how all the differences in the inverter responses can easily be modeled based on the mathematical structure used for the model.

Open Circuit and Short Circuit Test Result Summary

The short circuit rms currents from the eight PV inverters tested ranged from 0 to 1.91 pu, and the durations ranged from 0 to 10 cycles. This does not support a useful rule of thumb for PV inverter fault contributions. The open circuit rms voltage could reach 1.91 pu for the first cycle. Peak transient overvoltages may reach 2.08 pu and peak transient overcurrents may reach 7.53 pu. These values may be high enough to concern distribution engineers, but the impact can't be fully assessed without considering balance-of-system components and aggregation effects. The duration of fault contribution must also be considered. Each PV inverter has different behaviors that do not correlate to the nameplate or other data available to utilities. For this reason, distribution planners should have more accurate models for analyzing PV on distribution feeders. This problem is addressed by the creation of the Transient PV detailed in this dissertation. As will be seen later in this document, the model will be developed mathematically and also incorporated in OpenDSS by coupling the PV inverter transients to phasor dynamic solutions.

In addition, PV inverters should have type-test data available to support better modeling, and such tests have been proposed to the IEEE Std. 1547 working group for a full revision of the standard. Short circuit tests would encompass the basic fault types, and report the maximum transient current and maximum rms current over four time ranges:

- 0 to 1 cycles, for close and latch consideration
- 1 to 4 cycles, for equipment withstand
- 4 to 30 cycles, for interrupt ratings
- 30 cycles and beyond, for backup protection analysis (not covered in this paper)

Open circuit tests would encompass variations in output power and power factor, and report the maximum rms voltage from 1 to 10 cycles after the event. In the absence of good models, the type-test data could provide upper limits on the expected overvoltages and overcurrents. This is why the model developed in this dissertation is extremely important.

4.0   DETERMINING THE MATHEMATICAL STRUCTURE

This section discusses the process used to determine the mathematical structure for the Transient PV Inverter Model. Since the system (PV Inverter) is dynamical and we only have access to the input and output of the system, the first logical step is to consider System Identification techniques.

The definition of System Identification (SI) is - the process for modeling dynamical systems by measuring the input/output of the system. Within the realm of SI, both gray-box and black-box structures are analyzed. In addition, each structure is considered under both linear and nonlinear mathematical structures.

The linear methods considered are the ones common for steady state power electronics (i.e. inverters) and both the transfer function and state space representation are considered. For the nonlinear methods, SI represents the dynamic nonlinear systems with cascaded modular orientated techniques. The most common techniques are the Nonlinear Autoregressive with Exogenous (NARX) or the Hammerstein-Wiener (HW) method. Each of these methods are described in this section and evaluated against the inverter data collected in the laboratory.

4.1   GRAY-BOX MODELING

The first modeling approach attempted was to create a circuit topology in MATLAB Simulink to reproduce the transient data. Snapshots of the some of the circuit topologies are shown in Figure 34.
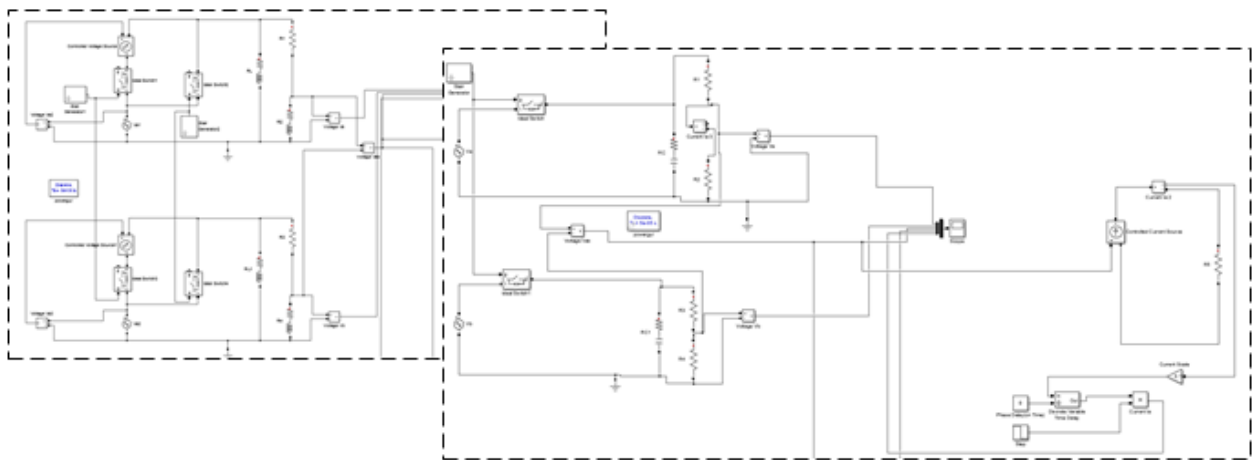
Figure 34. Snapshot of the Circuit Topology Created in MATLAB Simulink

This is a gray-box approach that allows the user to model the behavior of the system based on experimental data from the input and output of the system. However, this approach also requires insight into how the inverter controls operate during the transient event. Also, since the inverter's behavior is nonlinear, the nonlinearities would need to be addressed with nonlinear circuit components, thereby greatly increasing the complexity of the problem. In addition, the manufacturers do not supply this data, and each inverter behaves differently due to differences in manufacturer designs. Imagine creating a large RLC circuit, then trying to incorporate and tune

nonlinearities for each component [41]. Although this approach works (see Figure 35), and could eventually be incorporated for all inverter types, it limits the modeling to only known inverter structures.
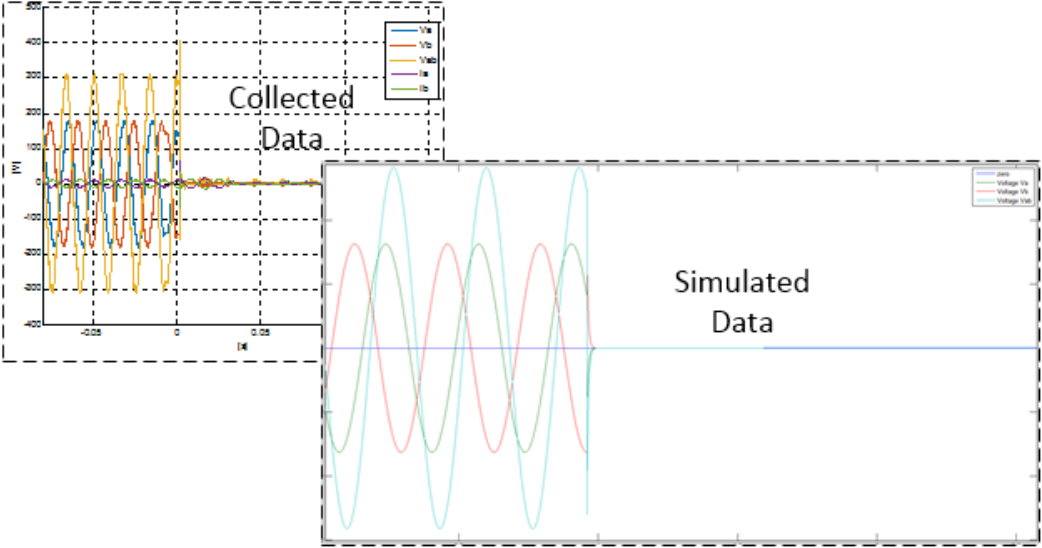
Figure 35. Collected and Simulated Data using the Grey-Box Approach

Some inverter structures could take weeks to model due to the complexity in the nonlinearities. The gray-box approach was not pursued further in this research due to the complexity introduced by the nonlinearities of the components and the need to know the internal controls of each inverter. The desire of this research is to develop a model that can easily be adapted to different inverters requiring only the inverters input and output data.

The next modeling method addressed is the black-box structure and is described in the following section. The black-box structure would allow for the inverter to be completely characterized by only using input and output data without needing to know anything about the internal controls of the inverter, and with nonlinearities already integrated into the model structure.

4.2   BLACK-BOX MODELING

Since the internal characteristics of the inverters are not known, they are most commonly viewed as 'black-box' models. There are two major approaches for modeling a 'black-box' system: analytical or experimental [42]. For Analytical methods, such as the gray-box approach mentioned previously, internal information of the system needs to be known. However, for experimental modeling and situations where internal information is unknown, the "black-box" system identification method is used. The "black-box" approach is what we want to use to create the transient inverter models; mainly for three reasons: First, we do not have to assume the internal operation of the inverter control system or structure (we do not need to know anything about internal structure of the inverter). Second, the model is entirely created using input/output data or nameplate information and operating condition of the inverter. Lastly, new inverter models can easily be created to account for differences in manufacturer designs by testing the inverter under the transient conditions outlined so far in this paper.

The following sub-sections outline the black-box model structures analyzed which led to the model structure used and best fitted for the Transient Inverter Model. Note that both linear and nonlinear black-box structures are addressed to provide complete mathematical analysis without assumptions as to linearity.

4.2.1   Linear Models

The first black-box model attempted was a linear model, since the idea was to start simple and work toward a more complex model. A linear model is described by a continuous response variable and is a function of one or more constants. For example, Equation 1 and Equation 2 give examples of linear functions.

$$f(x) = ax$$

Equation 1. Linear Equation with a Single Constant

$$f(x) = ax + b + c + ..$$

Equation 2. Linear Equation with Multiple Constants

In addition to describing linear systems/models as linear equations consisting of single continuous response variables, systems/models are most commonly described in terms of a Transfer Function or a State Space model.

4.2.1.1 Transfer Function

As described in earlier, the known dynamics of the inverter are the inputs and outputs of the inverter. By using the inverters input and output, the transfer function can be calculated since it is defined as the ratio of the output to the input of the system. If we can describe the output of the system by the function Y(s) and the input of the system by X(s), where the mathematical domain of the functions is Laplace, the transfer function could be described mathematically by Equation 3, or physically in Figure 36. Note that if the system was described mathematically in the time domain instead of Laplace, the function is then referred to as the impulse response.

66

$$H(s) = \frac{Y(s)}{X(s)}$$

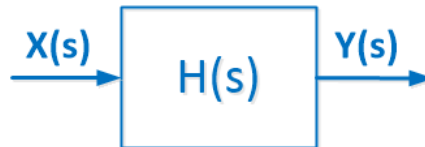**Equation 3.** Description of a Transfer Function in the Laplace Domain

Figure 36. Block Diagram Description of the Transfer Function

Representing the input and output of the system by use of the transfer function or impulse response is possible, but not a plausible solution. This is because these types of functions produce responses that are linear, meaning they have initial conditions and an equilibrium point. Measured data from the inverters were represented using the transfer function. Although transfer functions can model some transients, they are unable to represent the transients produced by PV inverters. Figure 37 shows a very simple transient response (voltage during a short-circuit event) and Figure 38 shows a type of response that is most common (voltage during an open-circuit event). Notice that the nonlinear response of the transient can almost be approximated using a linear function for simple cases as in Figure 37, but the nonlinear response of the transient cannot be reproduced using a linear function for cases such as in Figure 38.
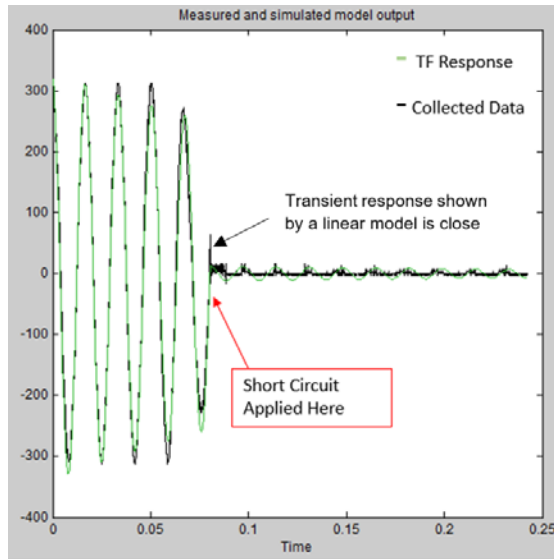
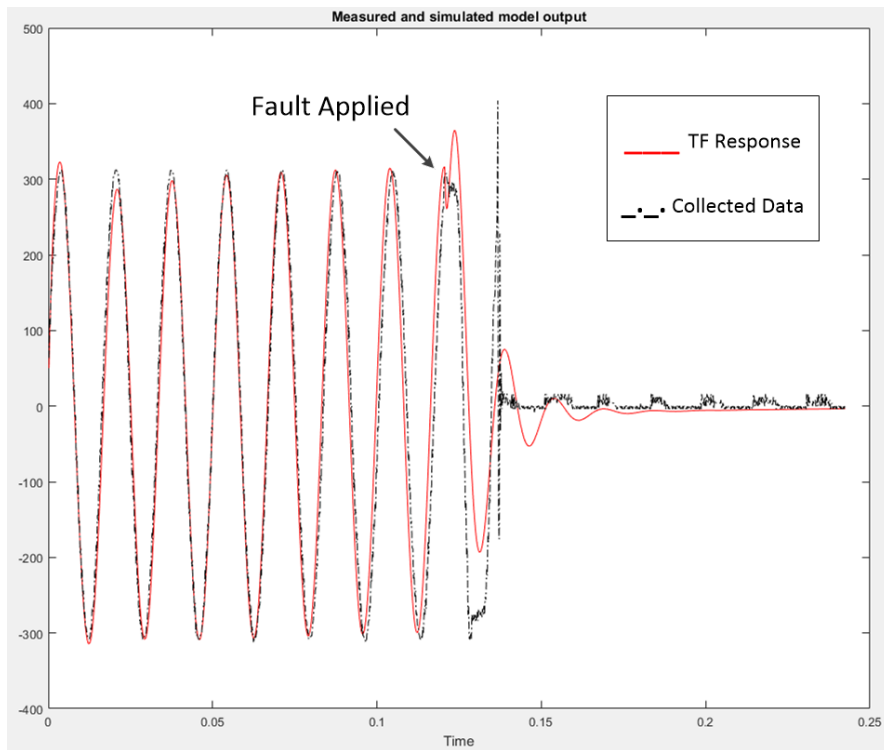**Figure 37.** Transient Voltage Response Compared to a Transfer Function Response (SC)

Figure 38. Transient Voltage Response Compared to a Transfer Function Response (OC)

68

One problem with linear models, is that they represent a system with respect to a small range about a single operating point. However, when transients are occurring within a dynamical system, the operating point can leave this range close to the steady-state operating point. The open-circuit and short-circuit response of PV inverters are outside the steady-state operating range. Using a nonlinear model allows the system to be represented over a wide range of operating points. The dynamic responses of the inverters are no longer in the linear range during transients we desire to model. <u>Due to the nonlinearity of the inverter's transient response, a linear model is not sufficient.</u> The same reason is applicable for state space representation since it also represents linear systems and is just another mathematical way to represent a linear system. The focus will now turn to nonlinear models.

4.2.2   Nonlinear Models

Now that it has been shown that linear model representations of the photovoltaic inverter transients is insufficient, the focus is moved to nonlinear representation for black-box models for the system identification. Note that one can estimate nonlinear discrete-time black-box models for both single-input/output (SISO) and multiple-input/output (MIMO) time-domain data, but for our data we can focus on SISO systems.

One way to specify a nonlinear model structure is to combine both the linear dynamic models with static (memoryless) nonlinear functions. These kinds of nonlinear models are called block-oriented models. Commonly used block-oriented models are the Nonlinear Autoregressive with Exogenous (NARX) structure and the Hammerstein-Wiener (HW) structure [43]. Both the NARX and HW nonlinear methods are described in the following sections.

69

4.2.2.1 Nonlinear Autoregressive with Exogenous (NARX) Structure

The first structure analyzed was the Nonlinear Autoregressive with Exogenous (NARX). NARX models define a predicted output as a nonlinear function of past inputs and outputs. Figure 39 shows the structure of the NARX model where *u* represents the input and *y* represents the output of the model.
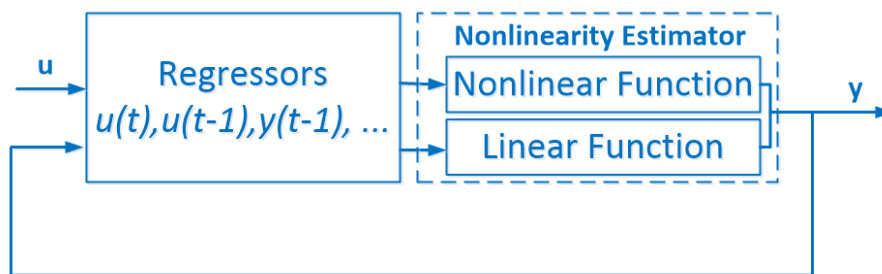

Figure 39. NARX Block Diagram

In order to compute the output of the model, the past input and past output values are used to calculate nonlinear values of the delayed input and output. These nonlinear delayed values are called standard regressors. In addition, these regressors can be functions of the delayed values from the input and output values. The regressors are then sent through a nonlinearity estimator which consists of both a linear and nonlinear function. However, all regressors are inputs to both the parallel linear and the nonlinear function blocks of the nonlinearity estimator.

The nonlinear estimator can consist of both the nonlinear function and the linear function, or a single linear or nonlinear function. The nonlinear estimator can take various mathematical forms like the ones in Section 4.2.2.3 called 'Nonlinear Estimators'.

As noted previously, the nonlinearity estimator block consists of parallel and linear blocks, therefore the estimator block is the addition of the two blocks and the output has the function described by Equation 4 where x is the vector of the regressors and r is the mathematical mean of the regressors.

$$F(x) = [L^T(x - r) + d] + [g(Q(x - r))]$$

Equation 4. Nonlinearity Estimator NARX Function

This method can rely on standard regressors, for example *u(t-1)* or *y(t-4)*, which uses delayed inputs and outputs. Or, customized regressors can be used, for example *sin(u(t-1))* or *u(t-1)*y(t-4)*, which uses nonlinear functions of delayed inputs and outputs. However, for the NARX structure, the nonlinear data does not directly effects the linear model making it difficult to track the operating point of the inverter through the transient region of operation. Figure 40 shows the response of a NARX model in comparison to the collected transient data.
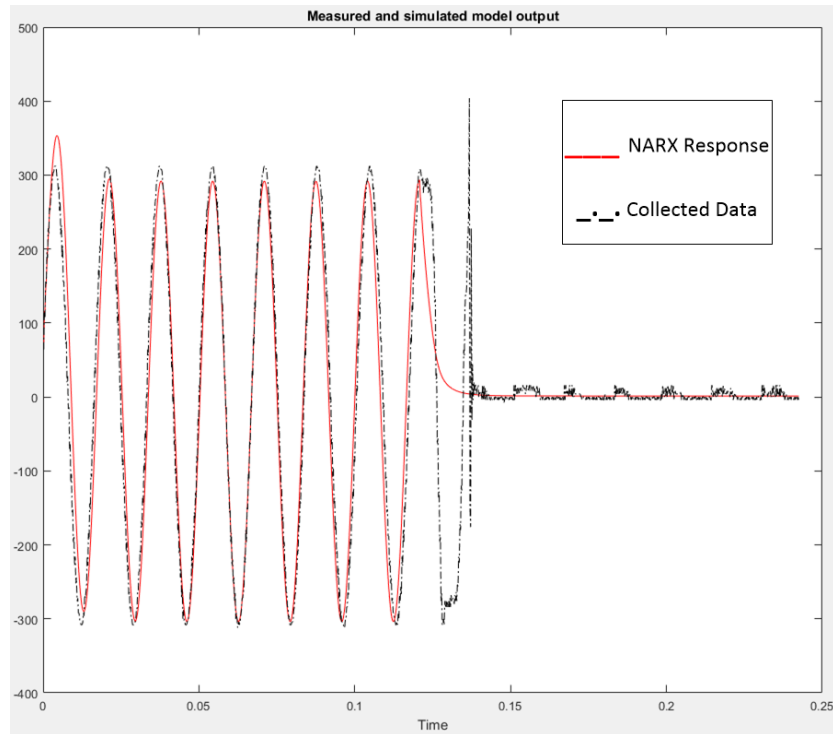
Figure 40. Transient NARX Voltage Response Compared to Collected Data

The NARX model would need to be mathematically tuned to accurately represent the nonlinear response, however, the nonlinear portion of the response cannot easily be manipulated in the NARX format. This leads to investigation into the Hammerstein-Wiener structure where each of the linear and nonlinear responses of the model can be tuned separately.

4.2.2.2 Hammerstein-Wiener (HW) Structure

The Hammerstein-Wiener (HW) models consist of three cascaded blocks, a linear block embedded between two static nonlinear gains, as shown in Figure 41. The first block represents the input nonlinearity (Hammerstein model) and the last bock represents the output nonlinearity (Wiener model) of the system. The center modular block contains the linear transfer function of the system. The nonlinear blocks in the HW model are represented by nonlinear functions f and

72

h, corresponding to the input and output nonlinearities respectfully. Both functions are implemented by using nonlinearity estimators [44].

By using the model block diagram described in Figure 41, the inputs and outputs are u(t) and y(t) respectfully, where u(t) can be a multiple variable input function.

Figure 41. Hammerstein-Wiener Block Diagram

The output of the first nonlinear block, Equation 5, is a nonlinear function transforming the input data u(t).

$$w(t) = f\big(u(t)\big)$$

Equation 5. Nonlinear Input for the Linear Block

Both w(t) and u(t) have the same dimensions. The output of the HW model, Equation 6, is a nonlinear function that represents the output of the nonlinear block and represents the final nonlinear system output.

$$y(t) = h\big(x(t)\big)$$

Equation 6. Nonlinear Output Function of the Hammerstein-Wiener Model

73

The linear block is a discrete transfer function matrix representing the dynamical component of the model. It is described in Equation 7 and Equation 8 in terms of its output in relation to its input, in the same manner used to describe a transfer function. However, the transfer function is now between two nonlinear gains. The transfer function has *ny* inputs and *nu* outputs.

$$x(t) = \frac{B_{j,i}(q)}{F_{j,i}(q)} w(t)$$

Equation 7. Linear Portion of the HW Model

$$j = 1, 2, \ldots, ny \ \ and \ \ i = 1, 2, \ldots, nu$$

Equation 8. Transfer Function Subscript Definitions

Figure 42 is an example of the nonlinear and linear function outputs for the HW model consisting of the AC input and AC output. The plot in the center is the system step response of the transfer function, and the left and right plots are the nonlinear input and output nonlinearities respectively using piecewise linear functions as the estimators.
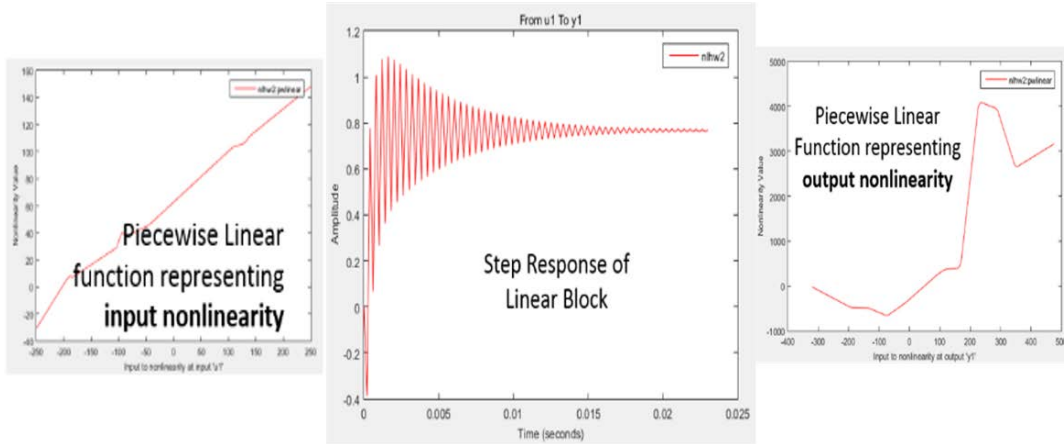
Figure 42. Hammerstein-Wiener Modular Block Response for Inverter A

The nonlinearities can be represented by multiple configurations such as a sigmoid network, wavelet network, saturation, dead zone, piecewise linear function, one-dimensional polynomial, or a custom network. Excluding both the input and output nonlinearities reduces the Hammerstein-Wiener structure to a linear transfer function and therefore the steady state inverter characteristic. The following section will briefly describe each of the nonlinearity estimators considered in this research to produce the correct transient model results.

4.2.2.3 Nonlinear Estimators

This section covers the nonlinear estimators considered during preliminary analysis on the inverter data in order to propose a black-box nonlinear model for the inverters transient response.

Sigmoid Network

The first nonlinear estimator tested was the Sigmoid Network. A Sigmoid Network is used to define a nonlinear function y=F(x) and is an iterative function governed by the expansion shown in Equation 9, where y is a scalar and x is an m-dimensional row vector.

$$F(x) = (x - r)PL + a_1 f((x - r)Qb_1 + c_1) + \cdots + a_n f((x - r)Qb_n + c_n) + d$$

Equation 9. Sigmoid Network Function Expansion

The sigmoid function, f, is described mathematically in Equation 10.

$$f(z) = \frac{1}{e^{-z} + 1}$$

Equation 10. Sigmoid Function

P and Q are m-*by*-p and m-*by*-q projection matrices. The projection matrices P and Q are determined by principal component analysis of estimation data. Usually, $p = m$. If the components of x in the estimation data are linearly dependent, then $p < m$. The number of columns of Q, q, corresponds to the number of components of x used in the sigmoid function [45].

When used in a NARX model, q is equal to the size of the Nonlinear Regressors (the numbers of inputs). When used in a Hammerstein-Wiener model, m = q = 1 and Q is a scalar. The dimension of the remaining variables are shown in Table 5.

Table 5. Sigmoid Network Variable Dimensions

Variable	Dimension
r	1-*by*-m vector and represents the mean value of the regressor vector computed from estimation data
d, a, c	Scalar
L	p-*by*-1 vector
b	q-*by*-1 vector

Some mathematical examples of the sigmoid function are the arctangent or the hyperbolic tangent; both are shown in Figure 43 along with additional examples of sigmoid functions.
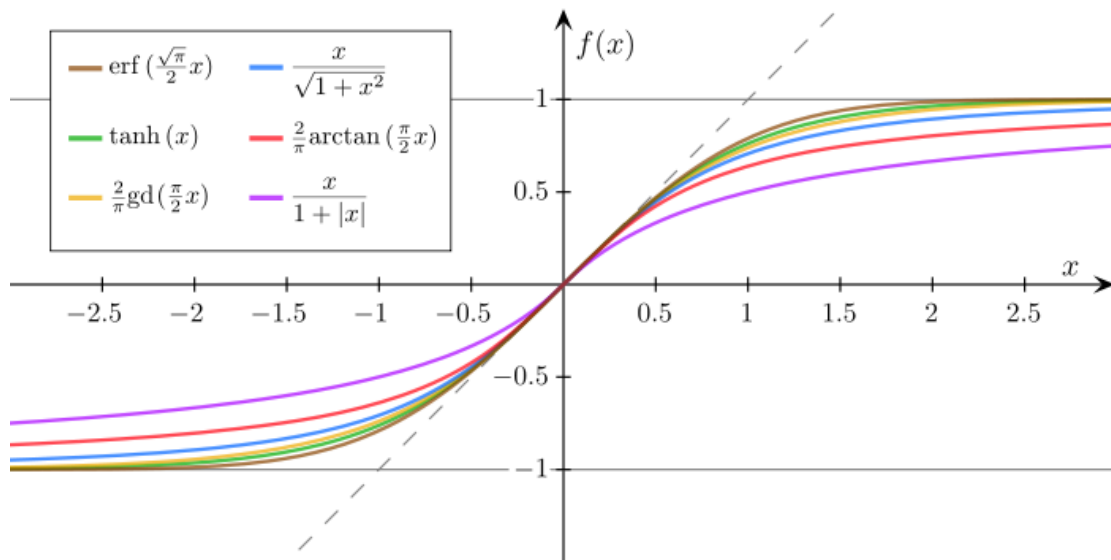

Figure 43. Examples of Sigmoid Functions [45]

77

The sigmoid function would only work if the operating point of the inverter followed this mathematical structure. Preliminary analysis has indicated that the sigmoid function is not a good enough representation for the nonlinearity of the inverter transient.

Wavelet Network

The second nonlinear estimator tested was the Wavelet Network. A Wavelet Network is used to define a nonlinear function y=F(x) and is an iterative function governed by the expansion shown in Equation 11, where *y* is a scalar and *x* is an m-dimensional row vector.

$$F(x) = (x - r)PL + a_{s-1}f\left(b_{s-1}((x - r)Q - c_{s-1})\right) + \cdots + a_{s-ns}f\left(b_{s-ns}((x - r)Q - c_{s-ns})\right)$$
$$+ a_{w-1}f\left(b_{w-1}((x - r)Q - c_{w-1})\right) + \cdots + a_{w-nw}f\left(b_{w-nw}((x - r)Q - c_{w-nw})\right) + d$$

Equation 11. Wavelet Network Expansion

The expansion consists of two functions: a scaling function, *f*, and a wavelet function, *g*. The functions are described in Equation 12 and Equation 13 respectively. Note that *x* is the number of regressors and *Nr* is the length of *x*.

$$f(x) = e^{-0.5xx'}$$

Equation 12. Scaling Function

$$g(x) = (N_r - xx')e^{-0.5xx'}$$

Equation 13. Wavelet Function

78

The projection matrices P and Q are determined by principal component analysis of estimation data. Usually, p = m. If the components of x in the estimation data are linearly dependent, then p < m. The number of columns of Q, corresponds to the number of components of x used in the scaling and wavelet function.

As in the Sigmoid Network, when the wavelet is used in a NARX model, q is equal to the size of the Nonlinear Regressors (the numbers of inputs). When used in a Hammerstein-Wiener model, m = q = 1 and Q is a scalar. The dimensions of the remaining variables are indicated in Table 6 below.

Table 6. Wavelet Network Variable Dimensions

Variable	Dimension
r	1-*by*-m vector and represents the mean value of the regressor vector computed from estimation data
d, a, b	Scalars
L	p-*by*-1 vector
c	1-*by*-q vector
P, Q	m-*by*-p and m-*by*-q projection matrices, respectively

As with the sigmoid nonlinearity, the wavelet function did not exhibit a high enough percent-fit to the data collected to pursue further. Percent-fit is based on the percentage of data points from the model, within a set confidence level (typically set to 95%), match the collected data.

Dead-Zone

The third nonlinear estimator tested was the dead-zone. The dead-zone nonlinear estimator is used for the Hammerstein-Wiener models. Just as it sounds, the dead-zone defines a nonlinear function y=F(x), where *F* is a function of *x* and can be defined by the Equation 14. Where *x* and *y* are scalars.

$$F(x) = \begin{cases} 0, & for\ a \le x \le b \\ x - a, & for\ x < a \\ x - b, & for\ x \ge b \end{cases}$$

Equation 14. Dead-Zone Function

An example of the dead-zone function is shown in Figure 44. The dead zone non-linearity refers to a condition in which the output becomes zero when the input crosses certain limiting value.
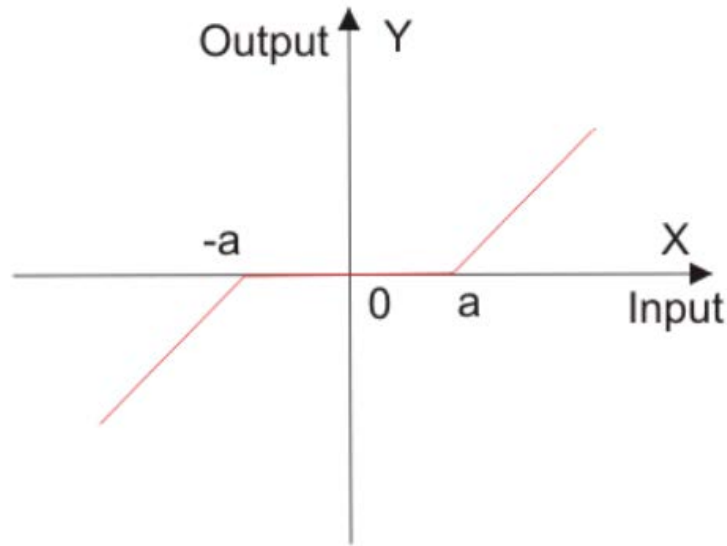

Figure 44. Dead-Zone Function

Although addressed as a possible solution for nonlinearities, the dead-zone function does not allow for enough changes in the operating point to produce the desired transient response.

Single Variable Polynomial

The fourth nonlinear estimator tested was the Single Variable Polynomial. The Single Variable Polynomial (SVP) is a nonlinear function described by y=F(x), where *F* is a single-variable polynomial function of x described by Equation 15.

$$F(x) = c(1)x^n + c(2)x^{n-1} + \cdots + c(n)x + c(n+1)$$

Equation 15. Single Dimensional Polynomial

The SVP nonlinear estimator will work for Hammerstein-Wiener Models, but will not be discussed further here since only allows for a single input variable, limiting the model's possibilities, including an expansion to three-phases.

Saturation

The fifth nonlinear estimator tested was Saturation. Nonlinear estimators based on saturation functions are similar to dead-zone functions, except one interval need not be zero. It is still a nonlinear function described by y=F(x), but F is now defined by Equation 16.

$$F(x) = \begin{bmatrix} x, & for \ a \le x < b \\ a, & for \ a > x \\ b, & for \ b \le x \end{bmatrix}$$

Equation 16. Saturation Function

Another way to view the saturation is to think of a gain "schedule", where the gain changes for the specified range *a* to *b*. Saturation is typically only used for HW models if the saturation is zero during the linear range of the model. This nonlinearity did not produce a high enough accuracy to propose as a solution.

Piecewise Linear

The sixth nonlinear estimator tested was the Piecewise Linear. The Piecewise Linear function is a nonlinear function y = F(x), where F is a piecewise-linear (affine) function of x having n breakpoints. The breakpoints can be defined by linear x-y coordinates described by Equation 17 below.

$$(X_k, Y_k) \ where \ k = 1, ..., n \ [\ Y_k = F(X_k)]$$

Equation 17. Breakpoints of a Piecewise Linear Function

The function, F, is the linear interpolation between the breakpoints and on either side of the breakpoints on the far end breakpoints. An example of the piecewise linear function is shown in Figure 45.
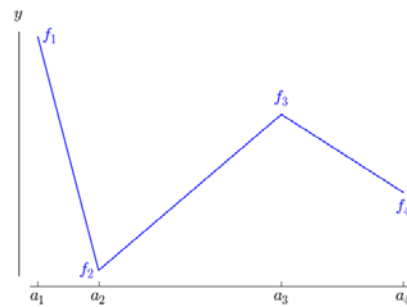

Figure 45. Piecewise Linear Function

In the piecewise linear function in the figure above, the function F is defined by four breakpoints f_1 through f_4, creating a nonlinear function defined by piecewise linear functions. Note, that the

83

end segments at f_1 and f_4 continue as linear extrapolations of the function. This method of a nonlinear estimator allows for an infinite number of breakpoints (i.e. operating points) of the function. This estimator produced the most accurate data fit due to being able to track the operating point during the transient. ***The piecewise linear estimator provided the best response for the PV Transient data,*** see Figure 46**.** Notice that for the plot on the right in Figure 46, the measured and simulated data are directly on top of each other, making it hard to distinguish two different lines. Clearer and more distinct plots will be shown later when the model is constructed in greater detail. For now, it is important to note the similarities in the Hammerstein-Wiener model using piecewise linear estimators in comparison to the measured data in the laboratory.
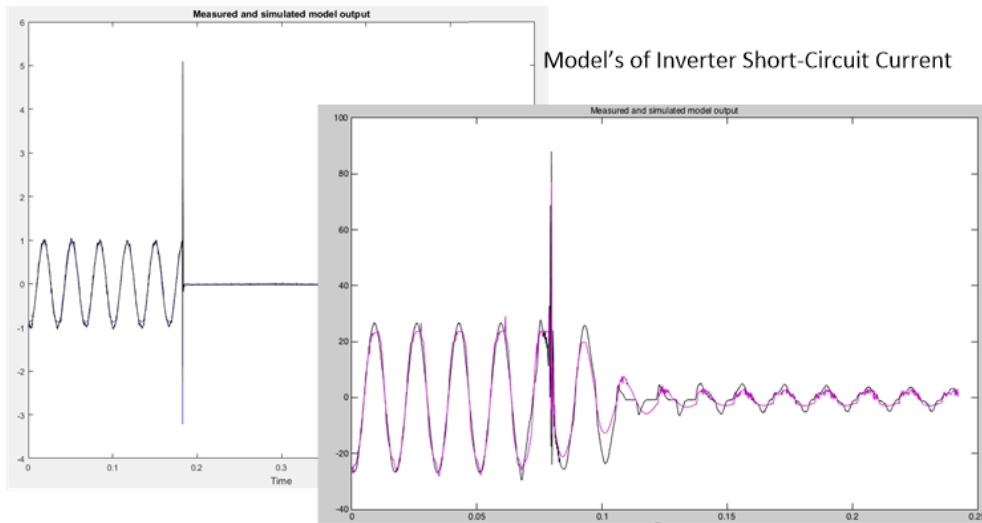

Figure 46. Results from the Piecewise Linear Estimator

Regressors

For HW and NARX mathematical structures, the output can be defined as a function of regressors which are transformations of past inputs and past outputs. Typical regressors are simply delayed input or output variables; referred to as standard regressors. It is also possible to use more advanced regressors in the form of arbitrary user-defined functions of delayed input and output variables. Such regressors are referred to as custom regressors. However, since we are using non-delayed input and output data directly, the nonlinear regression option does not fit the form of our data. In addition, the piecewise linear estimator in the HW structure matches the transients the best.

Other Nonlinear Estimators

The nonlinear estimators described in this dissertation are only a sample of possible mathematical nonlinear estimators, however they are the ones that are the most relevant and the ones deemed reasonable for the type of time variant dynamical inverter data collected. Additional examples of nonlinear estimators not discussed in this thesis are the Tree Partition, Neural Network, and Multilayered Neural Network [46]. These estimators did not come close to the nonlinearities of the inverter response data. Therefore, they are not discussed in detail.

4.3   MODEL STRUCTURE SUMMARY

After reviewing both linear and nonlinear mathematical structures to determine the appropriate transient PV inverter model, the one best suited is the Hammerstein-Wiener structure using piecewise nonlinear estimators for both the input and output nonlinearities. This allows the model to be constructed using only input and output data without having to make assumptions about the internal controls of the inverter. The following sections give more details about how the chosen structure was incorporated into open source software; placing an accurate transient PV model into the hands of all distribution engineers.

5.0 THE DEVELOPED TRANSIENT PV INVERTER MODEL

This section summarizes what this dissertation has accomplished to this point. Once the transient data was collected from the eight inverters, a model was needed which could accurately describe the transients mathematically. Figure 47 gives a visual summary of the processes used to determine the appropriate structure for the transient PV inverter model.
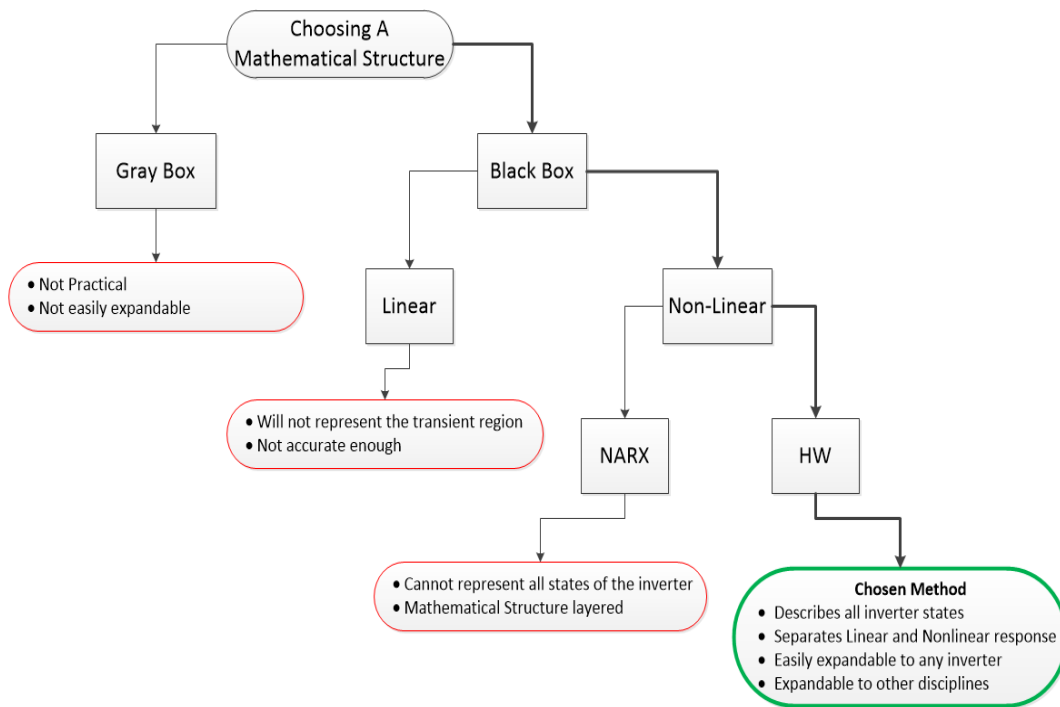

Figure 47. Process for Determining a Mathematical Structure for the Model

The chosen structure for the transient PV inverter model is the Hammerstein-Wiener using piecewise nonlinear estimators for both the input and output nonlinearities. This structure relies on only input and output data, while allowing for the separation of the model into both linear and nonlinear mathematical expressions. This allows the model to be used for both steady state and transient analysis. The user can also mathematically describe both the linear and nonlinear operation separately making it easy to program the model into any desired software platform. In addition to developing the model mathematically, this research also incorporated the model into two software platforms; MATLAB and OpenDSS. The transient PV inverter model was first developed in MATLAB since the laboratory data could easily be mathematically processed and manipulated within the software. However, the MATLAB model limits use to only MATLAB users. Detailed models of distribution feeders are not readily available in MATLAB.

The transient PV model developed in OpenDSS is open source and available to all users. This allows everyone access to a transient PV model as well as the software code. For those who already utilize OpenDSS, the model is complete. For those who prefer a different distribution simulation software, the code is readily accessible and can be implemented into any desired platform. Within OpenDSS, the transient PV inverter model is called the Voltage-Controlled Current Source (VCCS). The details of the model implementation into OpenDSS will be discussed in the following section.

6.0   IMPLEMENTING THE VCCS MODEL INTO OPENDSS

The transient PV inverter model was incorporated into OpenDSS as a power conversion element
called the Voltage-Controlled Current Source (VCCS); see Figure 48. The VCCS interfaces the
Hammerstein-Wiener framework to the dynamics mode in OpenDSS allowing transient analysis
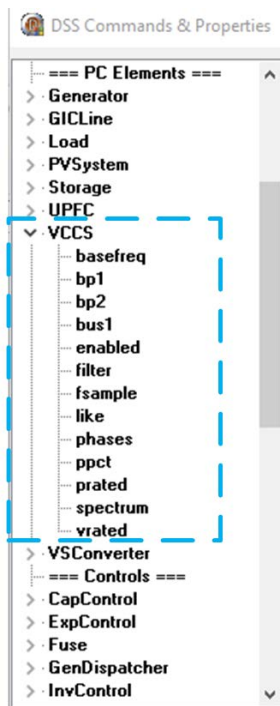with a varying time step [47].

Figure 48. VCCS as a PC Element in OpenDSS

The model senses the terminal voltage and updates the injected current at each OpenDSS time step. Figure 49 shows the relationship between the Hammerstein-Wiener and OpenDSS domains, and it defines the key signal locations to reference when reading the open source Delphi code. The top of the figure shows the Hammerstein-Wiener structure in time domain and the bottom of the figure shows the phasor-dynamic domain representation in OpenDSS. As noted previously, the Hammerstein-Wiener structure consists of three cascaded blocks; input nonlinearity represented by a piecewise linear function having breakpoints BP1, linear block represented by the digital filter H(z), and output nonlinearity represented by a piecewise linear function having breakpoints BP2.
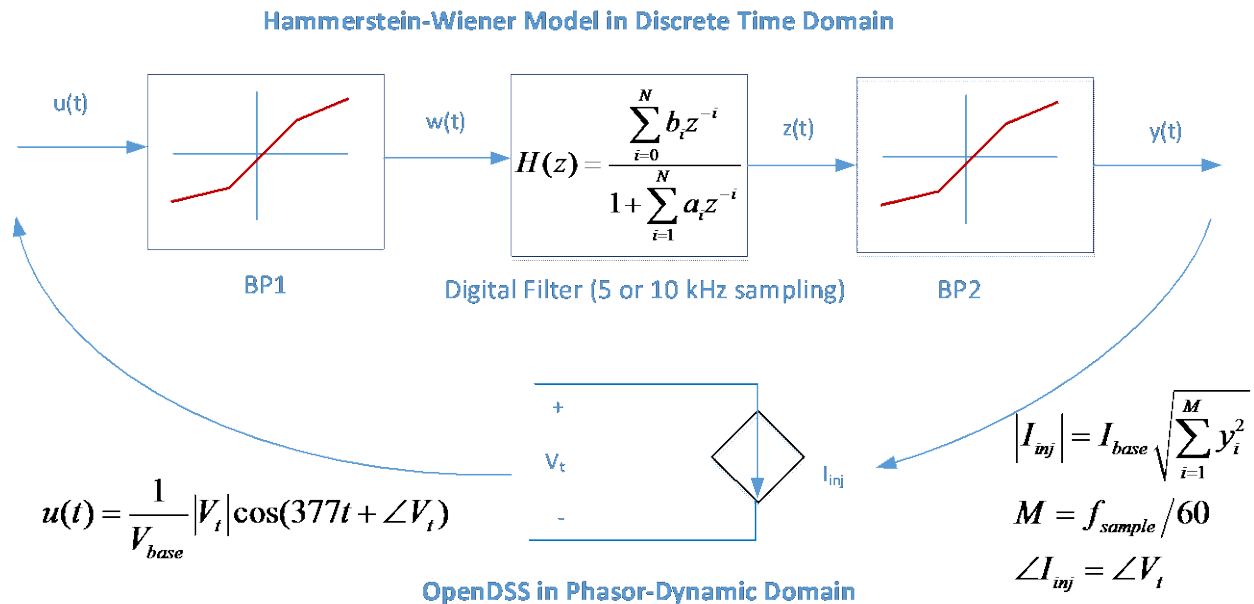

Figure 49. Interface Between Hammerstein-Wiener and OpenDSS Solution Variables

6.1   MODEL INPUTS

The VCCS model currently has two default short circuit transient models incorporated in OpenDSS; micro-inverter and single-phase inverter. Three-phase models can currently be incorporated by using three single-phase inverters. However, the model was incorporated so that the user can program a specific inverter model if they have the input and output response of the inverter. Else, the default inverter models can be used. Table 7 gives a list of the possible input parameters which can be edited by the user. In general, the user will only have to adjust the last three parameters: rated power (Prated), rated line-to-line voltage (Vrated), and percent power (Ppct).

Table 7. VCCS Input Parameters

Input Parameter	Definition	Notes
Basefreq	Base Frequency	Default assigned to be 60Hz
BP1	Breakpoints of the Input Nonlinearity	XYCurve defining the input piecewise linear block
BP2	Breakpoints of the Output Nonlinearity	XYCurve defining the output piecewise linear block
Bus1	Connected Bus Name	Name of bus to which source is connected (e.g. bus1=busname)
Enabled	VCCS on/off	Indicates whether this element is enabled (e.g. yes/no or true/false)
Filter	Filter Response	XYCurve defining the infinite impulse response (IIR) digital filter coefficients. X values are the numerator coefficients and Y values are the denominator coefficients, and note that a0=1 must be input explicitly. This also enforces equal order in numerator and denominator.
Fsample	Sampling Frequency	Sampling rate for linear block H(z), either 5 kHz (PortoSag) or 10 kHz (Dranetz) in this project
Like	Make 'like' another object	Make like another element (e.g. New VCCS.V1 like = V2 …)
Phases	Number of Phases	Only 1-phase implemented now, 3-phase under development
Ppct	Percent Power	Real power output in snapshot mode, based on Prated. Unity power factor assumed
Prated	Rated Power	Inverter's rated power in Watts
Vrated	Rated Voltage	Rated line-to-line voltage (3-phase) or line-to-neutral voltage (1-phase) in volts

An example of the XY curves defining the input and output nonlinearities can be seen in Figure 50. The left plot shows the input nonlinearity response BP1 and the right shows the output nonlinearity response BP2.
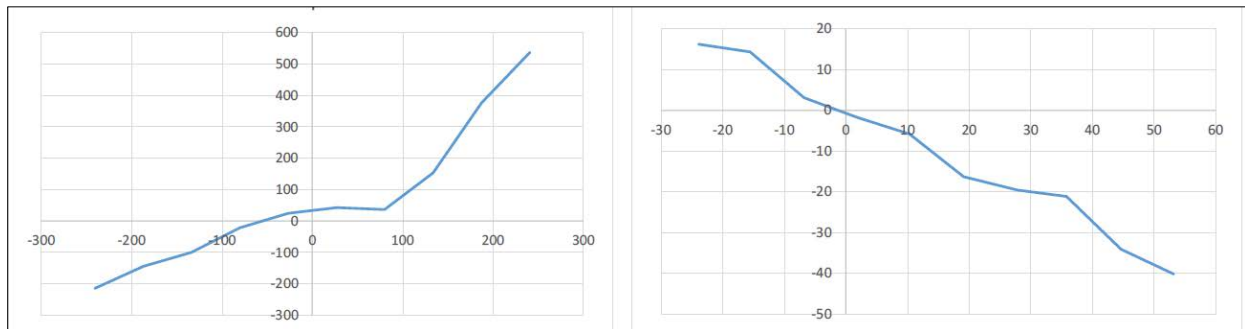

Figure 50. Sample 10-point Nonlinear Blocks BP1 (left) and BP2 (right)

The breakpoints are defined in text files as XY curves, and the filter coefficients are defined as an array. An example text file consisting of two XY curves (two 10-point piecewise input and output nonlinearity functions), and a 4th order filter shown in Figure 51. The example is based on a 190W micro-inverter. Note that the filter order expands with respect to the length of the transient response. Single phase inverters typically have a filter order of at least twenty-two.

```
New XYcurve.m190 bp1 npts=10 xarray=[-264.247209691872 -186.797096749935 -
113.999158872285 -82.6870353867463 -24.8137408902437 -11.9148284369882
27.0192252128813 135.149825825011 196.543272046783 241.739830586434]
~ yarray=[-56.6007772352605 18.4686074648929 90.5436353349481
121.436176790441 177.882600484537 191.555600465171 231.689431511064
332.957826097434 384.696875082151 420.213174126393]

New XYcurve.m190 bp2 npts=10 xarray=[-185.670885956717 -162.398919495745 -
139.126953016290 -115.852878563658 -92.5758885674808 -47.0112883890579 -
35.3480971557727 -27.0710140718451 13.4654018280332 23.7955752913491]
~ yarray=[39.9993291871476 18.6092700884592 0.271831180935148
0.476925527659269 15.4575150026444 14.1667309380808 7.00879990229796
3.58373421812038 -11.3765765505691 -38.8152025782624]

New XYcurve.m190 z npts=4 xarray=[1 -0.275515728217058 -0.0975731084864074
0.0275483933466857] // denominator
~ yarray=[0 -0.198600301682772 1 -0.856652694252797] // numerator
```

Figure 51. Example Text File Defining VCCS Breakpoints and Filter

The VCCS model also works in snapshot mode where the power flow is initialized, producing

steady state results; BP1, BP2, Filter, and Fsample have no effect. In a snapshot mode, the model

injected current will be constant, as determined by its ratings and initial power output level. The

main application for the VCCS is photovoltaic inverter modeling, and the input and output

parameters are defined in those terms. However, since the model is based on a nonlinear black

box structure based only on input and output data, the model could easily be expanded to other

disciplines or nonlinear modeling needs.

93

6.2 MODEL OUTPUTS

Table 8 below lists the default responses available from the VCCS model for both the micro-inverter and a single-phase inverter. Both are included in the OpenDSS library and do not require any programming by the user. The three phase inverter can be modeled using three single-phase inverter models with excellent results, however, including a three-phase model in the OpenDSS library is planned for the future. In addition to the library models, the user can easily program any inverter response into OpenDSS by defining the inverters breakpoints and filter coefficients as was shown earlier in Figure 51.

Table 8. VCCS Output Parameters

Output Parameter	Definition
V1	Peak Voltage
VAngle1	Voltage Angle
IAngle1	Current Angle
S1 (kVA)	Apparent Power
Ang1	Power Factor Angle
Vwave	Instaneous Voltage
Iwave	Instaneous Current
Irms	RMS Current
Ipeak	Peak Current
bp1out	Output of first Hammerstein-Wiener Block
filterout	Output of second Hammerstein-Wiener Block

6.3   VCCS EXAMPLE

This section gives a detailed example of the VCCS model using the micro-inverter model from the OpenDSS library. The results will then be compared to the transient data collected in the laboratory. In addition, the single-phase inverter response will be shown.

The OpenDSS code shown in Figure 52 models the 190 W micro-inverter (Inverter F). Each line of the example code has been numbered for sake of reference. The script runs a dynamics test on Inverter F, feeding a bolted fault with source impedance adjusted to match that of Pitt's electric power lab (lines 1-3). The text file containing the breakpoints and filter coefficients is accessed in line 4 and called in line 6. The VCCS model is defined in lines 5 and 6 to operate at 89.5% ouput power, rated 208V and 190W. In this example, Fsample is 10 kHz (corresponding to the instrument's sampling rate used to collect the data), so the OpenDSS time step must be at least 0.1 ms, but it can be longer (line 19). The Hammerstein-Wiener model can run at a faster time step within each OpenDSS time step. The bolted fault is defined in line 7. The fault's on-time value will determine when the HW model departs from its initial (steady state) condition. The monitors are setup in lines 8-11 and allow for easy access to the output variables. Lines 12-20 solve the circuit in dynamics mode so transient results can be obtained. The last line exports the monitor from line 10 to a CSV file for processing or expanded plotting options. OpenDSS download and manuals can be found at the following website: https://sourceforge.net/projects/electricdss/.

```
1) // EPSL impedance is 10% on 75 kVA positive sequence, 5% zero sequence,
   assume X/R = 2
2) new circuit.HWDynamic
3) ~ basekv=0.360 pu=1.0 angle=0 phases=3 bus1=SourceBus r1=0.029 x1=0.058
   r0=0.014 x0=0.029

4) redirect MicroInverter_M190.txt

5) New VCCS.SMA Phases=1 Bus1=SourceBus.1 Prated=190 Vrated=208 Ppct=89.5
6) ~bp1='m190_bp1' bp2='m190_bp2' filter='m190_z' fsample=10000

7) new fault.flt bus1=Sourcebus.1 phases=1 r=0.001 temporary=yes
   ontime=0.0821

8) new monitor.invvi element=vccs.sma terminal=1 mode=0
9) new monitor.invpq element=vccs.sma terminal=1 mode=1
10) new monitor.invst element=vccs.sma terminal=1 mode=3
11) new monitor.fltvi element=fault.flt terminal=1 mode=0

12) Set Voltagebases=[0.360]
13) set maxiterations=100
14) calcv
15) set mode=snap
16) solve
17) set mode=dynamic
18) set number=1250
19) set stepsize=0.0001 // matches fsample
20) Solve
21) export monitors invst
```

Figure 52. OpenDSS Example VCSS Script for a Micro-Inverter

The transient response obtained from the same inverter in the laboratory can be seen in Figure 53. Output results from the OpenDSS model are shown in Figure 54. Other than the VCCS instantaneous peak current being 586 mA lower than the peak seen in the laboratory, that the responses are identical. Since the VCCS and laboratory results are almost identical, the data overlaps each other. Therefore, they are shown in two different plots (Figure 53 and Figure 54). In Figure 54, the inverter's short-circuit current response is shown by the solid line, the dashed line tracks the peak current, and the dotted line represents the RMS current.

Figure 53. Micro-Inverter Short Circuit Current (Lab Data)

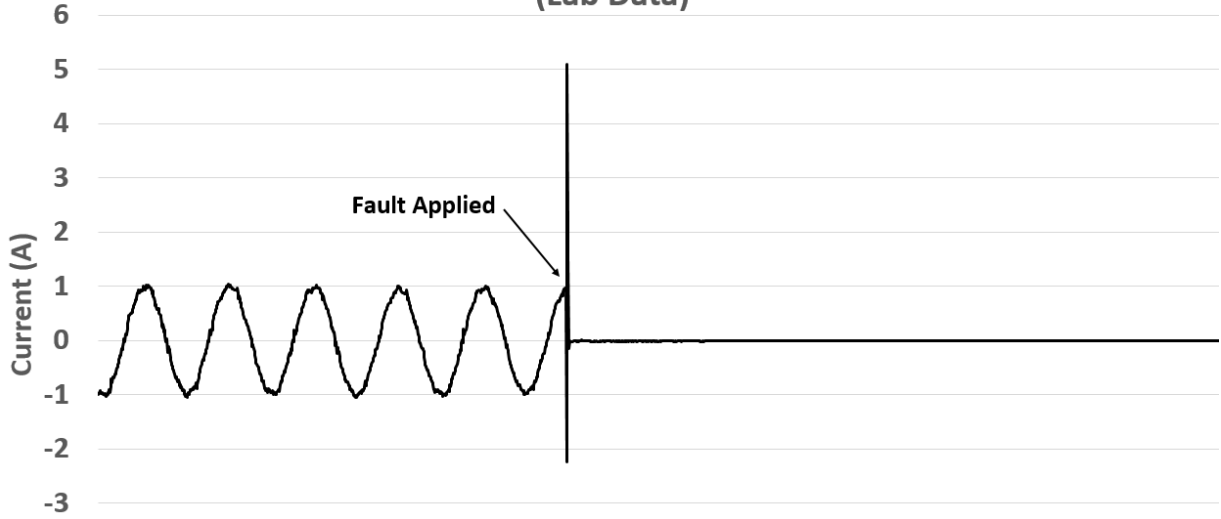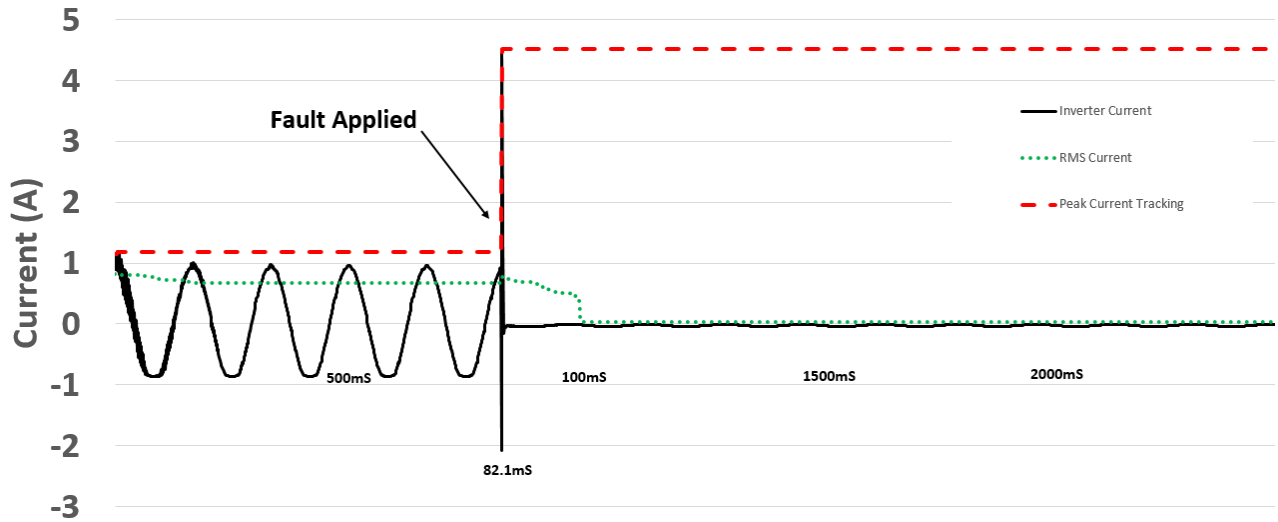**Figure 54.** Micro-Inverter Short Circuit Current (Model Output)

Figure 55 shows a snapshot of the VCCS micro-inverter output directly from OpenDSS and displays the same data as in Figure 54. Identical data was plotted so the plots could be distinguishable when printed or viewed as black and white while still displaying the OpenDSS output.
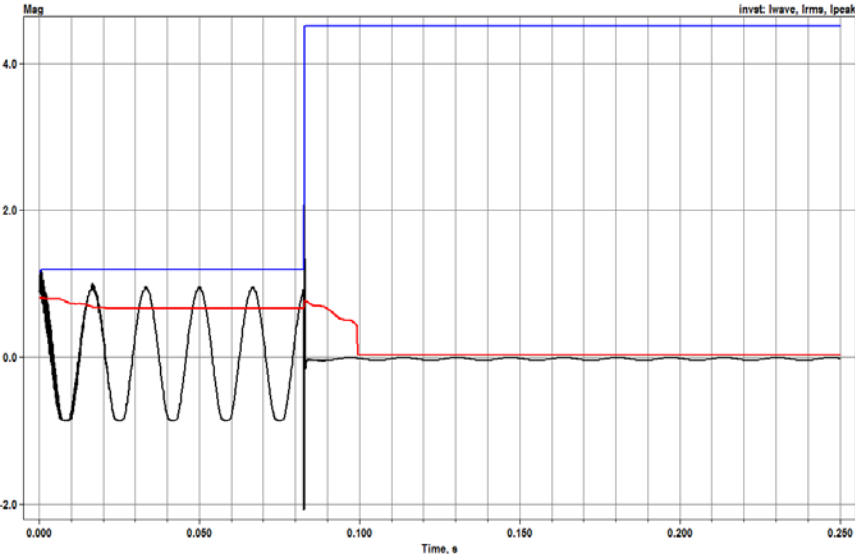

Figure 55. OpenDSS Snapshot of the Micro-Inverter Response

So far this section has given a detailed example of how to use the VCCS model in OpenDSS using the micro-inverter data from the OpenDSS library. To produce the response for a single-phase inverter, the user would only have to choose the single-phase inverter library file. The output of the single-phase VCCS model is shown in Figure 56.
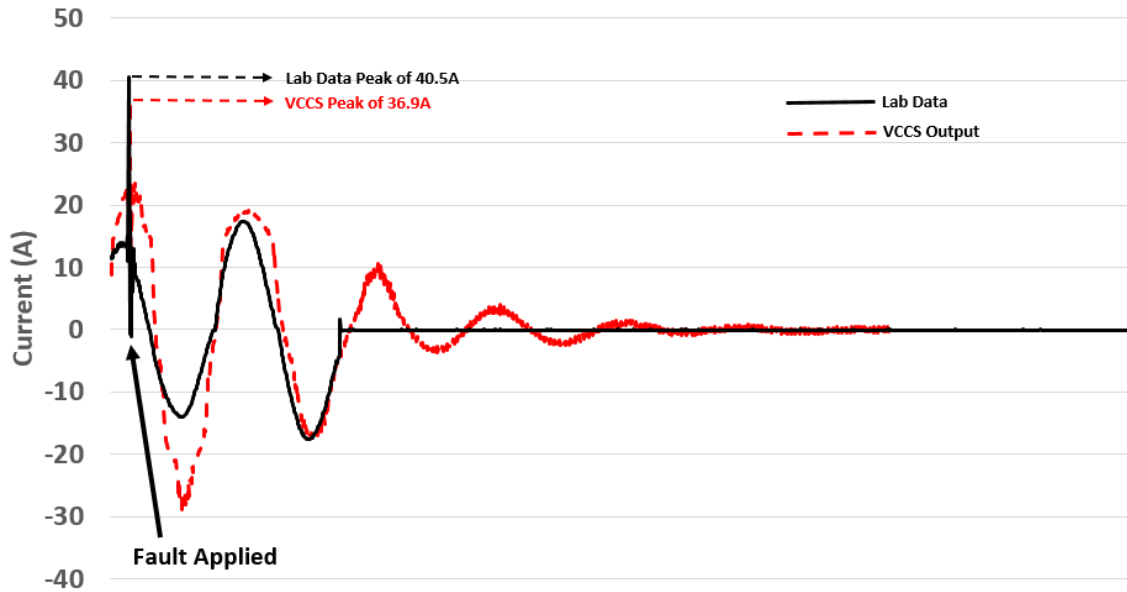
Figure 56. Single-Phase VCCS Model

Note that the VCCS produces a peak transient which is a few amps less than the actual laboratory data, and also displays some additional oscillation before reaching the final value. In reality, there would be some type of impedance between the fault and the inverter (lines or transformer) causing the current spike to be slightly lower than seen in the laboratory. The oscillations before settling are due to the large filter (order greater than 22) necessary to produce stored energy in the VCCS so as to produce current after the initial momentary transient spike. This was not seen for the micro-inverter since it does not contain enough energy storage (LC) to continue to produce current for a couple cycles after voltage is removed. However, this oscillation could be reduced by tuning the VCCS model (choosing a different set of breakpoints and filter coefficients).

VCCS Summary

Overall, both the VCCS single-phase and micro-inverter models in OpenDSS produce transient results equivalent to those captured in the laboratory. Both models and the VCCS source code are currently available and open sourced. The following link allows users to access the open source code for the VCCS model (code is written in Pascal): https://sourceforge.net/p/electricdss/code/HEAD/tree/trunk/Source/PCElements/vccs.pas. Since this dissertation research produced a transient PV inverter model both mathematically and in open source software, anyone can access and use the model making it a valuable resource. Additional information on the VCCS mathematical routines and data processing can be found in the OpenDSS Tech Notes "Voltage-Controlled Current Source" [48] which should be released to the public in November 2016.

7.0   SUMMARY

This section summarizes the dissertation by discussing (1) what the research accomplished, (2) the impact of the research, and (3) future work and research.

What this Research Accomplished

- Created a transient PV model which is easily adaptable for any current or future inverter.

- Solved the modeling problem corresponding to increasing PV installation.

- Developed the mathematical structure for the PV transient model based on actual laboratory data, AND incorporated the model into open-source software that is currently available to the public.

- Adaptable model is based on a black-box mathematical structure, it can easily be adapted to any system where only the input and output of the system is accessible.

- Paper submissions to ECCE [23] and journal paper on the inverter testing [49].

Impact of the Research

- Accurate transient PV model for planning and interconnection studies.

- The developed model is correlated to nameplate ratings and steady-state operating point.

- The PV transient model developed is expandable to additional inverter sizes, types, and manufacturers.

- The developed model describes both the linear and nonlinear transient effects of the PV inverters.

- Easy to use by utilities and incorporated into software that some of them currently use.

- The model was developed in open-source software.

- Will lead to the creation of PV generation standards since the transient conditions can now be accurately modeled.

Future Work

- A journal or conference paper is in progress which outlines the HW modeling process, the voltage sag events, and how to use the VCCS model on distribution system feeders.

- In addition to open circuit and short circuit tests performed in the laboratory, events were also collected for some of the inverters at 40%, 60%, 70%, 80%, and 90% sag levels. The results from these tests will be incorporated into a conference or journal paper.

- The OpenDSS model could be expanded to incorporate open circuit conditions.

- Creating the structure for a new inverter currently requires analyzing the structures one at a time. This process could be streamlined to make it faster to create multiple models at a time.

- Expand the HW models to include three-phase.

- Bypass the MATLAB toolbox.

- Specify new IEEE and UL standard test procedures that support HW black-box modeling.

In Summary, this dissertation makes an original contribution in providing a modeling solution for the transient behavior of photovoltaic inverters under load rejection and fault contribution transient events. The Hammerstein-Wiener mathematical model provides this solution for developing the photovoltaic inverter transient model. Advantages of the Hammerstein-Wiener model include being able to describe both the linear and non-linear transient effects of the inverter and allowing an avenue for describing the internal control of the inverter during the transient events. This model was incorporated in both MATLAB and OpenDSS which makes feeder analysis easy for planning engineers since it can provide both steady state and transient solutions for PV interconnections.

APPENDIX A

VOLTAGE SAG EVENTS

This section gives the results obtained from performing voltage sag testing on three micro-inverters, four single-phase inverters, and a three-phase inverter. The voltage sags are performed by using the portable sag generator, porto-sag, loaned from EPRI and discribed in section 3.0 . A sag duration of 12 cycles was used for each sag event. For each inverter the phase angle of the sag was set from 0 to 255 degrees in increments of 15 degrees to account for point-on-wave effects. In addition, for each series of events the power level was set to 25, 50, 75, and 100% output power. The sag events were captured using the sag generator's logging and control software. Both pre and post event data was collected to capture both the steady state and transient responses of each inverter under test (IUT). Additional details on the testing procedures and laboratory set-up can be found in section 3.6 or a prior published paper [49].

Single-Phase Inverter – Sag Events (100% *(short-circuit)*, 90%, 70%, 60%, 0% *(open-circuit)*)

Table 9 outlines the voltage sag event and whether the inverter tripped during the sag. Figure 57 through Figure 61 give plots from each item in the table.

Table 9. Single-Phase Sag Event Summary

Single-Phase Inverter - Event Type	Inverter Tripped
100% Sag - Short Circuit	Yes
90% Voltage	No
70% Voltage	Yes
60% Voltage	Yes
0% Sag - Open Circuit	Yes

Figure 57 gives the results of a 100% voltage sag (short-circuit) for a single phase inverter operating at 25% output power. The arrow on the plot indicates the time at which the voltage sag event occurred. The current initially spikes, but reaches a higher level of 2.1 pu, followed by the inverter rms current increasing eventually to 1.3 pu of the pre-fault current for 1.5 cycles. The inverter output current increases after the fault. However, within one cycle after the event, the current quickly decays to zero due to the inverter tripping due to the fault (i.e. voltage lost). Each single-phase IUT responded in a similar manner with respect to 100% voltage sags.
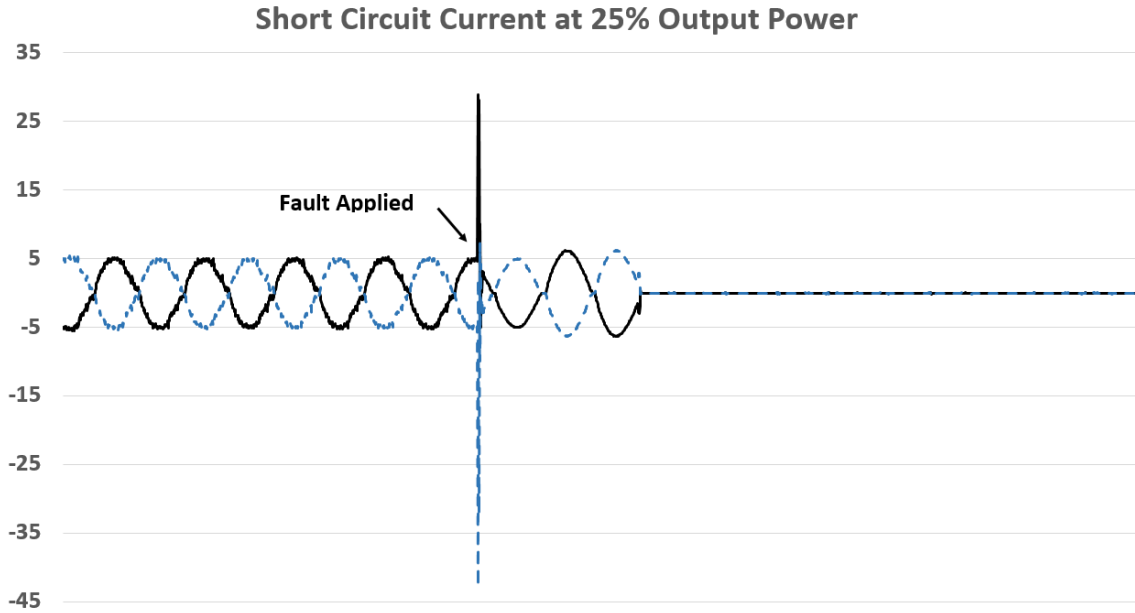
Figure 57. Single-Phase Inverter - 100% Sag (Short-Circuit)

Figure 58 displays both the voltage sag and the corresponding current response for a 90% sustained voltage (10% voltage loss) applied to the output terminals of the single-phase inverters. The vertical dashed lines indicate the start and end of the 12 cycle sag event. Results show that the current output increases during the event to account for the loss in voltage. After the sag event, both the voltage and current of the inverter return to their pre-event steady state values, and the inverter remains connected to the grid.
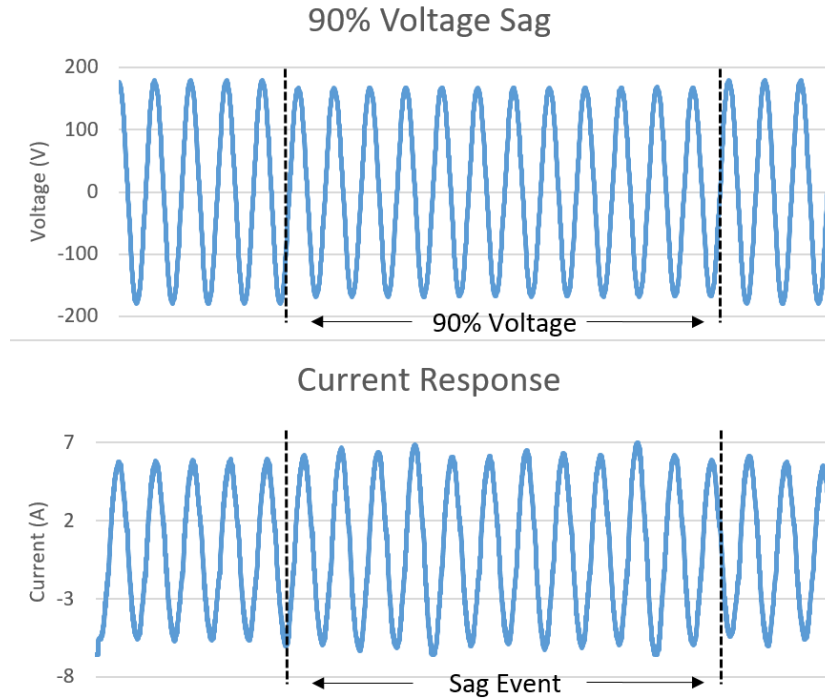
Figure 58. Single-Phase Inverter - 90% Voltage

Figure 59 and Figure 60 displays both the voltage sag and the corresponding current response for a 70% and 60% voltage respectively. Just like for the 90% sag, the vertical dashed lines indicate the start and end of the 12 cycle sag event. However, unlike for the 90% sag, the inverter current increases to account for the voltage reduction, but is unable to recover from the voltage sag and disconnects from the grid. The inverter disconnect can be seen by the current decays after the sag event.
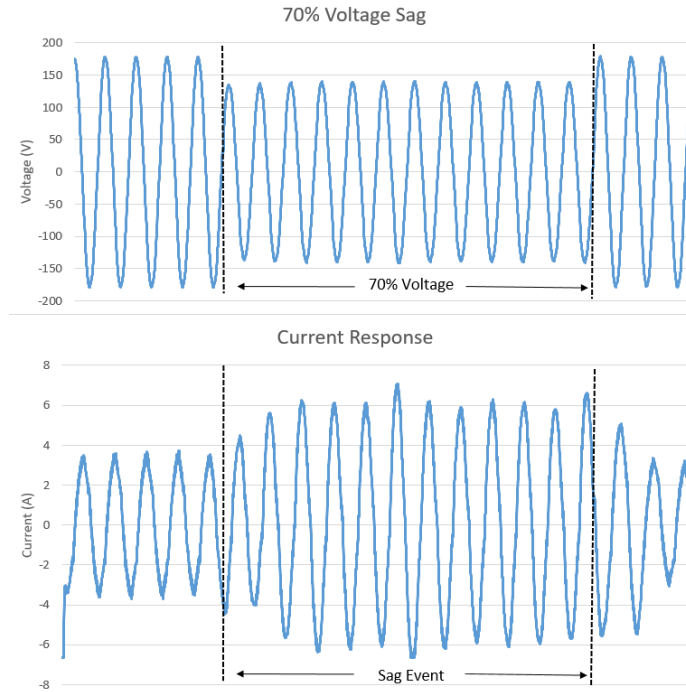
Figure 59. Single-Phase Inverter - 70% Voltage
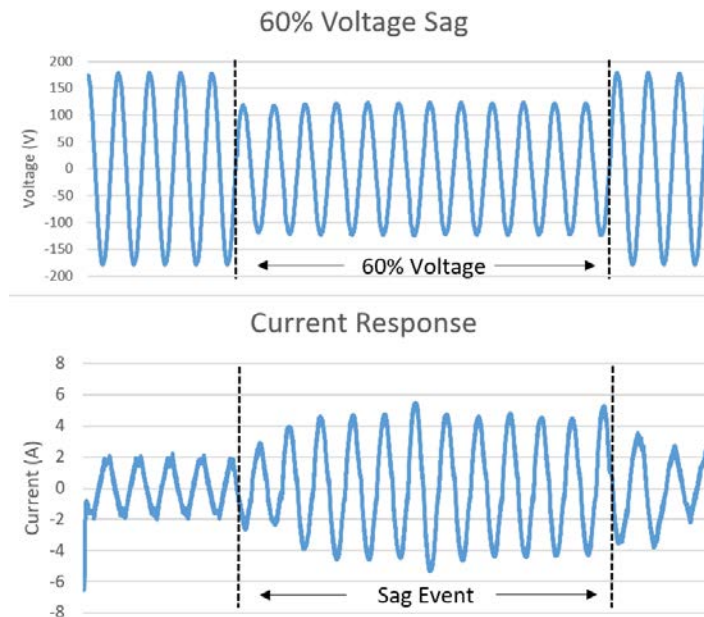
Figure 60. Single-Phase Inverter - 60% Voltage

108

Figure 61 displays the voltage response for a 0% sag event (open-circuit) for the single-phase inverter. When the voltage sag was applied, indicated by the arrow on the plot, the inverter produces a momentary overvoltage then rapidly decays within one cycle. The overvoltage peak and the decay rate are probably inherent to the inverter's internal RLC filter.
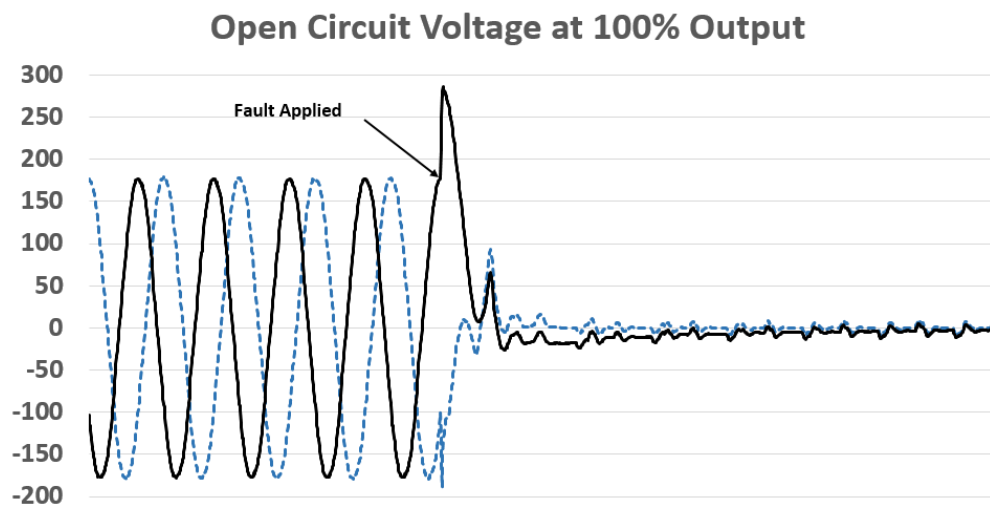

Figure 61. Single-Phase Inverter - 0% Sag (Open-Circuit)

Unlike the 0% voltage sags, each single-phase inverter produced a different initial peak overvoltage and decay rate. These differences are due to each inverter having different RLC responses. For example, some inverters have a DC link capacitor on the output causing a much slower voltage decay rate having a time constant up to 0.3 s. Overvoltage values for the single-phase inverters ranged from 1.46 to 1.78 pu and the first-cycle rms voltage peak ranged from 1.27 to 1.91 pu.

Micro-Inverter Sag Events (100% *(short-circuit)*, 90%, 80%, 60%, 40%, 0% *(open-circuit)*)

Table 10 outlines the voltage sag events for the micro-inverters and whether the inverter tripped during the sag. Figure 62 through Figure 67 give plots from each item in the table.

Table 10. Micro-Inverter Sag Event Summary

Micro-Inverter - Event Type	Inverter Tripped
100% Sag - Short Circuit	Yes
90% Voltage	No
80% Voltage	No
60% Voltage	Yes
40% Voltage	Yes
0% Sag - Open Circuit	Yes

Figure 62 gives the results of a 100% voltage sag (short-circuit) for a micro-inverter operating at 90% output power. The arrow on the plot indicates the time at which the voltage sag event occurred. The current initially spikes but instantly goes to zero. The peak transient currents ranged from 3.00 to 3.95 pu. Each micro-inverter responded in a similar manner with respect to 100% voltage sags.
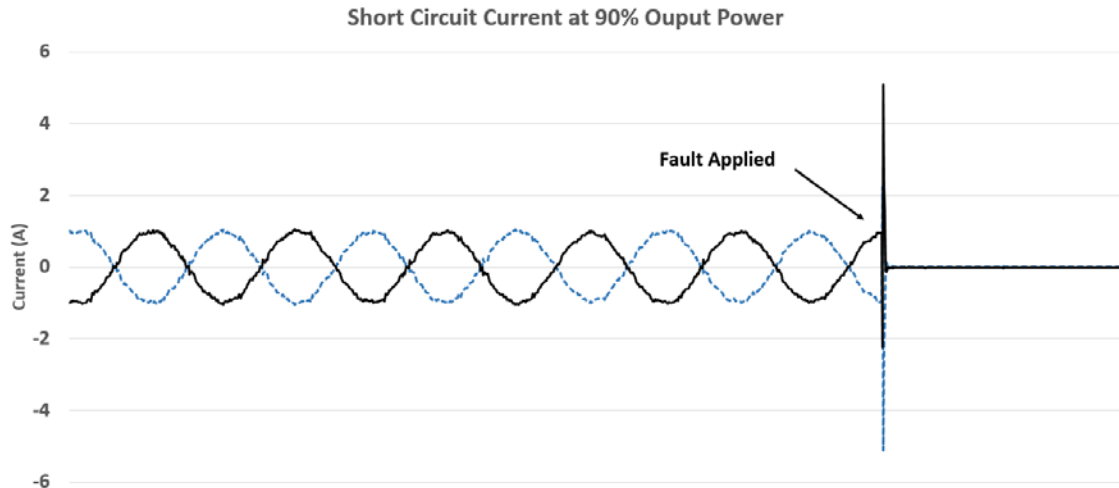
Figure 62. Micro-Inverter - 100% Sag (Short-Circuit)

Figure 63 and Figure 64 displays both the voltage sag and the corresponding current response for a 90% and 80% voltage sag respectively. Identical to the single-phase inverters response, the inverter is able to remain connected to the grid for both the 90% and 80% sags.
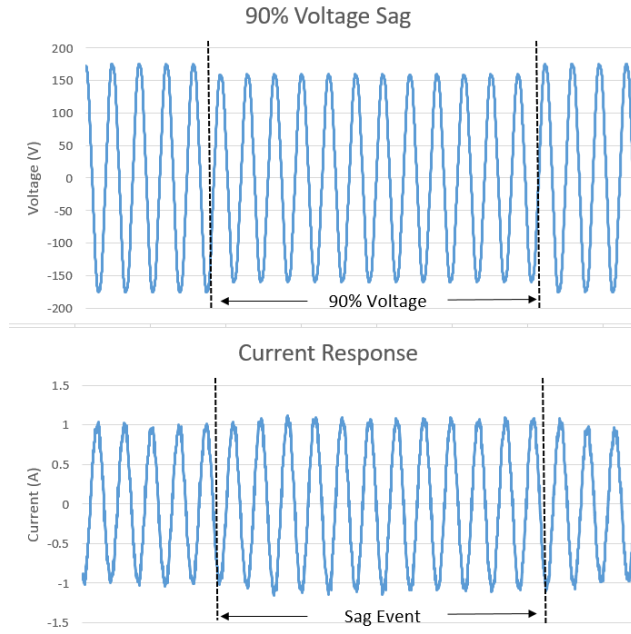
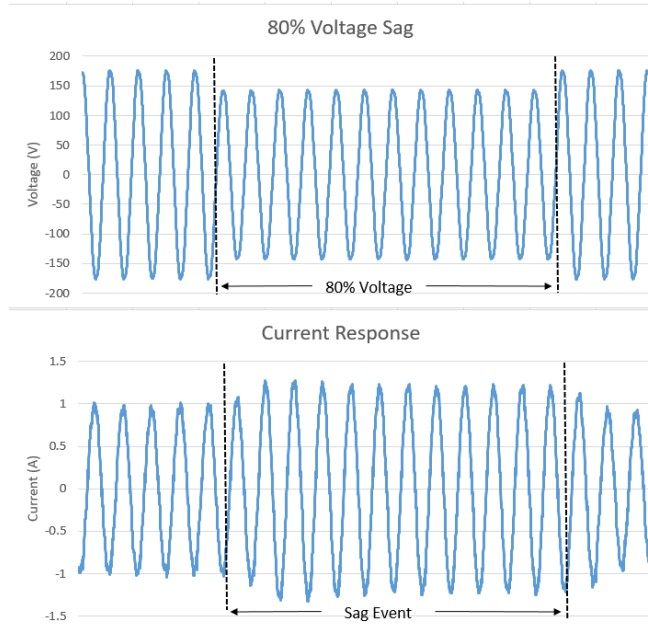**Figure 63.** Micro-Inverter - 90% Voltage

Figure 64. Micro-Inverter - 80% Voltage

Figure 65 and Figure 66 show the results from 60% and 40% sags. Unlike the single-phase inverter response, the micro-inverter is unable to retain current output once the voltage sag occurs. However, within 2-3 cycles after the event, the inverter attempts to counteract the decrease in voltage by producing a current greater than the original steady state current. Depending on the percent voltage sag, the inverter is only able to maintain current between 1 and 7 cycles. As expected, the inverter is unable to recover from the voltage sag and disconnects from the grid.
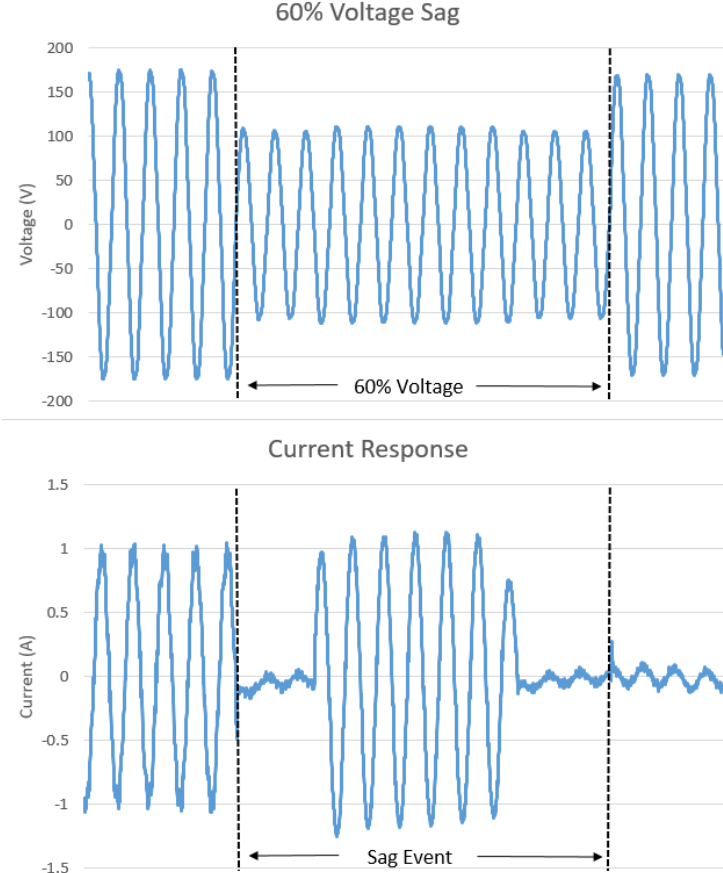
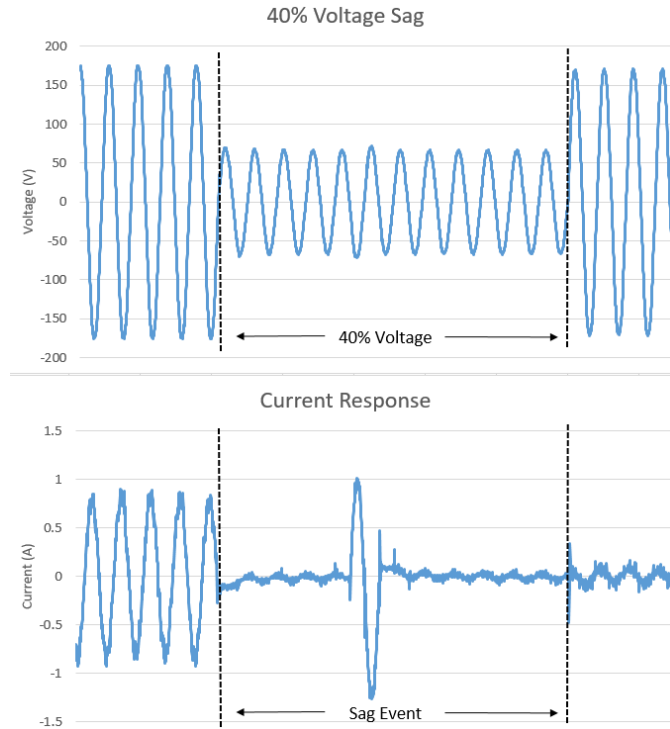**Figure 65.** Micro-Inverter - 60% Voltage

Figure 66. Micro-Inverter - 40% Voltage

Figure 67 displays the voltage response for a 0% sag event (open-circuit) for the micro-inverter. When the voltage sag was applied, indicated by the arrow on the plot, the inverter produces a momentary overvoltage slowly decays to zero. The overvoltage peak and the decay rate are probably inherent to the inverter's internal RLC filter.
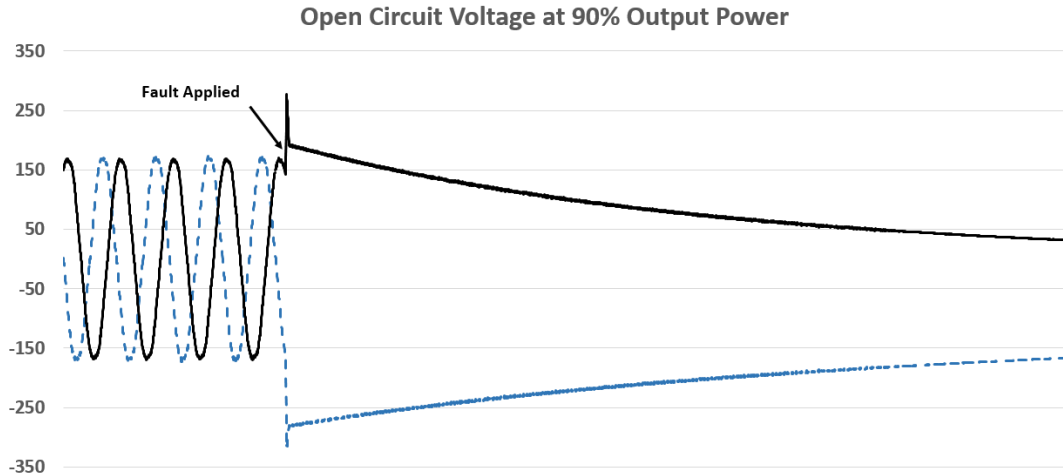
Figure 67. Micro-Inverter - 0% Sag (Open-Circuit)

Unlike the single-phase inverters where the open-circuit results were extremely different, the micro-inverter's all produced similar responses for both short-circuit and open-circuit results. The peak voltage for the micro-inverters ranged from 1.86 to 2.07 pu depending on the inverters output power and the point-on-wave of the event.

Three-Phase Inverter Sags (100% (short-circuit) and 0% (open-circuit)) and Single-line-to-ground faults (SLGF) with and without load (0% on A, 25% on A, 50% on A)

   Table 11 outlines the voltage sag events for the three-phase inverters. Both 0% and 100% sags were performed on all three phases of the inverter output, and single-line-to-ground-Faults (SLGF) are placed on phase A of the inverter. The SLGFs are applied with and without a resistive load at 0%, 25%, and 50% voltage sag levels. Figure 68 through Figure 72 give sample plots from some of the items in the table.

Table 11. Three-Phase Sag Event Summary

Event Type	Inverter Tripped	with/without Load
0% Sag - Open Circuit - All Phases	Yes	n/a
100% Sag - Short Circuit - All Phases	Yes	n/a
0% Sag - 12 cycle duration - Phase A	Yes	Resistive
25% Sag - 12 cycle duration - Phase A	No	Resistive
50% Sag - 12 cycle duration - Phase A	No	Resistive
0% Sag - 12 cycle duration - Phase A	Yes	No Load
25% Sag - 12 cycle duration - Phase A	No	No Load
50% Sag - 12 cycle duration - Phase A	No	No Load

Figure 68 and Figure 69 give the three-phase voltages and currents for the 0% and 100% voltage sags respectively. The open-circuit voltage behaves similar to the open-circuit response of the single-phase inverter shown in Figure 61. For the three-phase inverter tested, the overvoltage reached 2.08 pu for the 0% sag events and the overcurrents reached 1.47 pu for the 100% sag events. The inverter continued to produce current after the 100% sag for six to nine cycles, depending on the point-on-wave and the power output of the inverter when the fault was applied. In addition, the rms current reaches 1.02 pu of rating (1.36 pu of the pre-fault current) for the last several cycles. The inverter disconnects from the grid for both events. Additional results as well as the correlation between the pre-fault output level and the pu peak values can be found in [49].
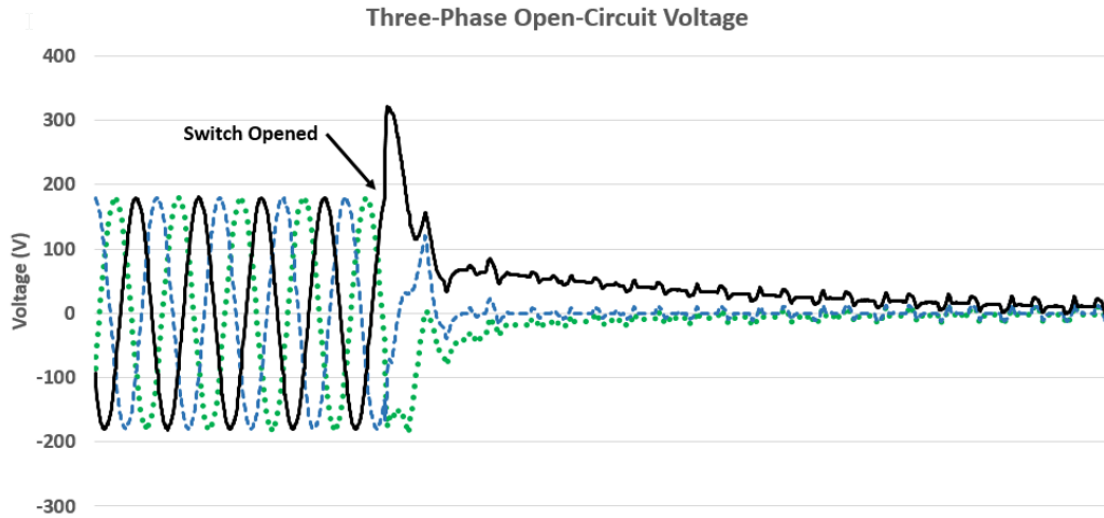
Three-Phase Open-Circuit Voltage

Switch Opened

Figure 68. Three-Phase Inverter - 0% Sag (open-circuit)
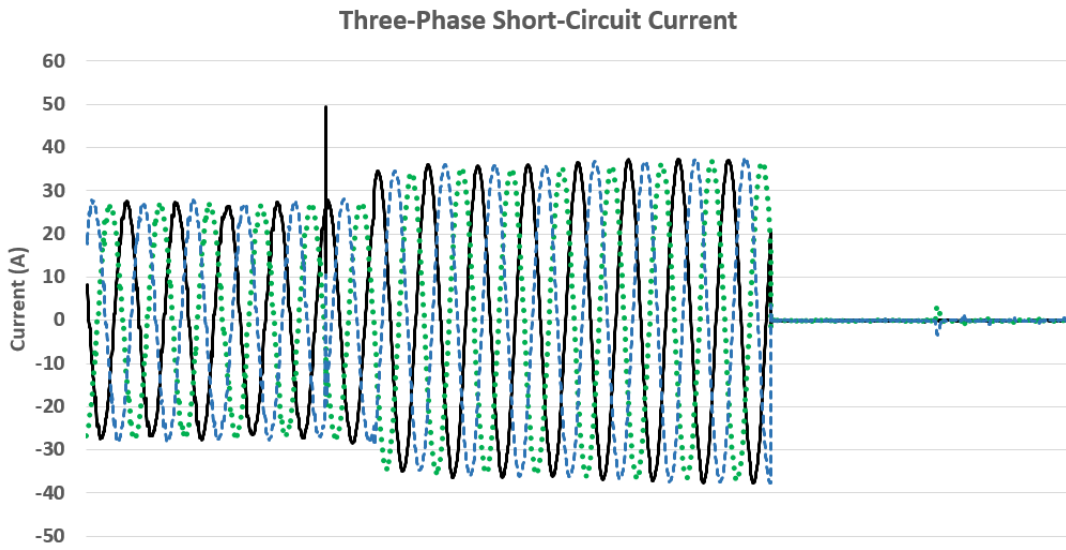
Three-Phase Short-Circuit Current

Figure 69. Three-Phase Inverter - 100% Sag (Short-Circuit)

117

A 25% voltage was placed on phase A while the inverter was operating at 100% output power. Figure 70 shows the voltages and currents for each phase during the event without residual resistive load. Figure 71 show the inverter and load currents for each phase during the event with resistive load. Note that the same voltages shown in Figure 70 were used for the results obtain in Figure 71. In both cases, all three phases of the inverter current increased to account for the reduction of voltage on phase A. However, for the case with the resistive load, the load current on phase A increases beyond phase B and C due to the voltage sag being applied to phase A. After the event, 12 cycles, all currents returned to the pre-fault current. The small current transients during the transition to the voltage sag and the return to 100% voltage do not cause the inverter to trip. The inverter remained connected to the grid for both the case with and without added resistive load. Similar results were obtained when the voltage on phase A was set to a 50% voltage sag.
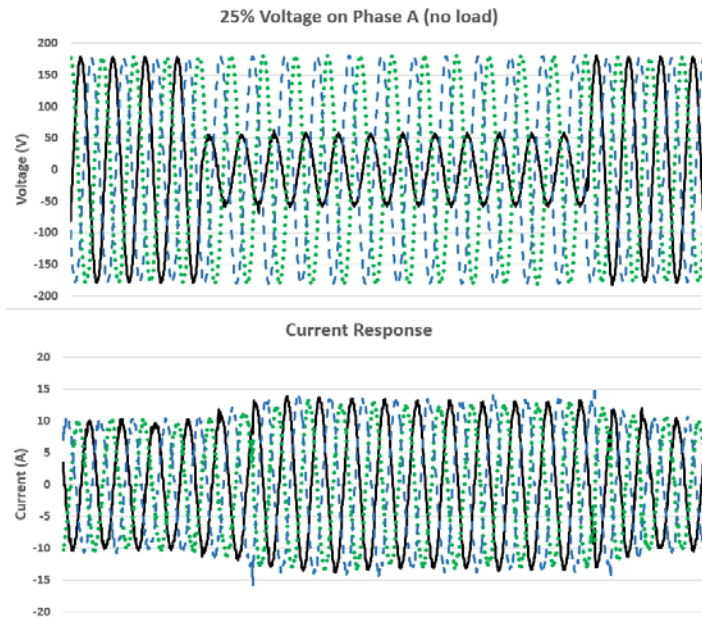

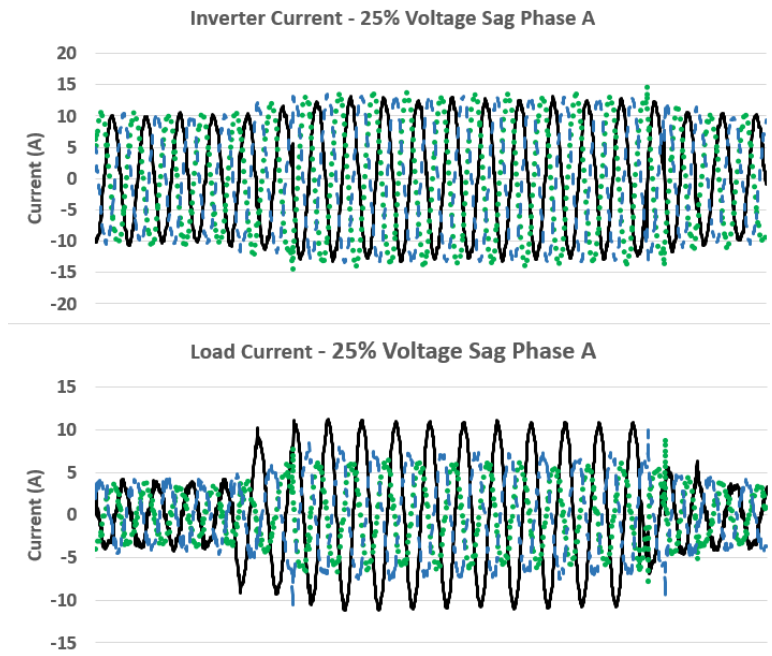**Figure 70.** Three-Phase Inverter - 25% Voltage on Phase A (no load)

Figure 71. Three-Phase Inverter - 25% Voltage on Phase A (R load)

A 12 cycle, 100% voltage sag (short-circuit), was placed on phase A both with and without resistive load. Figure 72 shows the voltage (top) and inverter currents (center) from each case and the load current for the resistive load (bottom). For the case with no load (top and middle plot), note that once the sag is applied, the currents increase and are sustained for 9 cycles before the inverter disconnects from the grid. However, for the case with resistive load (all three plots), phase A load current increases beyond the other phases as expected and is sustained for 9 cycles just like the inverter current. From looking at the load current, phase A only remains during the 9 cycles the inverter is connected. The remainder of the 12 cycles, 3 cycles, phase A current goes to zero. Once the voltage returns to pre-fault, current returns to the load while the inverter remains disconnected. The inverter disconnects during a SLGF independent of residual resistive load.
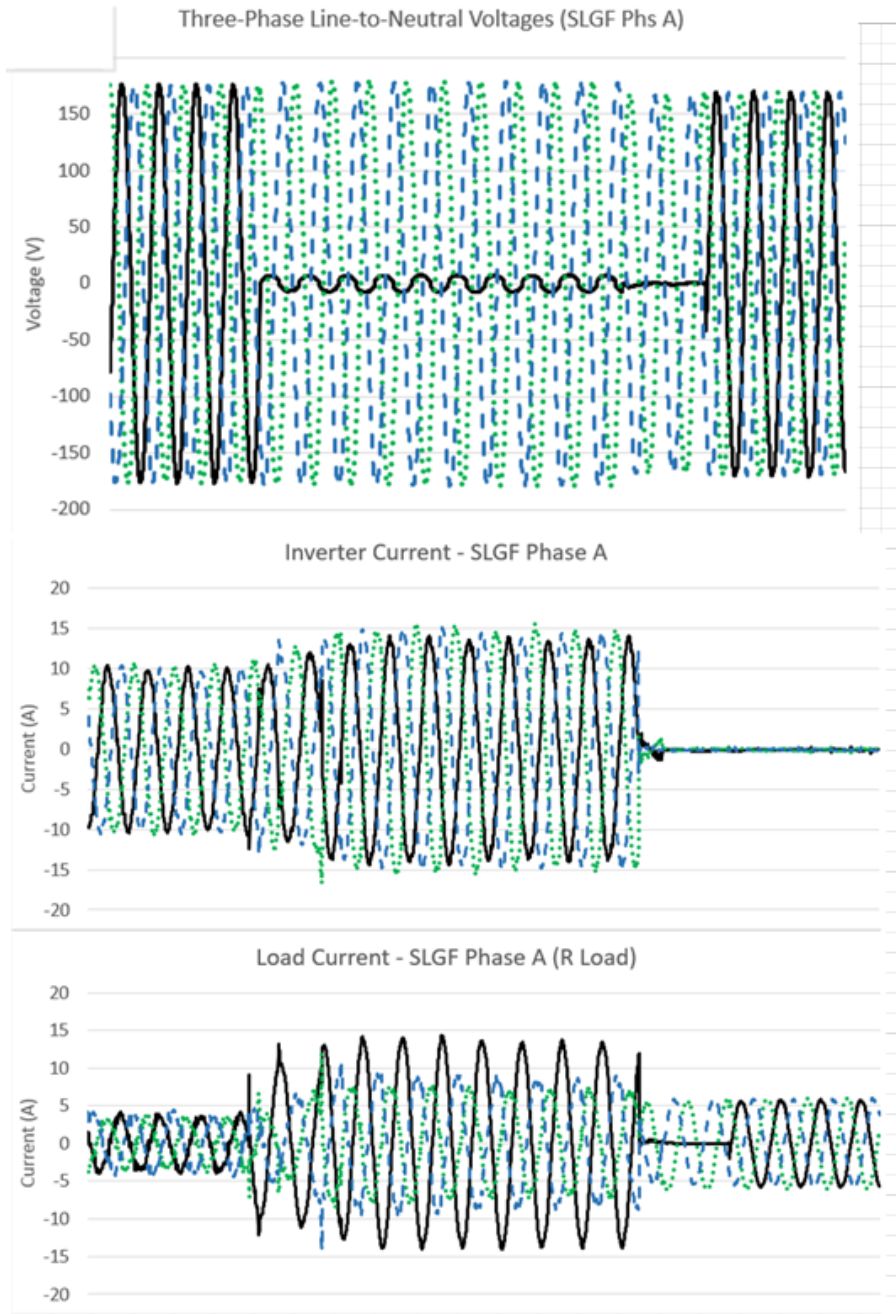
Figure 72. Three-Phase Inverter - SLGF on Phase A

In summary, the PV inverters were able to withstand a 20% voltage loss for 12 cycles without disconnecting from the grid. However, a voltage loss of 30% or greater led to the inverter disconnecting. Future work will include incorporating the sag responses into OpenDSS. Preliminary modeling has been done on the sag data and is shown in Appendix B.

APPENDIX B

HW MODELS FOR VOLTAGE SAG EVENTS

This section gives the preliminary modeling results obtained from using the collected sag data.

90% Sustained Voltage: Figure 73 gives the input voltage and output current for a sag event on a micro-inverter with 90% sustained voltage. A preliminary HW model was constructed, Figure 74 shows the input and output nonlinearities found to represent the model. Note that the nonlinearities follow a piecewise linear response as previously outlined in section 4.0 Figure 75 shows the HW model results where the light gray line represents the collected data, and the blue line represents the models response. (Note: if printed black/white, the collected data will be shown lighter than the models response.) The single-phase inverters had a similar response to a 90% sustained voltage.
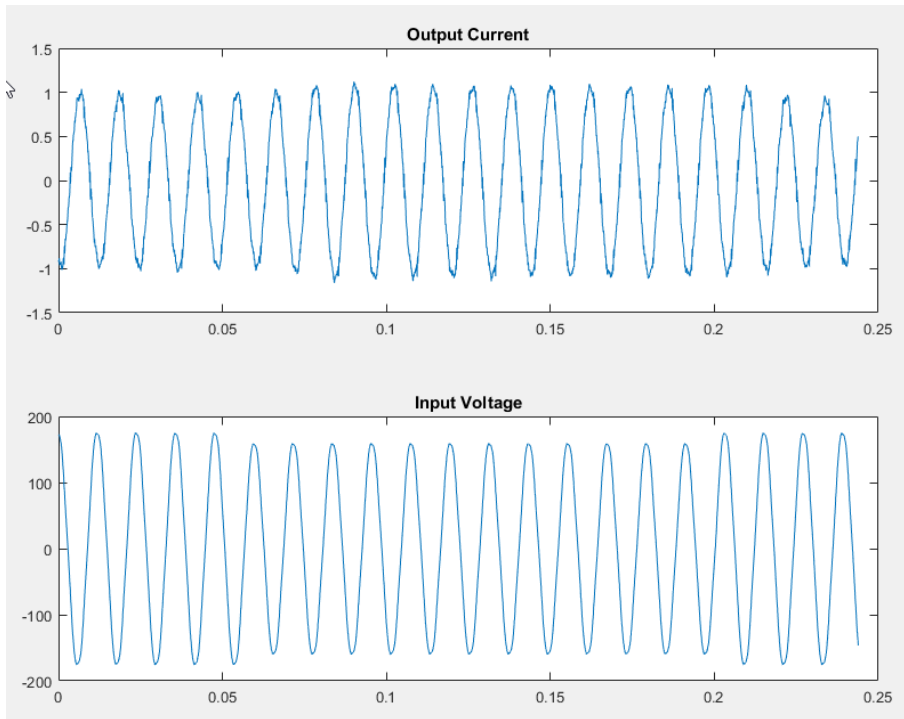
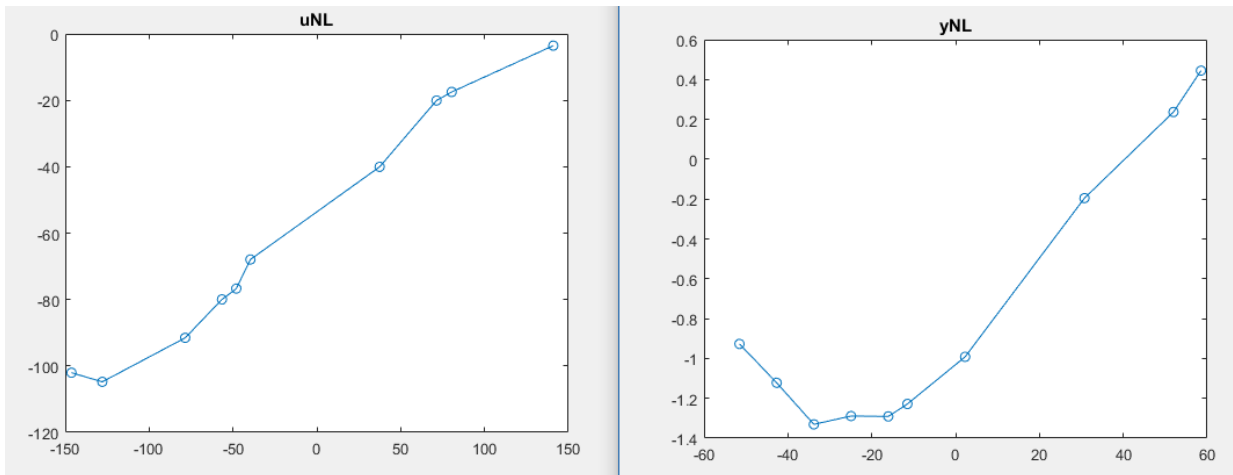**Figure 73.** Input Voltage and Output Current Response – 90% Voltage

Figure 74. Input and Output Nonlinearity - 90% Voltage
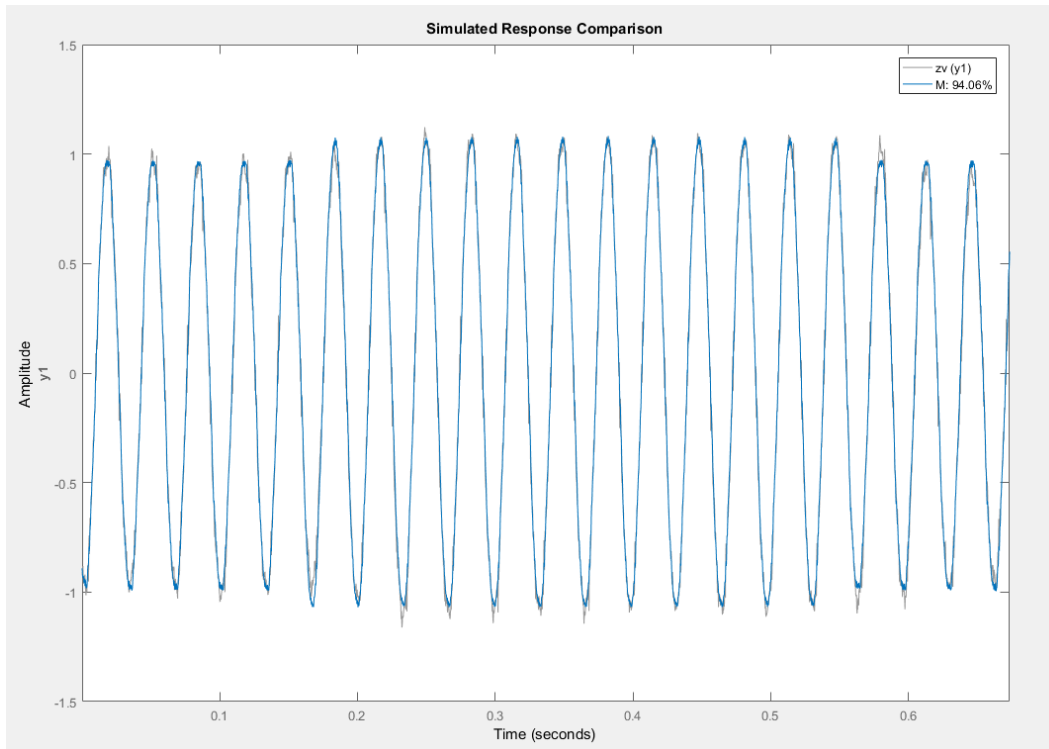
124

Figure 75. HW Model Results for 90% Voltage

80% Sustained Voltage: Figure 76 gives the input voltage and output current for a sag event on a micro-inverter with 80% sustained voltage. A preliminary HW model was constructed, Figure 77 shows the input and output nonlinearities found to represent the model. Note that the nonlinearities follow a piecewise linear response as previously outlined in section 4.0 Figure 78 shows the HW model results where the light gray line represents the collected data, and the blue line represents the models response. The single-phase inverters had a similar response to a 80% sustained voltage.
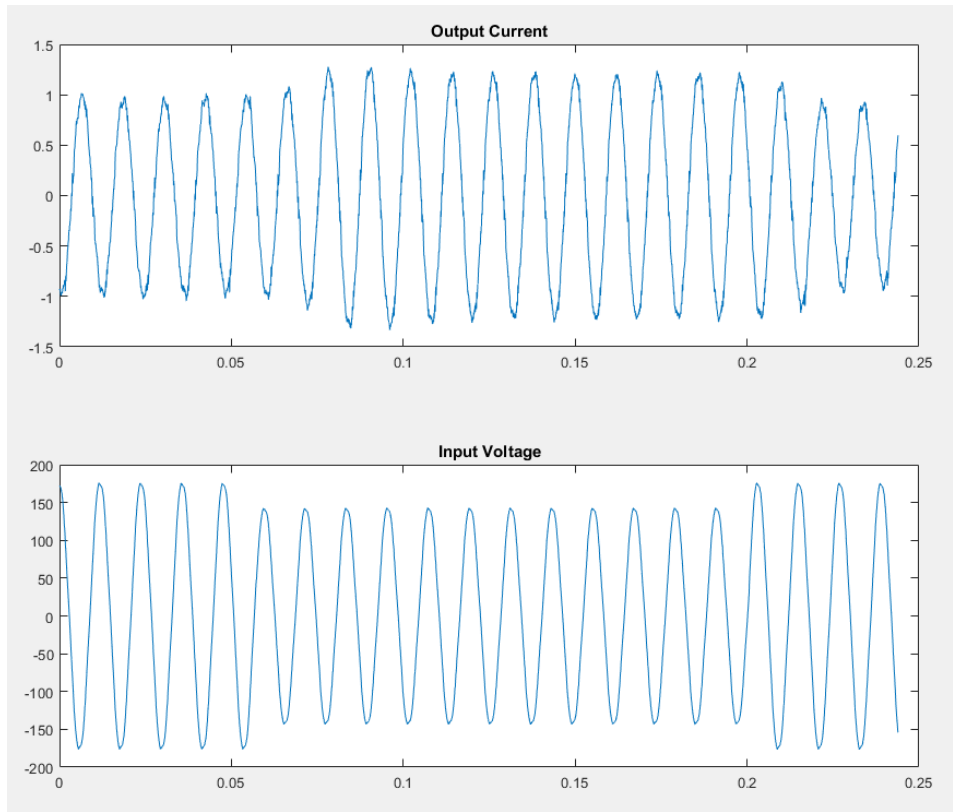
125

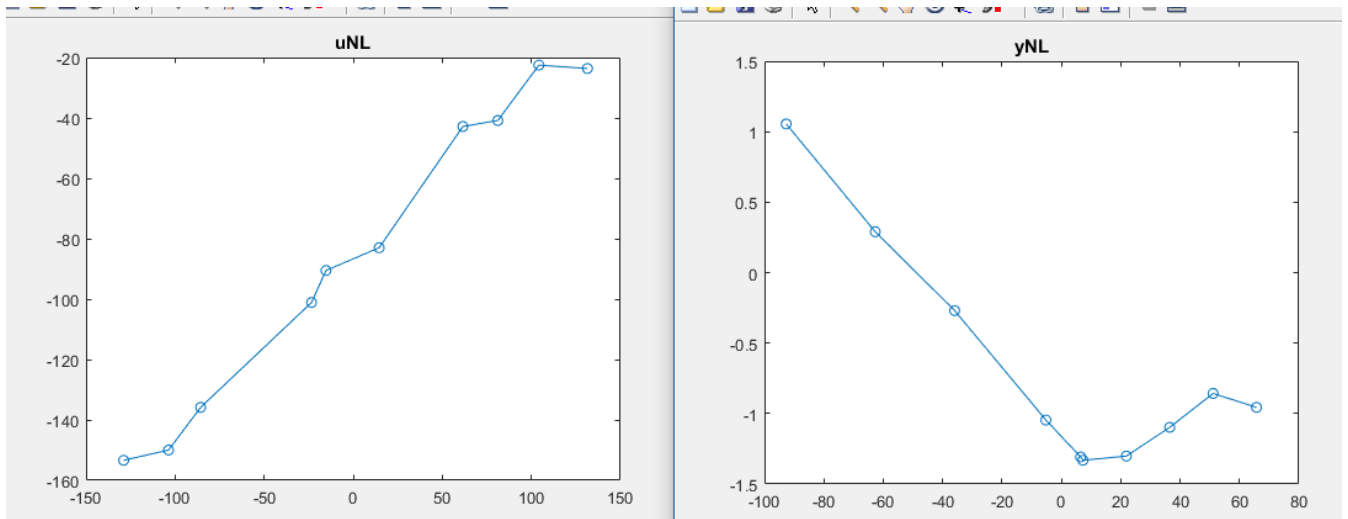**Figure 76.** Input Voltage and Output Current Response – 80% Voltage

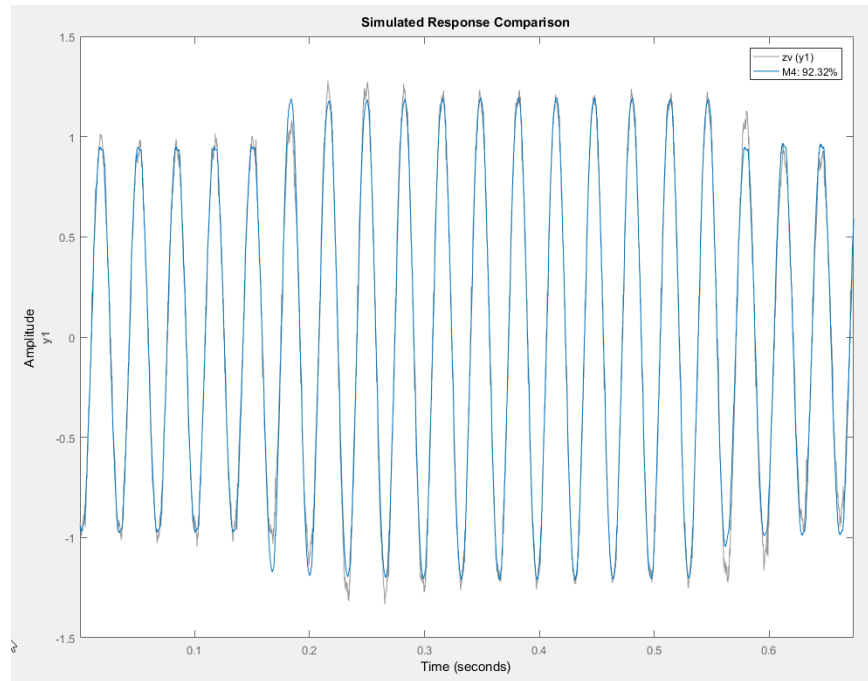**Figure 77.** Input and Output Nonlinearity - 80% Voltage

126

Figure 78. HW Model Results for 80% Voltage

60% Sustained Voltage: Figure 79 gives the input voltage and output current for a sag event on a micro-inverter with 60% sustained voltage. A preliminary HW model was constructed, Figure 80Figure 77 shows the input and output nonlinearities found to represent the model. Note that the nonlinearities follow a piecewise linear response as previously outlined in section 4.0 Figure 81 shows the HW model results where the light gray line represents the collected data, and the blue line represents the models response. The single-phase inverters did not have a similar response to a 60% sustained voltage. The single-phase inverter did disconnect like the micro-inverter, however, the single-phase inverters had an increase in current once the sag was applied, but then went directly to zero instead of flucuating between zero and sustained current.
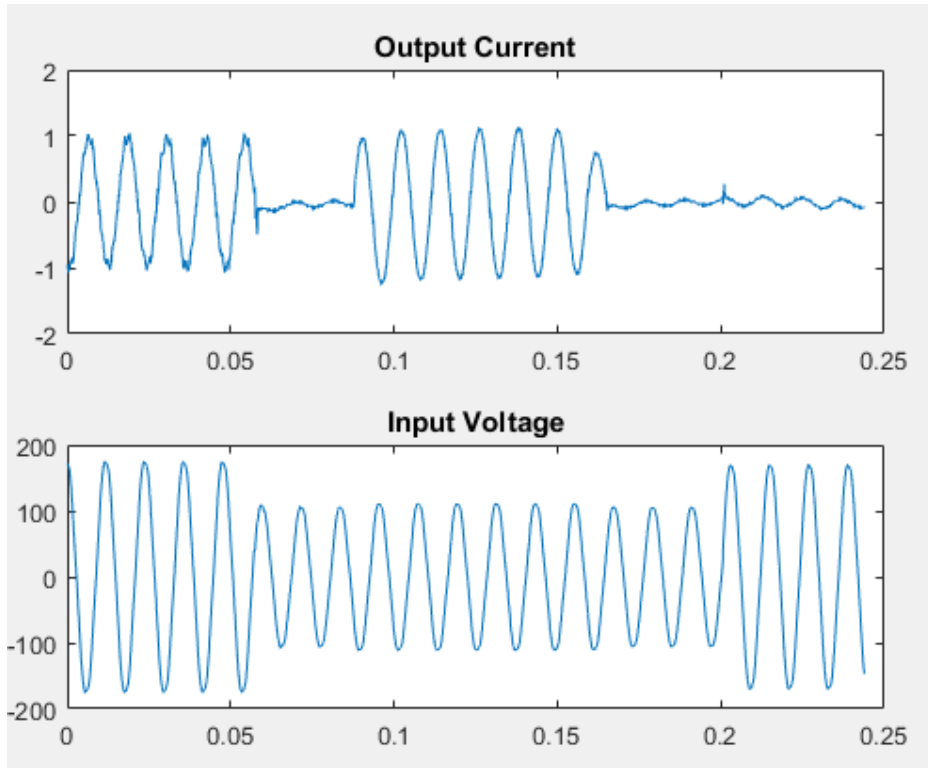
127

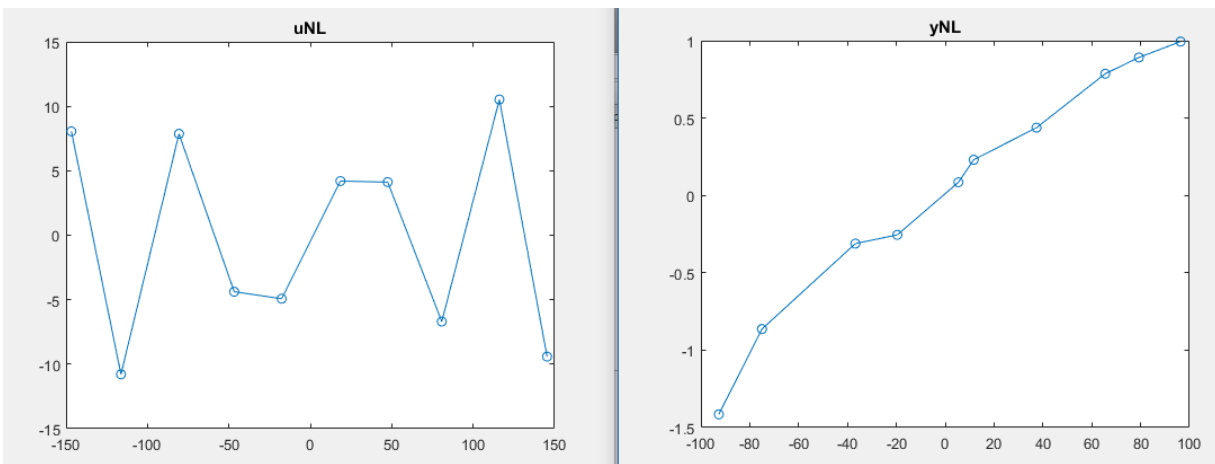**Figure 79.** Input Voltage and Output Current Response – 60% Voltage

Figure 80. Input and Output Nonlinearity - 60% Voltage

128
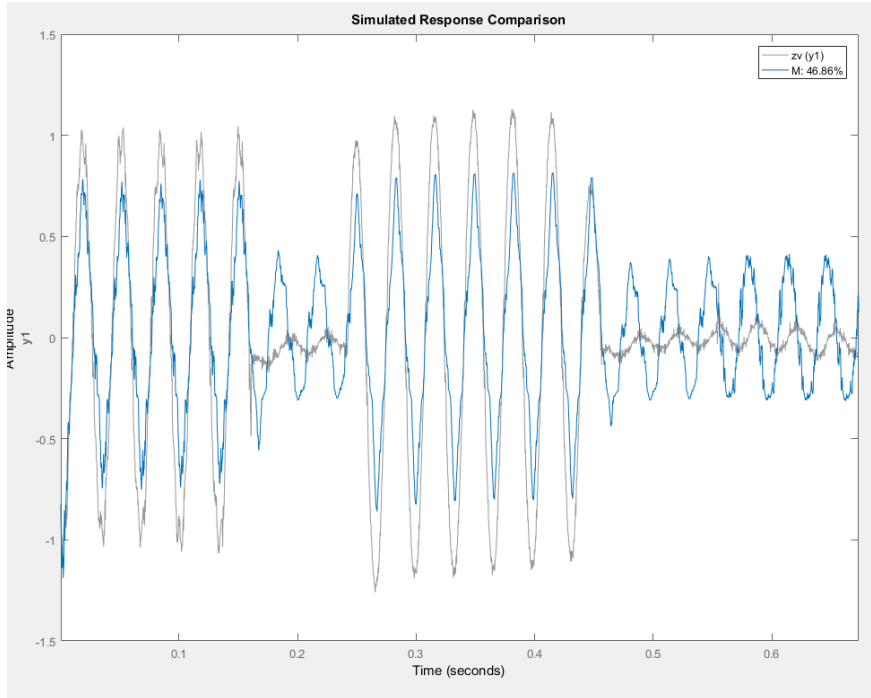
Figure 81. HW Model Results for 60% Voltage

0% Voltage Sag (open-circuit): Figure 82 and Figure 83 give the input and output nonlinearity and HW model response respectivitly for an open-circuit event on a single-phase inverter. For Figure 83, the light gray represents the captured inverter's voltage response and the blue line represents the models response.
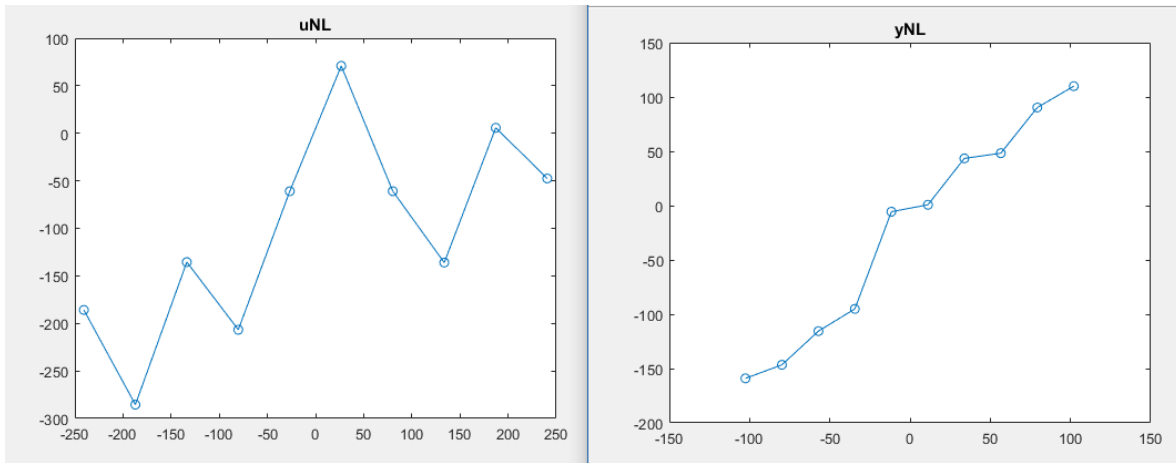
Figure 82. Input and Output Nonlinearity – Open-Circuit

Figure 83. HW Model Results for Open-Circuit Voltage

130

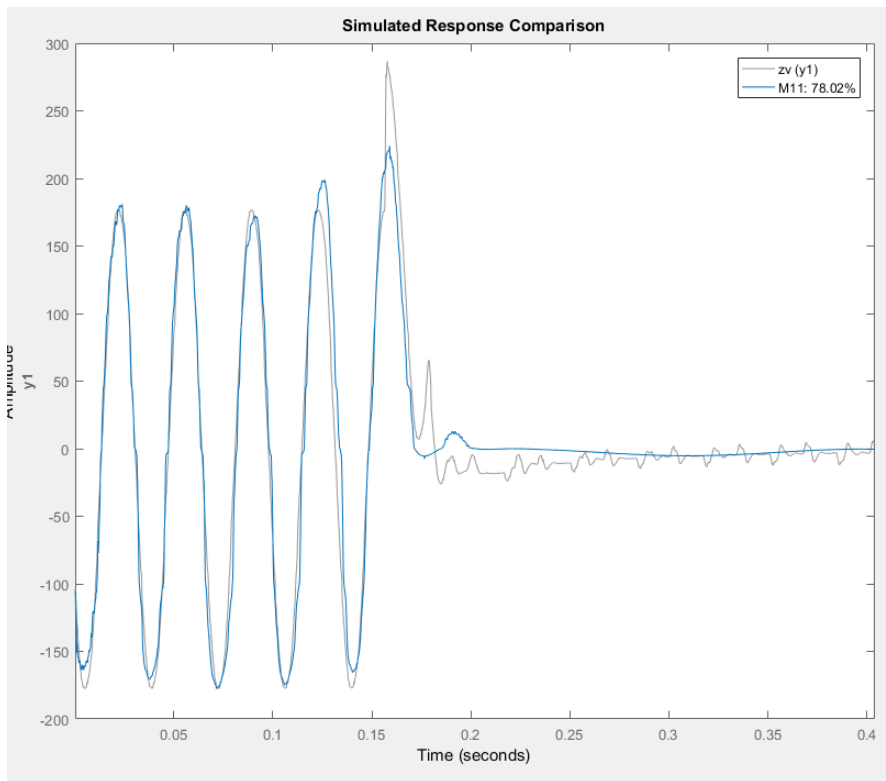As discussed in section 3.8.2, each inverter behaves differently during open-circuit testing. Future work consists of incorporating multiple open-circuit models to account for the different responses captured in the laboratory. Lastly, each HW model from the sag events could be optimized in the future to obtain a better fit to the collected data.

APPENDIX C

EXAMPLE OF THE VCCS IN AN IEEE TEST FEEDER

This example illustrates use of the VCCS model in an IEEE test feeder for DG protection analysis. See Figure 84, with feeder data defined in [50]. The DG was originally assumed to contribute fault current as a rotating machine, but here the source is a PV inverter, represented with a VCCS. Note that the VCCS does not emulate solar panel efficiency, power fluctuations, or smart inverter control; for those features, other components of OpenDSS can be used (e.g. PVSystem, InvControl, ExpControl). In Figure 84, a single-line-to-ground fault (SLGF) was applied at the feeder mid-point location, bus Bm or fault location 3.
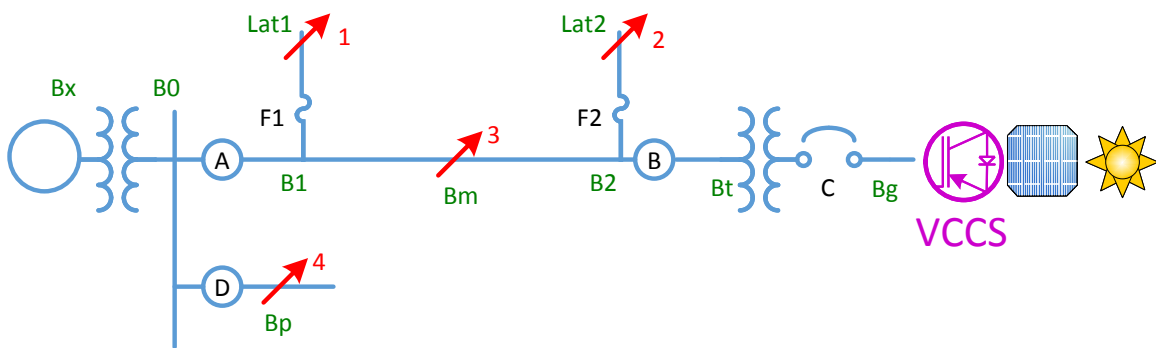

Figure 84. IEEE Test Feeder for DG Protection Analysis [50]

Figure 85 shows the current and voltage through recloser B, on the high side of the interconnection transformer, with a 1700-kW PV inverter source backfeeding the fault at Bm. The fault occurs at 0.2 seconds, just after steady-state DG output currents have stabilized. The faulted phase voltage (Figure 85 right) collapses almost immediately. In the plot, the currents are show on the left and the voltages on the right at recloser B with 1.7 MW PV and single-phase inverter model.
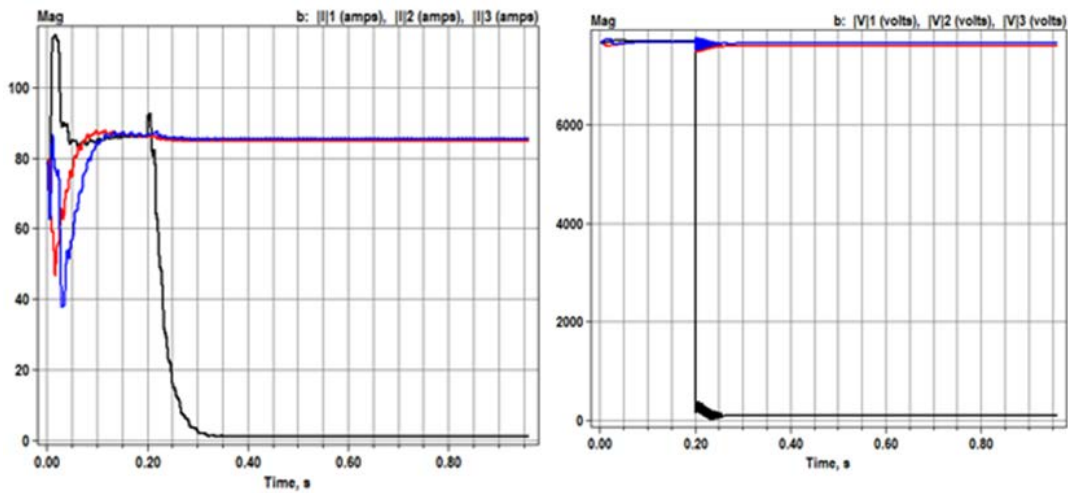
Figure 85. Currents (left) and Voltages (right) at Recloser B - 1.7 MW Inverter

Figure 86 shows the same fault response for a Thevenin equivalent source in place of the PV. The Thevenin impedance is sized to produce 6 pu short-circuit current at the source terminals based on 1700 kVA. As a result, the fault contribution is higher and the feeder primary voltage on the faulted phase, at recloser B, is maintained at a low level indefinitely. In the plot, the currents are show on the left and the voltages on the right at recloser B with 1.7 MW rotating machine (Thevenin equivalent).

133
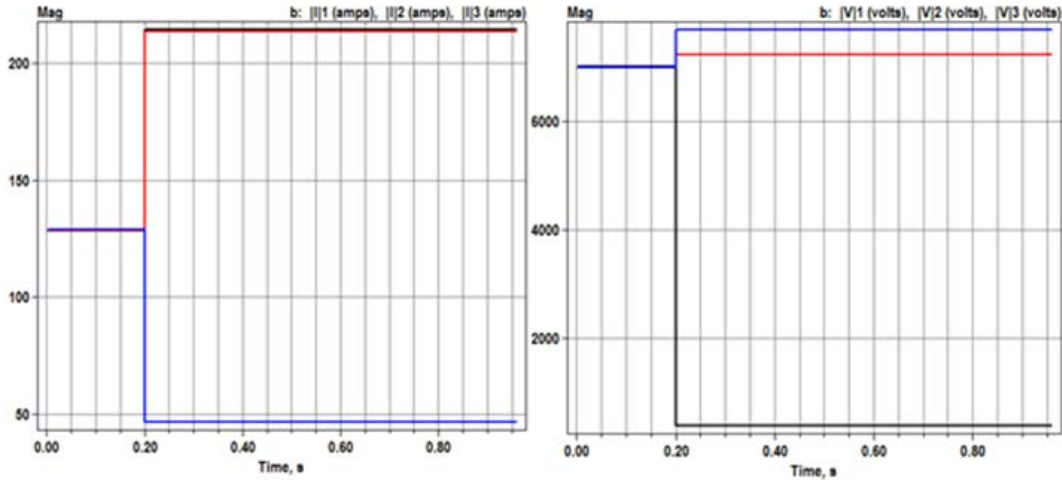
Figure 86. Currents (left) and Voltages (right) at Recloser B - 1.7 MW Rotating Machine

In conclusion, more details on the HW model response and initialization in OpenDSS can be seen in the OpenDSS Tech Note [48]. In addition, more details on the IEEE feeder example and per-unit scaling of the model can be viewed in the OpenDSS Tech Note as well. Future work will continue to improve stability and quality of the HW model fitting process.

BIBLIOGRAPHY

[1] Nachiket, "Solar Photovoltaic (PV) Market, Update 2015," Press Release, 21 October 2015. [Online]. [Accessed November 2015].

[2] M. Osborne, "Global solar demand in 2015 to hit 57GW on strong 30% growth rate," IHS, 31 March 2015. [Online]. Available: http://www.pv-tech.org/news/global_solar_demand_in_2015_to_hit_57gw_on_strong_30_growth_rate_ihs . [Accessed November 2015].

[3] R. J. Bravo, R. Yinger, S. Robles and W. Tamae, "Solar PV inverter testing for model validation," *2011 IEEE Power and Energy Society General Meeting*, San Diego, CA, 2011, pp. 1-7.

[4] A. Wills, T. B. Schon, L. Ljung and B. Ninness, "Identification of Hammerstein-Wiener Models," *IEEE,* 2012.

[5] MathWorks, "Hammerstein-Wiener Model Structure," Documentation, [Online]. Available: http://www.mathworks.com/help/ident/ref/idnlhw.html?refresh=true#burdu8p-16 . [Accessed 2015].

[6] A. Sarwar and M. J. Asghar, "Multilevel Converter Topology for Solar PV Based Grid-Tie Inverters," *IEEE International Energy Conference,* pp. 501-506, 2010.

[7] S. Jain and V. Agarwal, "A Single-Stage Gtrid Connected Inverter Topology for Solar PV Systems with Maximum Power Point Tracking," *IEEE Transactions on Power Electronics,* vol. 22, no. 5, pp. 1928-1940, 2007.

[8]   "The History of Solar," U.S. Department of Energy: Energy Efficiency and Renewable Energy.

[9]   W. Reece, "The History of Solar Power," [Online]. Available: https://www.experience.com/alumnus/article?channel_id=energy_utilities&source_page=additional_articles&article_id=article_1130427780670 . [Accessed 2015].

[10]   J. Perlin, "The Silicon Solar Cell Turns 50," August 2004. [Online]. Available: http://www.nrel.gov/education/pdfs/educational_resources/high_school/solar_cell_history.pdf . [Accessed 2015].

[11]   "Early History of Solar," Four Peaks Technologies, [Online]. Available: http://solarcellcentral.com/history_page.html . [Accessed 2015].

[12]   "How Much Does it Cost to Install Solar on an Average US House?," Solar Power Authority, 20 April 2012. [Online]. Available: http://solarpowerauthority.com/how-much-does-it-cost-to-install-solar-on-an-average-us-house/ . [Accessed 2015].

[13]   J. Roach, "Home Solar Panels Make Gains in America, Even in Rainy Seattle," NBC News, 4 August 2014. [Online]. [Accessed 2015].

[14]   J. Wiles, "Photovoltaic Power Systems and the NEC Suggested Practices," National Electrical Code, Quincy, 2001.

[15]   IEEE, "IEEE Standard for Interconnecting Distributed Resources with Electric Power Systems," IEEE Standards Coordinating Committee 21, 2008.

[16]   O. Hashimoto, T. Shimizu and G. Kimura, "A Novel High Performance Utility Interactive Photovoltaic Inverter System," pp. 2255-2260, 2000.

[17]   H. Watanabe, T. Shimizu and G. Kimura, "A Novel Utility Interactive Photovoltaic Inverter with Generation Control Circuit," pp. 721-725, 1998.

[18]   L. Cheng, R. Cheung and K. Leung, "Advanced Photovoltaic Inverter with Additional Active Power Line Conditioning Capability," pp. 279-283, 1997.

[19]   P. C. Loh, D. Vilathgamuwa, C. Gajanayake, Y. R. Lim and C. W. Teo, "Transient Modeling and Analysis of Pulse-Width Modulated Z-Source Inverter," *IEEE Transaction on Power Electronics,* vol. 22, no. 2, pp. 498-507, 2007.

[20] V. Valdivia, A. Roldan, A. Barrado, P. Zumel, C. Fernández and M. Sanz, "Black-Box Modeling of Three-Phase Voltage Source Inverters for System-Level Analysis," *Applied Power Electronics Conference and Exposition (APEC),* vol. 59, no. 9, pp. 3648-3662, 2011.

[21] O. Wasynczuk, "Modeling and Dynamic Performance of a Line-Commutated Photovoltaic Inverter System," *IEEE Transactions on Energy Conversion,* vol. 4, no. 3, pp. 337-343, 1989.

[22] F. Katiraei and J. Agüero, "Solar PV Integration Challenges," *IEEE Power and Energy Magazine,* vol. 9, no. 3, pp. 62-71, 2011.

[23] L. Wieserman and T. McDermott, "Fault current and overvoltage calculations for inverter-based generation using symmetrical components," *Energy Conversion Congress and Exposition (ECCE), 2014 IEEE,* pp. 2619-2624, 2014.

[24] M. E. Ropp and S. Gonzalez, "Development of a MATLAB/Simulink Model of a Single-Phase Grid-Connected Photovoltaic System," *IEEE Transaction on Energy Conversion ,* pp. 1-8, 2009.

[25] R. Arritt, "Protecting the Modern Distribution Grid - Preliminary Inverter Characterization for Overvoltages," *EPRI Technical Update,* pp. 1-27, 2014.

[26] Swanson School of Engineering, "Pitt and Eaton celebrate opening of new Electric Power Engineering Lab," 9 January 2014. [Online]. Available: http://www.engineering.pitt.edu/SSOE-Resources/News/2014/Pitt-and-Eaton-celebrate-opening-of-new-Electric-Power-Engineering-Lab/ . [Accessed 2015].

[27] P. Barker, "Overvoltage considerations in applying distributed resources on power systems," in Power Engineering Society Summer Meeting, 2002 IEEE, 2002, pp. 109-114 vol.1.

[28] R. A. Walling, R. Saint, R. C. Dugan, J. Burke, and L. A. Kojovic, "Summary of Distributed Resources Impact on Power Delivery Systems," IEEE Transactions on Power Delivery, vol. 23, pp. 1636-1644, 2008.

[29] R. F. Arritt and R. C. Dugan, "Distributed generation interconnection transformer and grounding selection," in Power and Energy Society General Meeting - Conversion and Delivery of Electrical Energy in the 21st Century, 2008 IEEE, 2008, pp. 1-7.

[30] R. J. Bravo, R. Salas, R. Yinger, and S. Robles, "Solar photovoltaic inverters transient over-voltages," in 2013 IEEE Power & Energy Society General Meeting, 2013, pp. 1-5.

[31] R. J. Bravo, R. Yinger, and S. Robles, "Three phase solar photovoltaic inverter testing," in 2013 IEEE Power & Energy Society General Meeting, 2013, pp. 1-5.

[32] R. F. Arritt and R. C. Dugan, "Review of the Impacts of Distributed Generation on Distribution Protection," in Rural Electric Power Conference (REPC), 2015 IEEE, 2015, pp. 69-74.

[33] M. E. Ropp and S. Gonzalez, "Development of a MATLAB/Simulink Model of a Single-Phase Grid-Connected Photovoltaic System," IEEE Transactions on Energy Conversion, vol. 24, pp. 195-202, 2009.

[34] A. Nelson, A. Hoke, S. Chakraborty, M. Ropp, J. Chebahtah, T. Wang, et al., "Experimental evaluation of load rejection over-voltage from grid-tied solar inverters," in Photovoltaic Specialist Conference (PVSC), 2015 IEEE 42nd, 2015, pp. 1-6.

[35] M. Ropp, A. Hoke, S. Chakraborty, D. Schutz, C. Mouw, A. Nelson, et al., "Ground Fault Overvoltage with Inverter-Interfaced Distributed Energy Resources," IEEE Transactions on Power Delivery, vol. PP, pp. 1-1, 2016.

[36] Ametek, "Standalone TerraSAS Photovoltaic Simulator," ProgrammablePower.

[37] A. Lichauer and S. Whaite, "Three-phase Voltage Sag Generator Final Report," University of Pittsburgh, 2014.

[38] Electric Power Research Institute "The Impact of Voltage Sags on Industrial Plant Loads". 31 December 2003. [Online] Available: http://www.epri.com/abstracts/Pages/ProductAbstract.aspx?ProductId=00000000000101 7288 .

[39] Dranetz. (August 30, 2016). PowerXplorer PX5. Available: http://www.dranetz.com/product-services/powerxplorer-px5/ - tab-1

[40] "System Identification Toolbox" Mathworks. [Online] Available:
      https://www.mathworks.com/products/sysid/

[41] N. Patcharaprakiti, K. Kirtikara, K. Tunlasakun, J. Thongpron, D. Chenvidhya, A.
      Sangswang, V. Monyakul and B. Muenpinij, "Modeling of Photovoltaic Grid Connected
      Inverters Based on Nonlinear System Identification for Power Quality Analysis," in
      Electrical Generation and Distribution Systems and Power Quality Disturbances, 2011,
      pp. 53-82.

[42] K. N. Yong He, "Nonlinear Model Identification for Inverter of AMB-Flywheel System,"
      Journal of Selected Areas in Mechatronics (JMTC), pp. 1-6, 2012.

[43] Y. Zhu, "Estimation of Nonlinear ARX Models," Conference on Decision and Control,
      pp. 2214-2219, 2002.

[44] "Documentation," MathWorks, [Online]. Available:
      http://www.mathworks.com/help/ident/ref/sigmoidnet.html . [Accessed October 2015].

[45] "Sigmoid Functions," 27 December 2014. [Online]. Available:
      https://upload.wikimedia.org/wikipedia/commons/6/6f/Gjl-t%28x%29.svg . [Accessed
      26 November 2015].

[46] "Documentation," MathWorks, [Online]. Available:
      https://www.mathworks.com/help/ident/ref/nlarx.html . [Accessed November 2016].

[47] Roger C. Dugan, "Reference Guide: The Open Distribution System Simulator
      (OpenDSS)" [Online].

[48] L. Wieserman and T. McDermott, "OpenDSS Tech Note: Voltage-Controlled Current
      Source" [Online]. Available on the OpenDSS website January 2017.

[49] L. M. Wieserman, T. E. McDermott, and R. C. Dugan, "Open and Short Circuit Testing
      of Photovoltaic Inverters," *IEEE Transactions on Power Delivery,* submitted.

[50] T. E. McDermott, "A test feeder for DG protection analysis," in *Power Systems
      Conference and Exposition (PSCE), 2011 IEEE/PES*, 2011, pp. 1-7.